JAEA-Data/Code
2011-013

JAEA-Data/Code

Construction of Average Adult Japanese Voxel Phantoms for Dose Assessment

Kaoru SATO, Fumiaki TAKAHASHI, Daiki SATOH and Akira ENDO

Division of Environment and Radiation Sciences
Nuclear Science and Engineering Directorate

December 2011
Japan Atomic Energy Agency
日本原子力研究開発機構

Construction of Average Adult Japanese Voxel Phantoms for Dose Assessment

Kaoru SATO, Fumiaki TAKAHASHI, Daiki SATOH and Akira ENDO

Division of Environment and Radiation Sciences
Nuclear Science and Engineering Directorate
Japan Atomic Energy Agency
Tokai-mura, Naka-gun, Ibaraki-ken

(Received September 16, 2011)

The International Commission on Radiological Protection (ICRP) adopted the adult reference voxel phantoms based on the physiological and anatomical reference data of Caucasian on October, 2007. The organs and tissues of these phantoms were segemented on the basis of ICRP Publication 103. In future, the dose coefficients for internal dose and dose conversion coefficients for external dose calculated using the adult reference voxel phantoms will be widely used for the radiation protection fields. On the other hand, the body sizes and organ masses of adult Japanese are generally smaller than those of adult Caucasian. In addition, there are some cases that the anatomical characteristics such as body sizes, organ masses and postures of subjects influence the organ doses in dose assessment for medical treatments and radiation accident. Therefore, it was needed to use human phantoms with average anatomical characteristics of Japanese.

The authors constructed the averaged adult Japanese male and female voxel phantoms by modifing the previously developed high-resolution adult male (JM) and female (JF) voxel phantoms. It has been modified in the following three aspects: (1) The heights and weights were agreed with the Japanese averages; (2) The masses of organs and tissues were adjusted to the Japanese averages within 10%; (3) The organs and tissues, which were newly added for evaluation of the effective dose in ICRP Publication 103, were modeled. In this study, the organ masses, distances between organs, specific abdosrbed fractions (SAFs) and dose conversion coefficients of these phantoms were compared with those evaluated using the ICRP adult reference voxel phantoms. This report provides valuable information on the anatomical and dosimetric characteristics of the averaged adult Japanese male and female voxel phantoms developed as refernce phantoms of adult Japanese.

Keywords: Adult Japanese, Japanese average, Voxel Phantoms, Dosimetry, Organ Dose, Radiation Exposure, ICRP Publication 103

線量評価用平均的成人日本人ボクセルファントムの構築

日本原子力研究開発機構原子力基礎工学研究部門
環境・放射線科学ユニット
佐藤　薫、高橋　史明、佐藤　大樹、遠藤　章

(2011 年 9 月 16 日受理)

2007年10月、国際放射線防護委員会（ICRP）は、コーカサス人の生理学的、解剖学的標準データに基づいた成人レファレンスボクセルファントムを採用した。これらのファントムの臓器及び組織は、ICRP Publication 103に基づいて区分されている。今後、成人レファレンスボクセルファントムを用いて計算された、内部被ばく評価のための線量係数及び外部被ばく評価に用いる線量換算係数が放射線防護分野において利用される。一方、一般的に成人日本人の体格及び臓器重量は、成人コーカサス人よりも小さい。加えて、医療処置及び放射線事故時の線量評価においては、被験者の体格、臓器重量、姿勢等の解剖学的特徴が臓器線量に影響するケースがあることから、日本人の平均的な解剖学的特徴を有する人体ファントムを利用することが必要である。

著者らは、以前に開発した高解像度成人男性（JM）及び女性（JF）ボクセルファントムを修正することにより、平均的成人日本人男女のボクセルファントムを構築した。以下の3点について修正を行った。(1)身長及び体重を日本人の平均値に一致させた。(2)臓器・組織の重量を日本人の平均値の±10%以内になるように調整した。(3)ICRP Publication 103において実効線量の評価のために新たに追加された臓器・組織をモデル化した。本研究では、これらのファントムの臓器重量、臓器間距離、比吸収割合（SAFs）、線量換算係数について、ICRP成人レファレンスボクセルファントムを用いて計算した値と比較した。本報告書は、成人日本人のレファレンスファントムとして開発した、平均的成人日本人男女ボクセルファントムの解剖学的及び線量評価上の特性についての有用な情報を示す。

原子力科学研究所（駐在）：〒319-1195 茨城県那珂郡東海村白方白根 2-4

Contents

目　次

List of figures

List of tables

1. Introduction

ICRP approved the fundamental recommendations[1)] on the radiation protection of man and environment against ionizing radiation on March, 2007. In this recommendation, ICRP updated the organs, tissues, and their tissue weighting factors that should be considered in the effective dose calculation; the salivary glands, extrathoracic (ET) regions, oral mucosa, prostate and lymphatic nodes were added, based upon more information on stochastic effects of radiation on organs and tissues. The calculations of absorbed doses in these organs and tissues are necessary for the dose assessment methods given in ICRP Publication 103.[1)] In addition, ICRP decided to use the adult reference voxel phantoms[2)] based on the physiological and anatomical data[3)] of adult Caucasian male and female for evaluations of new reference values of equivalent doses for each organs and effective doses for whole body. The new reference values of dose coefficients and dose conversion coefficients, which are calculated by using the ICRP adult reference voxel phantoms, will be presented.

The dose coefficients and dose conversion coefficients recommended by ICRP are practical for the purposes of radiation protection. However, the anatomical characteristics such as organ masses, body sizes and postures are different from each individual. In dose assessments against medical treatments and radiation accidents, there are some cases that the anatomical characteristics influence the organ doses. Therefore, many human phantoms containing the voxel phantoms with different anatomical chracteristcs were developed, and were used for the calculations of organ doses agaist various radiation exposures.[4-22)] Veit and Zankl clarified that there is a correlation between organ doses and patient diameter.[13,14)] This finding was based on the analysis of the organ doses of the infant (BABY) and pediatric (CHILD) voxel phantoms.[5,6)] However, it was very difficult to individually represent the sizes and shapes of organs, tissues and bodies of all patients. In recent years, non-uniform rational B-spline (NURBS) surface modeling technique was applied to the descriptions of the organ, tissue and content boundaries in human phantoms.[15)] NURBS surface modeling technique can easily change the sizes and shapes of organs, tissues and bodies. Thus, several human phantoms were created by using NURBS surface modeling technique, and were used to the analysis of effects of body size on patient dose assessment.[15-22)]

The Caucasoid have large size body compared with Mongolian populations containing Japanese. Therefore, it is important to analyze the differences in the organ doses and the SAFs containing the self-specific absorbed fractions (Self-SAFs) between Japanese and Caucasian. The Japan Atomic Energy Agency (JAEA) has been developed the computed tomography (CT) based four adult Japanese male (JM[23)] and Otoko[24)]) and female (JF[25)] and Onago[26)]) voxel phantoms to clarify the impacts of the differences in body sizes between Japanese and Caucasian on dose assessment. In addition, these voxel phantoms were used for the calculations of SAFs for the intake of radionuclides and dose conversion coefficients for external radiation fields.[23-36)] Among the four adult Japanese male and female voxel phantoms, Otoko and Onago were first Japanese voxel phantoms. Their voxel size was 0.98×0.98×10 mm^3.[24,26)] In most cases, this voxel size is enough to estimate organ doses. However, in some cases where the deposited energy of small or thin organs is evaluated, more realistic voxel phantom may be needed. Therefore, the JM and JF phantoms were developed as the second-generation adult Japanese voxel phantoms whose voxel size was 0.98×0.98×1 mm^3.[23,25] This size voxel enables us to realistically represent shapes of thin and small size organs and tissues, and to accurately calculate organ doses and SAFs; the JM and JF phantoms are human models, which accurately represent anatomical structure of specific subject. Although the anatomical charcteristics of each subject are important for the dose assessments against medical treatment and radiation accident, it is not practical to individually construct human models for dose assessment against each subject. Therefore, human models with anatomical characteristics of average Japanese are necessary for dose assessments against medical treatment and radiation accident. To solve the issue, the authors constructed the averaged adult Japanese male and female voxel phantoms by modifying the body sizes and organ masses of JM[23)] and JF[25)]. The organs and tissues of the JM and JF phantoms were segmented under consideration of tissue category of the tissue weighing factors given in the ICRP Publication 60.[37)] Therefore, JM and JF were called 'the JM-60 phantom' and 'the JF-60 phantom', respectively. In the averaged adult Japanese male and female voxel phantoms, the salivary glands, ET region, oral mucosa, prostate and lymphatic nodes, which the tissue weighting factors were newly assigned by ICRP Publication 103,[1)] were also segmented. Thus, these phantoms were called 'the JM-103 phantom' and 'the JF-103 phantom', respectively. Now, the JM-103 phantom is using for the study on dose assessment of adult Japanese male in CT examinations.[38)] In future, the JM-103 and JF-103 phantoms will be also used as the basic models for constructions of the adult Japanese models with different body sizes. These human models will apply to the construction of the organ dose database in web-based dose assessment system, WAZA-ARI[39,40)] for CT examinations in Japan. This report describes the construction methods, and anatomical and dosimetric characteristics of the JM-103 and JF-103 phantoms. To examine the anatomical and dosimetric characteristics of JM-103 and JF-103, examples of the SAFs, Self-SAFs and dose conversion coefficients of these phantoms were calculated, and were compared with those of the JM-60 and JF-60 phantoms and the ICRP adult reference voxel phantoms.

2. Construction of the JM-103 and JF-103 phantoms

As shown in Table 2-1, the body sizes[41] of adult Japanese were smaller than those[3] of adult Caucasian. Although the height and weight of JM-60 were almost the same as the averages of adult Japanese,[23] JF-60 has a diminutive body compared with body size of average adult Japanese female.[25] Thus, the adjustment of body size to Japanese average was performed against only JF-60.

Table 2-1 Heights and weights of JM-60, JF-60, and the averages of adult Japanese and Caucasian.

Gender	Phantom and Subject	Height (cm)	Weight (kg)
Male	JM-60	171	65
	Average adult Japanese	170	64
	Average adult Caucasian	176	73
Female	JF-60	152	44
	Average adult Japanese	155	52
	Average adult Caucasian	163	60

In the previous paper,[23,25] the authors reported that the differences in organ and tissue masses between JM-60 and Japanese averages were mostly within 30%, and the masses of organs and tissues of JF-60 were generally smaller than the averages[41] of adult Japanese female, corresponding to its small size body. Thus, the mass modifications of organs and tissues were necessary for JM-60 and JF-60. In the latest fundamental recommendations,[1] ICRP updated the organs, tissues and their tissue weighting factors that should be considered in the effective dose calculations (Table 2-2); the tissue weighting factors were also assigned to the salivary glands, ET region, oral mucosa, prostate and lymphatic node. The evaluations of their absorbed doses will be also required for dose assessments in the radiation protection fields. However, the tissue segmentations of JM-60 and JF-60 were based on the tissue weighting factors[37] given in ICRP Publication 60 (Table 2-3). Thus, the above five organ and tissue models were constructed, and were incorporate into JM-103 and JF-103.

Table 2-2 Tissue weighting factors in ICRP Publication 103.[1]

Tissue or organ	Tissue weighting factors, w_T
Lungs. Stomach, Colon, Red bone marrow, Breast, Remainder*	0.12
Gonads (Ovary or Testis)	0.08
Thyroid, Esophagus, Bladder, Liver	0.04
Bone surface, Skin, Brain, Salivary glands	0.01

*Adrenals, Extrathoracic (ET) region, Gall bladder, Heart, Kidneys, Lymphatic nodes, Muscle, Oral mucosa, Pancreas, Prostate, Small intestine, Spleen, Thymus, Uterus/Cervix

Table 2-3 Tissue weighting factors in ICRP Publication 60.[37)]

Tissue or organ	Tissue weighting factors, w_T
Gonads (Ovary or Testis)	0.20
Red bone marrow, Colon, Lungs, Stomach	0.12
Bladder, Breast, Liver, Esophagus, Thyroid	0.05
Skin, Bone surface	0.01
Remainder*	0.05

*Adrenals, Brain, Upper large intestine, Small intestine, Kidneys, Muscle, Pancreas, Spleen, Thymus, Uterus

2.1 Techniques of phantom constructions

Since the breast is located at the outer surface of the chest, the mass modification should be performed under consideration of outer body configuration. In addition, the densities of salivary glands and lymphatic nodes are almost the same as those of most soft tissues (See, Appendix C). Thus, these tissues cannot be easily segmented from the CT images by using the grey value threshold only. The characteristics with respect to their densities and shapes restrict their mass modifications and modeling based on the two dimensional image processing only. To solve these issues, the two dimensional[5,6,8,24,26)] and three dimensional[15-17)] image processing were applied to the constructions of JM-103 and JF-103 (Figure 2-1). In the two dimensional image processing, the Visilog 6.8 for Windows (Noesis Inc, France) and Photoshop 5.5 for Windows (Adobe Incorporated, USA) were used for modifications of shapes and sizes of organs and tissues, and assignments of their identification numbers to voxels belonging to each segmented region. A vector-based three dimensional imaging, modeling and measurement software, 3D-DOCTOR 4.0 for Windows (Able Software Corp, USA) and three dimensional polygon modeler software, Metasequoia LE R2.4 for Windows were used for the three dimensional image processing. The three dimensional geometrical images were constructed from the two dimensional organ segmented images by using 3D-DOCTOR 4.0. A three dimensional mesh voxelizer software, Binvox 0.37 for Linux[42)] was employed for the constructions of the two dimensional organ segmented images.

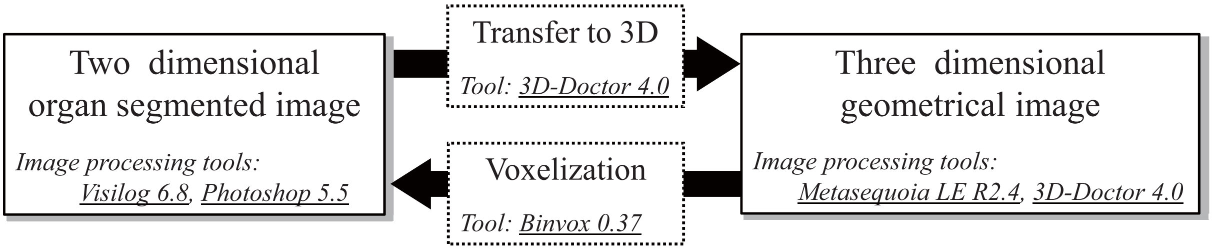

Figure 2-1 Image processing procedures and imaging software used for constructions of the JM-103 and JF-103 phantoms.

2.2 Adjustment of height and weight to Japanese averages

Generally, the voxel sizes of phantoms affect the masses and thicknesses of membranous organs and tissues, and also change the marrow distribution in bone tissue. Thus, it was considered that a voxel size ($0.98 \times 0.98 \times 1$ mm^3) and a spatial distribution of marrows in bone tissues of the JF-60 phantom should be kept in the JF-103 phantoms. To solve these issues, the body size of JF-60 was adjusted by adopting the two image processing methods. The Visilog 6.8 was used for these image processing. Firstly, the three voxel layers were added to just inner skin of whole body in JF-60 for the enlargement of body size. The image processing was performed by using the function named 'dilation'. The dilation function can fill small holes and gulfs, and enlarge the size by adding the voxel layers to outer surface of objects on images. After the enlargement of whole body, the addition layers of voxels were redefined as adipose tissues. In the first step, the weight of JF-60 increased by 10% to 48.4 kg. Secondly, the resolution ($512 \times 512 \times 1634$ pixels) of JF-60 was changed by an image processing function named 'zoom'. The zoom function can generate an image with a new resolution using the interpolation methods selected by user. In this process, a new resolution of JF-60 was set to $526 \times 526 \times 1666$ pixels. In the second step, the weight of JF-60 increased by 8% to 52 kg. Finally, the height and weight of JF-60 were able to adjust to the average height (155 cm) and weight (52 kg)[41] of adult Japanese female.

2.3 Modifications of organs, tissues and content masses

In this study, the authors determined that the masses of organs, tissues and contents in the JM-103 and JF-103 phantoms should be adjusted to Japanese averages[41] within 10%. In addition to dilation function (see, Section 2.2), an image processing function named 'erosion' in Visilog 6.8 was generally adopted for reduction of the organ, tissue and content masses. The erosion can remove small points, and shrink the size by deleting the voxel layers from outer surface of objects on images. The dilation and erosion functions can produce the images of organs and tissues with different sizes and geometrically similar shapes. The enlargement and reduction of organs and tissues were mainly performed in the horizontal directions (e.g. ventral-dorsal and left-right directions) of the phantom body, since the unplanned alterations of organ and tissue shapes may create the anatomically unreasonable human structure. In the case that the inflation and deflation treatments on horizontal direction were impossible, the image processing against the vertical direction (e.g. head-leg axis) was done under consideration of anatomy. The following several image processing methods were applied to the mass modifications of organs, tissues and contents in the JM-103 and JF-103 phantoms.

2.3.1 Membranous organs and their contents

In order to modify the masses of membranous organs, the boundaries between organs and contents were redefined by reprocessing original CT images for the JM-60 and JF-60 phantoms. The artifacts in CT images are generally derived from the vital signs and the scatter of X-ray emitted from CT devices at adjacency of bones, teeth and implants with different densities. The artifact is one of several difficulties in distinguishing membranous organs from their contents. For example, the boundary between wall and content in heart is not clear, because of its heartbeat and blood flow. Therefore, the artifacts in heart were removed by exploiting image processing functions of Visilog 6.8 and Photoshop 5.5. Similarly to the heart, the boundaries between wall and content were also redefined in other membranous organs such as gastrointestinal tracts, gall bladder and bladder.

2.3.2 Adipose and muscle

Adipose and muscle are distributed over the whole body, and have heavier masses than other organs and tissues. Thus, it is very difficult to adjust their masses to Japanese averages. In this study, the anatomically reasonable tissues were newly reconstructed from adipose and muscle tissues. The segmentation procedures contributed to the decreases in the masses of both tissues. For example, the largest artery (aorta) and vein (vena cava) in human body and their contents were constructed for the purpose of mass modifications of adipose and muscle. In addition, the mass ratios between adipose and muscle were also corrected to Japanese averages in order to ensure the anatomical justice. The boundaries between adipose and muscle in the JM-60 and JF-60 phantoms were reprocessed by adopting an image processing filter named 'diffusion' in Photoshop 5.5. The diffusion filter can generate a haze to soften objects on images; the diffusion filter can reduce contrast of the boundaries of objects on images. To keep distribution of adipose and muscle in body, the reprocessing of boundaries between two soft tissues was performed from head to foot.

2.3.3 Brain and lungs

The brain and lungs are surrounded with the cranium and ribs. The mass modifications of the two organs are considerably restricted by these bone structures. Therefore, the constructions of membranous tissues such as meninges and pleura were performed to reduce the masses of brain and lungs. The meninges are the membrane system with three layers, and envelope the central nervous system containing cerebrum (brain), medulla oblongata and spinal cord. By using image processing

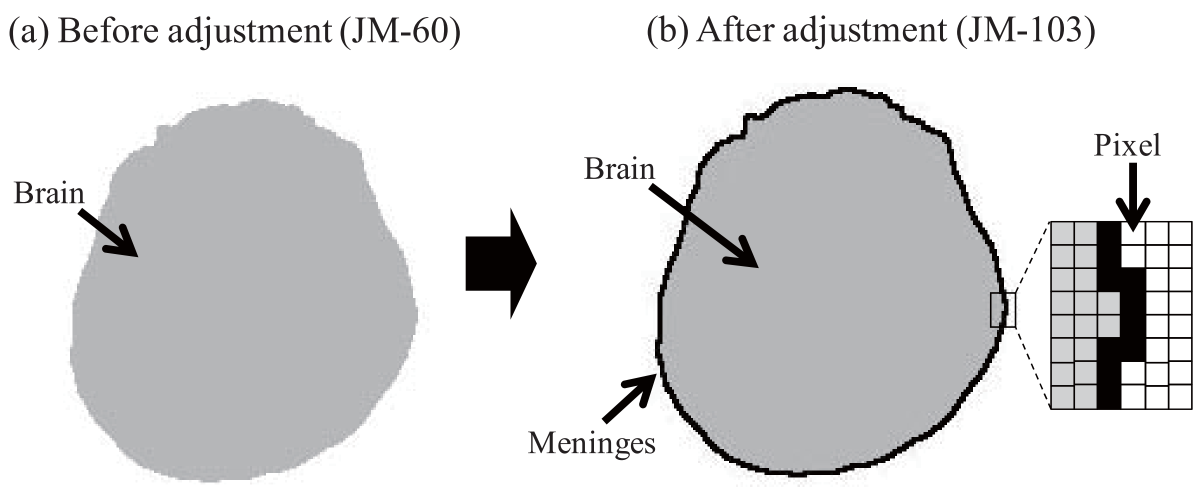

Figure 2-2 Cross sectional view of brain at 100 mm from top of the head.
(a) Before adjustment (JF-60) and (b) After adjustment (JF-103).

functions such as erosion and dilation in Visilog 6.8, one or two voxel layers at the outer surface of brain were assigned to the meninges (Figure 2-2). The pleura are thin membranous tissues that surround the lungs. The construction method of pleura is similar to that of the meninges in brain; the one or two voxel layers at outer surface of lungs were redefined as pleura.

2.3.4 Female breast tissue

The breast tissue, which consists of only breast adipose, was constructed for adult male phantom, JM-103. On the other hand, it was assumed that the breast tissue in adult female consists of breast adipose and mammalian gland. The average mass (300 g) of breast tissue in adult Japanese female was referred to the data of Tanaka and Kawamura.[41] The mass ratio (0.4)[3] of mammalian gland to whole breast tissue was adopted for mass calculation of the two breast tissues. The authors estimated the average masses of mammalian gland and breast adipose in adult Japanese female at 120 g and 180 g, respectively. The breast tissue of the JF-60 phantom was modified according to the following image processing procedures. Firstly, OBJ format three dimensional geometrical data (hereafter, 'polygon data') of the breast tissue in JF-60 was constructed from its DICOM format two dimensional organ segmented image data by using 3D-DOCTOR 4.0. Secondly, Metasequoia LE R2.4 and 3D-DOCTOR 4.0 were utilized to change the shape and size of breast tissue polygon data (Figure 2-3); the breast mass (581g) of JF-60 was adjusted to the average of breast mass in adult Japanese female within 3%. Thirdly, the modified polygon data of breast tissue was placed in arbitrary space of the JF-103 phantom under consideration of anatomical positions, and was voxelized by employing Binvox 0.37 for Linux;[42] as a result of voxelization, the RAW format two dimensional organ segmented image data of breast tissue was produced from its modified polygon data. Lastly, the produced RAW format image data of breast tissue was incorporated into DICOM format two dimensional organ segmented image data of JF-103 by using Visilog 6.8.

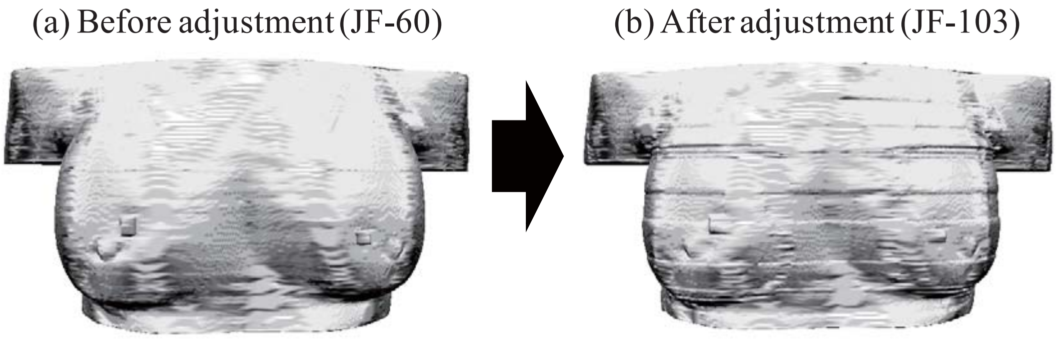

Figure 2-3 Changes in breast shape during adjustment process.
(a) Before adjustment (JF-60) and (b) After adjustment (JF-103).

2.3.5 Bone tissues

A previously developed bone marrow distribution model (hereafter, 'the Approx-distribution model')[36] was also applied to the JM-103 and JF-103 phantoms. In the Approx-distribution model, the bone tissues were classified into the twenty anatomical regions based on the divisions given in ICRP Publication 70[43] and 89.[3] Each anatomical region was divided into seven materials, according to the grey values; the marrow distributions in bone tissues were approximately represented by 140 segmented sub-regions (7 materials × 20 anatomical regions). Since the body size of JM-60 was almost the same as the Japanese averages, JM-103 made use of the bone tissue model of JM-60 without the modifications of its masses and shapes.

As described in Section 2.2, the zoom function in Visilog 6.8 can generate an image with an optional resolution; the shapes and sizes of objects on images can be changed by assigning the resolution in the x-axis and y-axis directions. Therefore, the bone tissue model of JF-60 was scaled up by employing the zoom function. As a result of scaling, the resolution and voxel size of a new scaled bone tissue model were set to 526×526×1666 pixels and 0.98×0.98×1 mm^3, respectively. Thereafter, the new scaled bone tissue model was incorporated into the JF-103 phantom. Figure 2-4 compares the mass fractions of (a) each material and (b) each anatomical region to whole bone tissue in the JF-103 with those in JF-60 phantoms. Mass distributions of seven materials and twenty anatomical regions in the bone tissue of JF-103 were in good agreement with those of JF-60, respectively. These results indicate that the JF-103 phantom has similar anatomical characteristics to the bone tissue of the JF-60

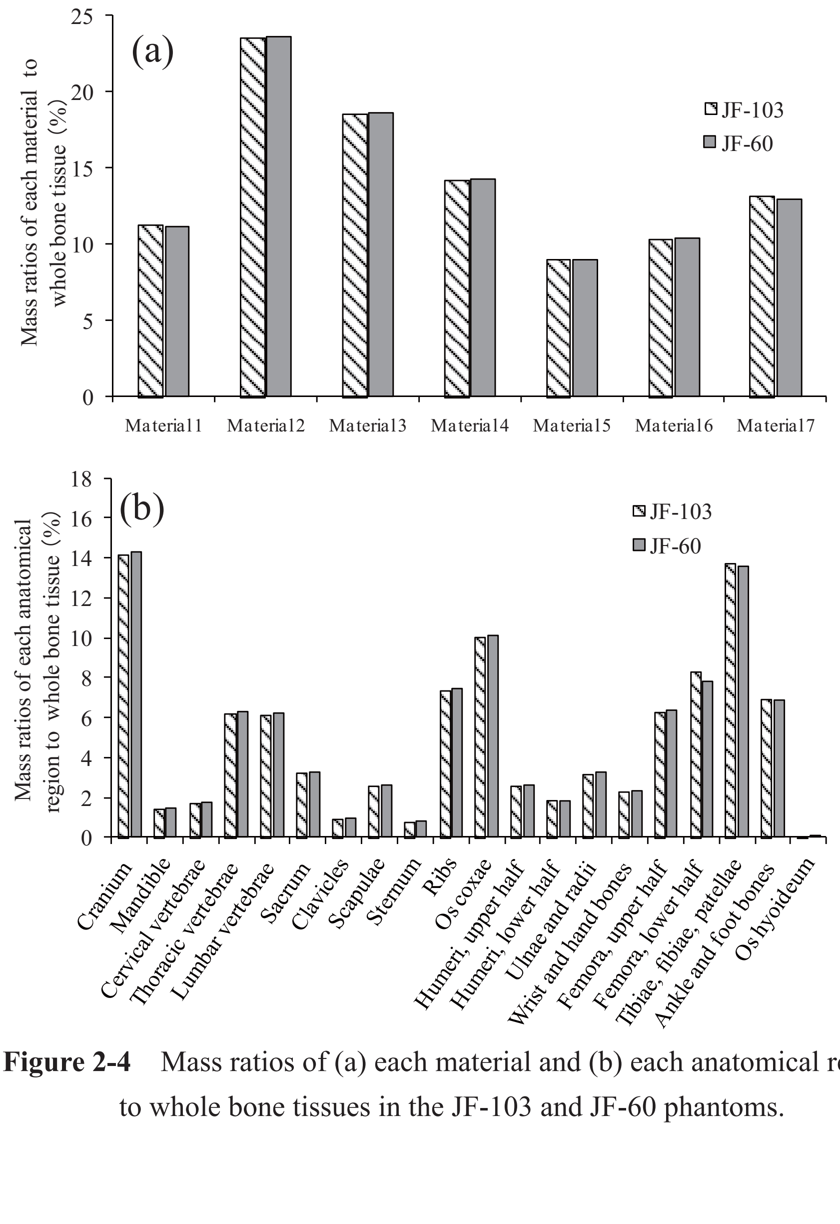

Figure 2-4 Mass ratios of (a) each material and (b) each anatomical region to whole bone tissues in the JF-103 and JF-60 phantoms.

phantom, which was modeled from an actual person. Therefore, it can be concluded that there is no anatomical problem in applying the JF-103 phantoms to the dose calculation for bone tissue.

2.4 Construction of five organs and tissues, to which the tissue weighting factors were newly added by ICRP Publication 103

In the 2007 recommendations[1)] of ICRP, the Commission added the ET region, oral mucosa, salivary glands, prostate and lymphatic nodes to the organs and tissues that should be considered in the effective dose calculation. As previously mentioned, the JM-60 and JF-60 phantoms cannot utilize for the dose calculation of the above five organs and tissues. Thus, the five organs and tissues were modeled, and were set in the JM-103 and JF-103 phantoms.

2.4.1 ET region and oral mucosa

In the morphometric model of respiratory tract given in ICRP Publication 66,[44)] ET region is a thin membranous tissue, which consists of four layers such as mucus, epithelium, basement membrane and subepithelial layer. The targets called 'basal cells' are assumed to be at average depth of 40-50 μm from mucus surface. In dose assessment against ET region, the absorbed dose in its target should be calculated.[44)] However, it is impossible to represent the thin layer structures by using voxel with a size of 0.98×0.98×1 mm^3. Thus, ET regions of JM-103 and JF-103 were automatically defined by segmenting one voxel layer from the outer surface of the airways at the around the anterior and posterior nasal passages and pharynx.

In oral cavity, the stem cells, which are located in the basal cell layer of mucosa, are taken to be a 10 μm layer at a depth of 190-200 μm.[45)] Similarly to the ET region, a thickness of target layer including stem cells is very thin, and cannot be exactly modeled by about 1 mm^3 size voxel. Therefore, one voxel layer at the outer surface of oral cavity in JM-103 and JF-103 was assigned to the oral mucosa.

2.4.2 Salivary glands and prostate

The salivary glands are included in the alimentary tract system, and are mainly located in the around oral cavity. The major salivary glands are the parotid, submandibular and sublingual glands. The sizes, positions and shapes of the salivary glands were in detail described in the ICRP Publication 100[45)] and anatomical text book.[46)] Each average mass of salivary glands in adult Japanese was based on the previous reports.[41)] In interpretation of CT images, the salivary glands cannot be easily distinguished from the surround soft tissues such as adipose and muscle. Therefore, the organ model construction methods described in Section 2.3.4 were also adopted in modeling the salivary glands. The salivary glands were constructed as follows. The polygon data of salivary glands were created by employing a Metasequoia LE R2.4. The 3D-DOCTOR 4.0 was used for determination of each insertion position of three salivary gland polygon data into JM-103 (Figure 2-5). Thereafter, the polygon data of salivary glands were voxelized by using Binvox 0.37. The voxel sizes of salivary glands were also set in the 0.98×0.98×1 mm^3. As a result, the two dimensional organ segmented images of salivary glands were produced. The incorporation of the two dimensional organ segmented images of salivary glands into the JM-103 phantom was performed through the image processing functions in Visilog 6.8. The relative positional relationships between cranium, mandible, cervical vertebrae and Os hyoideum in JM-103 were almost the same as those in JF-103. Therefore, the polygon data of salivary glands constructed for JM-103 was scale-downed, and was also incorporated into JF-103.

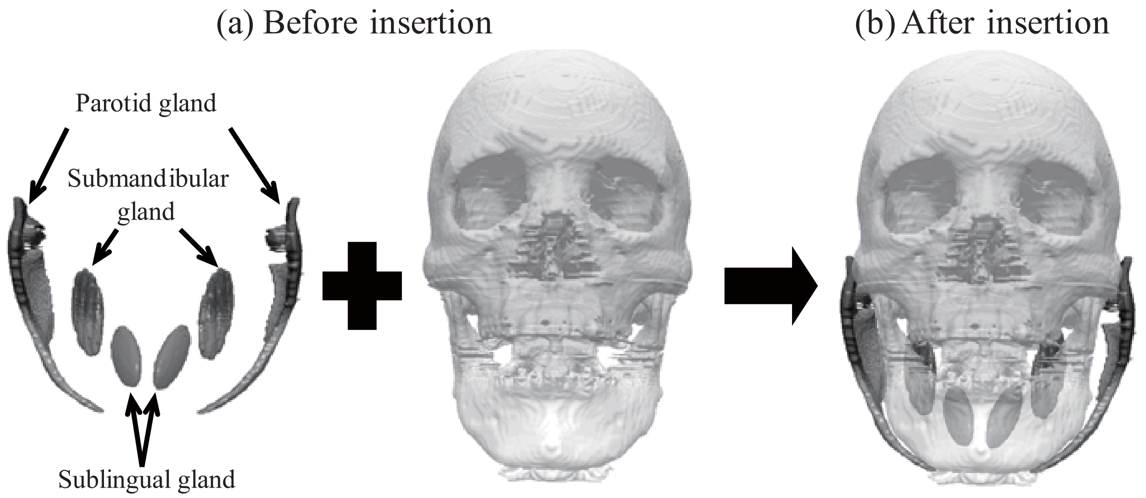

Figure 2-5 Insertion process of salivary gland polygon models into skull polygon model. (a)Before insertion and (b) After insertion.

The prostate is one of reproductive organs in male, and is located under bladder. The prostate mass was referred to the average mass[41] of adult Japanese male. The modeling methods of female breast tissues and salivary gland were also employed for the construction of prostate model.

2.4.3 Lymphatic tissue

The lymphatic tissue plays an important role in the immune system. These tissues are widely distributed in whole body, and cannot be identified on the CT images. Therefore, the modeling of lymphatic tissue was performed by using image processing techniques described in Sections 2.3.4 and 2.4.2. The sizes, shapes and distributions of lymphatic tissues were based on the anatomical text book.[46] Figure 2-6 shows the polygon models of lymphatic tissue constructed for the JM-103 and JF-103 phantoms. In this study, it was assumed that the lymphatic tissue consists of nodes and vessels. The diameter of vessels and the transverse diameter of nodes in lymphatic tissue models were set to be 2 and 6 mm, respectively. The masses of lymphatic tissue models were according to the reference values (Male and female: 220 and 170 g, respectively)[41] of the adult Japanese. In the ICRP adult reference voxel phantoms,[2] the lymphatic tissues were placed in six regions such as extrathoracic airways, thoracic airways, head, trunk, arms and legs. Therefore, the authors also incorporated the constructed lymphatic tissue models into the above six regions of JM-103 and JF-103.

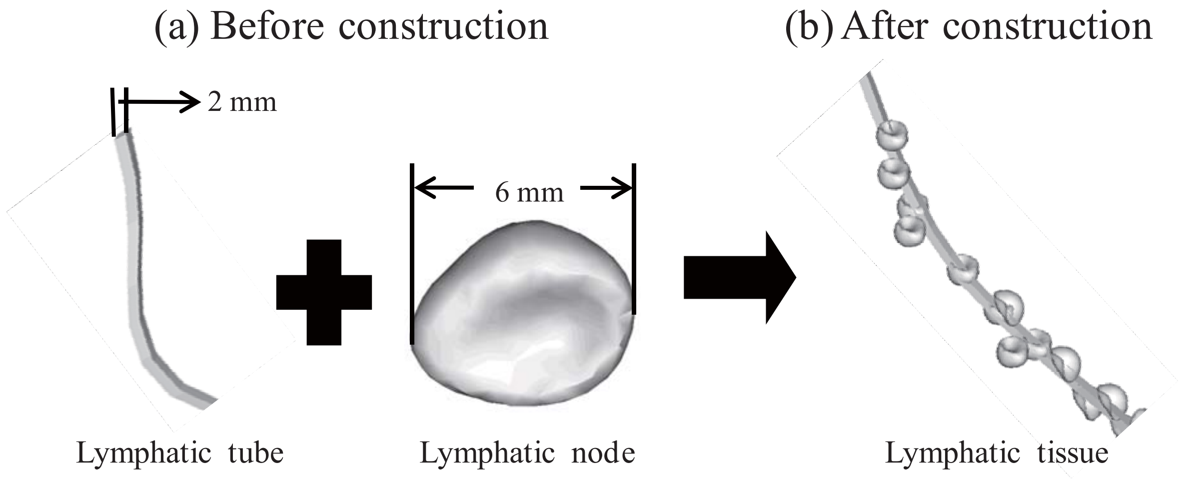

Figure 2-6 Construction of lymphatic tissue polygon model for the JM-103 and JF-103 phantoms. (a)Before construction and (b) After construction.

2.5 Elemental compositions and densities of the JM-103 and JF-103 phantoms

Tables 2-4 and 2-5 give the elemental compositions and densities of tissues, organs and organ contents assigned to the JM-103 and JF-103 phantoms, respectively. Except for the bone tissue, lymphatic tissue and prostate, the composition data were obtained from the data for adult given in the ICRP Publication 89[3] and the ICRU Report 44.[47] Except for the lymphatic tissue, prostate, bone tissues and teeth, the densities were referred to the ICRU Report 46.[48] The teeth density by Schlattl et al.[49] was adopted for that in the JM-103 and the JF-103 phantoms. The materials for bone tissue, which consists of hard bone and bone marrow containing active and inactive marrows, were referred to the elemental compositions and densities by Veit et al.[6] The elemental compositions and densities of the lymphatic tissue and prostate were obtained from the ICRP Publication 110.[2] In order to calculate the absorbed doses separately in the active and inactive marrows, and hard bone, the seven materials assigned to the bone tissues were used for the Approx-distribution model[36] explained in Section 2.3.5 (Tables 2-4 and 2-5).

Table 2-4 List of materials, their elemental compositions (percentage by mass) and densities for the JM-103 phantom.

Material	ID	H	C	N	O	Na	Mg	P	S	Cl	K	Ca	Fe	I	Ar	Density (g/cm^3)
Bulk soft tissues	m31	10.5	25.6	2.7	60.2	0.1		0.2	0.3	0.2	0.2					1.03
Muscle	m32	10.2	14.3	3.4	71.0	0.1		0.2	0.3	0.1	0.4					1.05
Skin	m33	10.0	20.4	4.2	64.5	0.2		0.1	0.2	0.3	0.1					1.09
Adipose	m34	11.4	59.8	0.7	27.8	0.1			0.1	0.1						0.95
Breast	m35	11.4	59.8	0.7	27.8	0.1			0.1	0.1						0.95
Lungs	m36	10.3	10.5	3.1	74.9	0.2		0.2	0.3	0.3	0.2					0.26
Teeth	m37	2.2	9.5	2.9	42.1		0.7	13.7				28.9				2.75
Bladder	m41	10.5	9.6	2.6	76.1	0.2		0.2	0.2	0.3	0.3					1.04
Brain	m42	10.7	14.5	2.2	71.2	0.2		0.4	0.2	0.3	0.3					1.04
Eyes	m43	9.6	19.5	5.7	64.6	0.1		0.1	0.3	0.1						1.07
Heart	m44	10.4	13.9	2.9	71.8	0.1		0.2	0.2	0.2	0.3					1.05
Kidneys	m45	10.3	13.2	3.0	72.4	0.2		0.2	0.2	0.2	0.2	0.1				1.05
Liver	m46	10.3	18.6	2.8	67.1	0.2		0.2	0.3	0.2	0.3					1.05
Pancreas	m47	10.6	16.9	2.2	69.4	0.2		0.2	0.1	0.2	0.2					1.04
Spleen	m48	10.3	11.3	3.2	74.1	0.1		0.3	0.2	0.2	0.3					1.06
GI-tract	m49	10.6	11.5	2.2	75.1	0.1		0.1	0.1	0.2	0.1					1.03
Thyroid	m50	10.4	11.9	2.4	74.5	0.2		0.1	0.1	0.2	0.1			0.1		1.05
Blood (heart content)	m51	10.2	11.0	3.3	74.5	0.1		0.1	0.2	0.3	0.2		0.1			1.06
Testes	m52	10.6	9.9	2.0	76.6	0.2		0.1	0.2	0.2	0.2					1.04
Lympha	m53	10.8	4.2	1.1	83.1	0.3			0.1	0.4						1.03
Prostate	m54	10.4	23.1	2.8	62.7	0.1		0.2	0.3	0.2	0.2					1.03
Stomach content	m81	10.5	25.6	2.7	60.2	0.1		0.2	0.3	0.2	0.2					0.68
Colon content	m82	10.5	25.6	2.7	60.2	0.1		0.2	0.3	0.2	0.2					0.72
Bone01 (marrow-70wt%)	m11	9.0	41.0	2.8	37.4	0.1	0.1	3.2	0.1			6.3	0.001			1.12
Bone02 (marrow-54wt%)	m12	8.1	34.9	3.1	39.1	0.1	0.1	4.9	0.2			9.7	0.001			1.25
Bone03 (marrow-45wt%)	m13	7.5	31.5	3.3	40.0	0.1	0.1	5.8	0.2			11.5				1.32
Bone04 (marrow-36wt%)	m14	6.9	28.1	3.5	40.9	0.1	0.1	6.7	0.2			13.4				1.39
Bone05 (marrow-24wt%)	m15	6.2	23.5	3.7	42.1	0.05	0.2	8.0	0.2			16.0				1.49
Bone06 (marrow-10wt%)	m16	5.3	18.2	4.0	43.6	0.02	0.2	9.5	0.3			18.9				1.64
Bone07 (marrow:00wt%)	m17	4.7	14.4	4.2	44.6		0.2	10.5	0.3			21.0				1.77
Air	m99		0.01	75.5	23.2										1.3	1.204E-3

The composition data are referred to the data for adult given in the ICRP Publication 89[3] and 110[2], the ICRU Report 44[47] and the Veit et al.[6]

Table 2-5 List of materials, their elemental compositions (percentage by mass) and densities for the JF-103 phantom.

Material	ID	H	C	N	O	Na	Mg	P	S	Cl	K	Ca	Fe	I	Ar	Density (g/cm^3)
Bulk soft tissues	m31	10.5	25.6	2.7	60.2	0.1		0.2	0.3	0.2	0.2					1.03
Muscle	m32	10.2	14.3	3.4	71.0	0.1		0.2	0.3	0.1	0.4					1.05
Skin	m33	10.0	20.4	4.2	64.5	0.2		0.1	0.2	0.3	0.1					1.09
Adipose	m34	11.4	59.8	0.7	27.8	0.1			0.1	0.1						0.95
Breast	m35	11.6	51.9		36.5											0.94
Lungs	m36	10.3	10.5	3.1	74.9	0.2		0.2	0.3	0.3	0.2					0.26
Teeth	m37	2.2	9.5	2.9	42.1		0.7	13.7				28.9				2.75
Stomach content	m38	10.5	25.6	2.8	60.1	0.1		0.2	0.3	0.2	0.2					0.43
Bladder	m41	10.5	9.6	2.6	76.1	0.2		0.2	0.2	0.3	0.3					1.04
Brain	m42	10.7	14.5	2.2	71.2	0.2		0.4	0.2	0.3	0.3					1.04
Eyes	m43	9.6	19.5	5.7	64.6	0.1		0.1	0.3	0.1						1.07
Heart	m44	10.4	13.9	2.9	71.8	0.1		0.2	0.2	0.2	0.3					1.05
Kidneys	m45	10.3	13.2	3.0	72.4	0.2		0.2	0.2	0.2	0.2	0.1				1.05
Liver	m46	10.3	18.6	2.8	67.1	0.2		0.2	0.3	0.2	0.3					1.05
Pancreas	m47	10.6	16.9	2.2	69.4	0.2		0.2	0.1	0.2	0.2					1.04
Spleen	m48	10.3	11.3	3.2	74.1	0.1		0.3	0.2	0.2	0.3					1.06
GI-tract	m49	10.6	11.5	2.2	75.1	0.1		0.1	0.1	0.2	0.1					1.03
Thyroid	m50	10.4	11.9	2.4	74.5	0.2		0.1	0.1	0.2	0.1			0.1		1.05
Blood (heart content)	m51	10.2	11.0	3.3	74.5	0.1		0.1	0.2	0.3	0.2		0.1			1.06
Ovaries	m52	10.5	9.3	2.4	76.8	0.2		0.2	0.2	0.2	0.2					1.05
Uterus	m53	10.6	31.5	2.4	54.7	0.1		0.2	0.2	0.1	0.2					1.02
Lympha	m54	10.8	4.2	1.1	83.1	0.3			0.1	0.4						1.03
Bone01 (marrow-70wt%)	m11	9.0	41.0	2.8	37.4	0.1	0.1	3.2	0.1			6.3	0.001			1.16
Bone02 (marrow-53wt%)	m12	8.0	34.5	3.1	39.2	0.1	0.1	5.0	0.2			9.9	0.001			1.26
Bone03 (marrow-45wt%)	m13	7.5	31.5	3.3	40.0	0.1	0.1	5.8	0.2			11.5				1.32
Bone04 (marrow-36wt%)	m14	6.9	28.1	3.5	40.9	0.1	0.1	6.7	0.2			13.4				1.39
Bone05 (marrow-25wt%)	m15	6.3	23.9	3.7	42.0	0.1	0.2	7.9	0.2			15.7				1.49
Bone06 (marrow-10wt%)	m16	5.3	18.2	4.0	43.6	0.02	0.2	9.5	0.3			18.9				1.64
Bone07 (marrow-00wt%)	m17	4.7	14.4	4.2	44.6		0.2	10.5	0.3			21.0				1.77
Air	m99		0.01	75.5	23.2										1.3	1.204E-3

The composition data are referred to the data for adult given in the ICRP Publication 89[3)] and 110[2)], the ICRU Report 44[47)] and the Veit et al.[6)]

3. Anatomical characteristics of the JM-103 and JF-103 phantoms

3.1 Body sizes and organ masses

Table 3-1 shows the physical characteristics of the adult Japanese male (JM-103 and JM-60[23)]) and female (JF-103 and JF-60[25)]) voxel phantoms, and the ICRP adult reference male (hereafter, 'the AM phantom') and female (hereafter, 'the AF phantom') voxel phantoms.[2)] The physical characteristics of the AM and AF phantoms were referred to the ICRP Publication 110.[2)] The body size of JM-60 was almost the same as the averages[41)] of adult Japanese male. On the other hand, JF-60 had a diminutive body compared with the body size of average adult Japanese female. The heights and weights of the JM-103 and JF-103 phantoms were almost the same as the averages of adult Japanese male and female, and were smaller than those of AM and AF.

The voxel sizes (0.98×0.98×1 mm^3) of JM-103 and JF-103 were smaller than those of AM and AF. Therefore, the organs and tissues of JM-103 and JF-103 were more realistically modeled compared with those of AM and AF. The differences in voxel sizes between these voxel phantoms also affected the capacity of phantom data; the data capacity of the JM-103 and JF-103 phantoms was several ten times as large as those of the AM and AF phantoms. The data capacity of phantom influences data handling in the computing environment. However, the small size voxel enables us to accurately calculate the organ doses, because the voxel size of JM-103 and JF-103 is smaller than mean free path (1.8 mm) of 0.01 MeV photons in the ICRU soft tissue.[47)]

Table 3-1 Physical characteristics of the JM-103, JM-60,[23)] JF-103, JF-60,[25)] AM and AF phantoms.[2)]

Property	JM-103	JM-60	AM	JF-103	JF-60	AF
Gender	male	male	male	female	female	female
Age	54	54	-	54	54	-
Height (cm)	171 (170)	171	176	155 (155)	152	163
Weight (kg)	65 (64)	65	73	52 (52)	44	60
Number of total voxel	67,340,831	69,471,853	1,946,375	54,461,853	47,802,315	3,886,020
Voxel horizontal length (mm)	0.98	0.98	2.137	0.98	0.98	1.775
Voxel vertical height (mm)	1	1	8	1	1	4.84
Voxel volume (mm^3)	0.9604	0.9604	36.54	0.9604	0.9604	15.25
Number of total slice	1835	1835	220	1666	1634	346
Number of total segmented region	214	192	140	215	194	140
Total capacity of phantom data (MB)	1800	1800	28	1700	1600	56

Values in parenthesis are the avregae heights and weights[41)] of adult Japanese male and female.

Numbers of total segmented region in JM-103 and JF-103 were 214 and 215, respectively, although the 192 regions for JM-60 and the 194 regions for JF-60 were segmented, respectively. The organ segmented data including these segmented regions were stored as ASCII text data with the array explained in Appendix A.

Tables 3-2 and 3-3 summarize the masses of some organs, tissues and contents in JM-103, JM-60,[23] JF-103, JF-60,[25] AM and AF,[2] along with averages[41] of adult Japanese. The mass data of each segmented region of JM-103 and JF-103 were calculated by using the data shown in Tables C-1 and C-2 (see, Appendix C). The adipose masses of the JM-103 and JF-103 phantoms were about 31% and 41% of the AM and AF phantoms, respectively. The adipose tissues are widely distributed in whole body. Thus, it was suggested that the thickness and distribution of subcutaneous and visceral adipose tissue in trunk of adult Japanese were different from those of adult Caucasian.

The skin masses of the JM-103 and JF-103 phantoms were smaller than the AM and AF phantoms about 41% and 30%, respectively (Tables 3-2 and 3-3). Similarly to the JM-60 and JF-60 phantoms,[23,25,36] an outer voxel layer of whole body of JM-103, JF-103, AM and AF[2] was defined as the skin tissues. Therefore, the thicknesses and masses of the skin tissues in these voxel phantoms were highly dependent on voxel size. For example, the thicknesses of skin tissues in AM and AF are about 2.137 mm and 1.775 mm,[2] respectively, and are about twice those (about 0.98 mm) of JM-103 and JF-103. The average skin masses of adult Japanese male and female were evaluated as the total mass of the epidermis and dermis.[41] The authors also assumed that the skin tissues of JM-103 and JF-103 included the epidermis and dermis; the skin masses of JM-103 and JF-103 were adjusted to the averages of adult Japanese within 10%. On the other hand, it was assumed that the skin tissues of AM and AF also consisted of the epidermis and dermis.[2] Thus, there is no difference in the anatomical definition of skin tissue between the two averaged adult Japanese voxel phantoms (JM-103 and JF-103) and the ICRP adult reference voxel phantoms (AM and AF). These facts mean that the differences in skin masses between the two averaged adult Japanese voxel phantoms and the ICRP adult reference voxel phantoms were mainly caused by the differences in voxel sizes rather than the anatomical characteristics.

The wall and content masses in bladder of the JM-103 phantom were about 78% and 51% of the AM phantom, respectively (Table 3-2). The large differences in masses were also found in comparison between the JF-103 and AF phantoms (Table 3-3). In particular, the mass differences in bladder content directly influence the shapes and sizes of bladder wall. Thus, it can be expected that the morphometric characteristics of bladder in the adult Japanese were distinctly different from those in the adult Caucasian.

In addition to the above cases, the large differences in masses of several organs and tissues were also found in comparison between the JF-103 and the AF phantoms (Table 3-3). The masses of breast, stomach, small intestine and colon of JF-103 were smaller than those of AF about 38%, 24%, 22%, 32%, respectively. In particular, a mass difference in the breast between the JF-103 and AF phantoms was relatively large. It was suggested that the mass differences in these organs were also attributed to the anatomical differences between adult Japanese and Caucasian.

There are no average mass data of ET region and oral mucosa in the adult Japanese. In addition, thicknesses of their tissues are very thin.[44,45] Therefore, these tissues were represented by segmenting one voxel layer with about 1 mm thickness from outer surface of airway at the around head region (see, Section 2.4.1). Consequently, the masses of these tissues in the JM-103 and JF-103 phantoms might be overestimated compared with those in average adult Japanese. Most of organs, tissues and contents in JM-103 and JF-103 agreed well with the averages[41] of adult Japanese male and female within 10%.

In the skeletal system containing teeth, active and inactive marrows, and hard bone, their masses in the JM-103 and JF-103 phantoms were greatly different from those[41] of average adult Japanese (Tables 3-2 and 3-3). The tooth masses of JM-103 and JF-103 were about 135% and 135% of averages of adult Japanese male and female, respectively. The mass differences in the teeth between the two averaged adult Japanese voxel phantoms (JM-103 and JF-103) and Japanese averages were caused by the density differences; the authors adopted the tooth density (2.75g/cm^3) by Schlattl et al.[49] If the masses of teeth are calculated according to the reference data (adult male: 2.10g/cm^3, adult female: 2.06g/cm^3) by Tanaka and Kawamura,[41] the tooth masses of JM-103 and JF-103 agreed well with Japanese averages within 5%.

The masses of hard bone in the JM-103 and JF-103 phantoms were about 162% and 143% of averages of adult Japanese male and female, respectively (Tables 3-2 and 3-3). The differences in masses of active and inactive marrows between JM-103 and average Japanese were about 19% and 94%, respectively. Similar differences were also found in the masses of two marrow tissues of JF-103 and average Japanese. The mass differences in skeletal system were mainly caused by the differences in the tissue identification methods; the average masses of adult Japanese were evaluated by using the autopsy data.[41] In the autopsy, the cortical and trabecular bones, active and inactive marrows, cartilage, miscellaneous tissue and periarticular tissue containing peripheral connective tissues listed in Tables 3-4 and 3-5 were anatomically dissected, and were manually weighed. On the other hand, the skeletal system cannot be clearly segmented from CT images on the basis of only image processing and their tissue densities. Thus, the marrow distributions in skeletal system of the JM-103, JM-60, JF-103 and JF-60 phantoms were approximately represented by the Approx-distribution model.[36] By this reason, the classifications of skeletal system in the average mass data[41] of organs and tissues of adult Japanese are different from those in the JM-103, JM-60, JF-60 and JF-103 phantoms (Tables 3-4 and 3-5); the masses of each bone tissue in the two averaged adult Japanese voxel phantoms cannot be simply compared with Japanese averages. In this study, the active and inactive marrows, cartilage and periarticular tissue were defined as 'Total bone marrow', and other three tissues in skeletal tissue except teeth were classified into 'Total hard bone'. The densities of Total bone marrow are usually lower than those of Total hard bone. Thus, 'Total bone marrow' and 'Total hard bone' were easily segmented and quantified on the basis of grey values, closely relating to the tissue densities. The masses of Total bone marrow and Total hard bone were based on the masses and mass fractions in each skeletal segmented region except teeth shown in Tables D-1 and D-2 (see, Appendix D).

As shown in Tables 3-4 and 3-5, the masses of Total bone marrow in the JM-103 and JF-103 phantoms were adjusted to Japanese averages within 5% according to the previous methods.[36] In addition, the masses of active marrow in JM-103 and JF-103 were also in good agreement with the reference values in adult by ICRP Publication 89[3] within 10%, although the masses of active marrow in JM-103 and JF-103 were heavier than the averages of adult Japanese male and female about 19% and 23%, respectively. These characteristics suggest that JM-103 and JF-103 will be fully available for dose evaluations of active marrow in adult Japanese.

In the new ICRP fundamental recommendations,[1] the tissue weighting factors were also assigned to breast, stomach, small intestine, colon and bladder. Furthermore, it was expected that the mass differences of adipose tissue in trunk between the two averaged adult Japanese voxel phantoms and the ICRP adult reference voxel phantoms induced the differences in positions and shapes of many organs and tissues in human body. Thus, it was suggested that the differences in masses of these organs and tissues induced the differences in the organ dose between the two averaged adult Japanese voxel phantoms and the ICRP adult reference voxel phantoms.

Table 3-2 Masses of some organs, tissues and contents of JM-103, JM-60[23] and AM[2] and the averages[41] of adult Japanese male.

Organ, tissue and content	Mass (kg)			
	JM-103	JM-60	AM	Average of Japanese adult male
Adipose	14.192 (1.02)	18.734 (1.35)	20.458 (1.47)	13.900
Adrenal	0.015 (1.04)	0.012 (0.84)	0.014 (1.00)	0.014
Bladder content	0.102 (1.02)	0.117 (1.17)	0.200 (2.00)	0.100
Bladder	0.039 (0.97)	0.037 (0.93)	0.050 (1.25)	0.040
Brain	1.529 (1.04)	1.688 (1.15)	1.450 (0.99)	1.470
Breast	0.023 (1.03)	0.090 (4.09)	0.025 (1.14)	0.022
Colon content	0.360 (1.00)	0.592 (1.64)	0.300 (0.83)	0.360
Colon	0.326 (0.99)	0.248 (0.75)	0.370 (1.12)	0.330
Esophagus	0.036 (0.91)	0.036 (0.91)	0.040 (1.00)	0.040
ET region	0.043 (-)	- (-)	0.039 (-)	-
Eye	0.014 (0.92)	0.014 (0.92)	0.015 (0.97)	0.015
Eye lens	0.0004 (0.95)	0.0004 (0.95)	0.0004 (0.95)	0.0004
Gall bladder content	0.049 (0.98)	0.010 (0.19)	0.054 (1.08)	0.050
Gall bladder	0.008 (1.02)	0.007 (0.82)	0.014 (1.74)	0.008
Hard bone	7.304 (1.62)	7.320 (1.63)	5.500 (1.22)	4.500
Heart content	0.362 (0.91)	0.417 (1.04)	0.510 (1.28)	0.400
Heart	0.389 (1.02)	0.529 (1.39)	0.330 (0.87)	0.380
Kidney	0.333 (1.04)	0.265 (0.83)	0.310 (0.97)	0.320
Liver	1.462 (0.91)	1.305 (0.82)	1.800 (1.13)	1.600
Lung	1.215 (1.01)	1.361 (1.13)	1.208 (1.01)	1.200
Lymphatic tissue	0.224 (1.02)	- (-)	0.138 (0.63)	0.220
Marrow (active)	1.192 (1.19)	1.197 (1.20)	1.170 (1.17)	1.000
Marrow (inactive)	2.526 (1.94)	2.536 (1.95)	2.480 (1.91)	1.300
Muscle	28.198 (1.03)	26.178 (0.95)	29.000 (1.05)	27.500
Oral_mucosa	0.010 (-)	- (-)	0.005 (-)	-
Pancreas	0.136 (1.05)	0.118 (0.91)	0.140 (1.08)	0.130
Prostate	0.011 (0.94)	- (-)	0.017 (1.42)	0.012
Salivary gland	0.086 (1.05)	- (-)	0.085 (1.04)	0.082
Skin	2.189 (0.91)	2.225 (0.93)	3.728 (1.55)	2.400
Small intestine content	0.351 (1.00)	0.330 (0.94)	0.350 (1.00)	0.350
Small intestine	0.557 (0.94)	0.423 (0.72)	0.650 (1.10)	0.590
Spleen	0.139 (1.00)	0.139 (1.00)	0.150 (1.07)	0.140
Stomach content	0.240 (1.00)	0.383 (1.60)	0.250 (1.04)	0.240
Stomach	0.141 (1.01)	0.122 (0.87)	0.150 (1.07)	0.140
Tooth	0.061 (1.35)	0.061 (1.35)	0.050 (1.11)	0.045
Testis	0.036 (0.99)	0.036 (0.99)	0.035 (0.95)	0.037
Thymus	0.031 (1.03)	0.031 (1.03)	0.025 (0.83)	0.030
Thyroid	0.020 (1.06)	0.022 (1.15)	0.020 (1.05)	0.019
Tongue	0.062 (0.92)	- (-)	0.073 (1.09)	0.067
Trachea	0.009 (0.99)	0.010 (1.11)	0.010 (1.11)	0.009

Values in parenthesis are the ratios of masses of JM-103, JM-60 and AM to averages of adult Japanese male, respectively.

Table 3-3 Masses of some organs, tissues and contents of JF-103, JF-60[25] and AF,[2] and the averages[41] of adult Japanese female.

Organ, tissue and content	Mass (kg)			
	JF-103	JF-60	AF	Average of Japanese adult female
Adipose	13.815 (0.91)	11.074 (0.73)	23.596 (1.55)	15.200
Adrenal	0.012 (0.92)	0.006 (0.47)	0.013 (1.00)	0.013
Bladder content	0.090 (1.06)	0.061 (0.72)	0.200 (2.35)	0.085
Bladder	0.032 (1.06)	0.020 (0.67)	0.040 (1.33)	0.030
Brain	1.335 (1.01)	1.342 (1.02)	1.300 (0.98)	1.320
Breast	0.309 (1.03)	0.581 (1.94)	0.500 (1.67)	0.300
Colon content	0.289 (1.03)	0.502 (1.79)	0.320 (1.14)	0.280
Colon	0.244 (0.94)	0.232 (0.89)	0.360 (1.38)	0.260
Esophagus	0.031 (1.05)	0.049 (1.62)	0.035 (1.17)	0.030
ET region	0.030 (-)	- (-)	0.019 (-)	-
Eye	0.012 (0.99)	0.015 (1.25)	0.015 (1.22)	0.012
Eye lens	0.0003 (0.94)	0.0008 (2.79)	0.0004 (1.33)	0.0003
Gall bladder content	0.035 (0.92)	0.002 (0.06)	0.046 (1.20)	0.038
Gall bladder	0.006 (1.03)	0.004 (0.62)	0.010 (1.71)	0.006
Hard bone	4.866 (1.43)	4.639 (1.36)	4.000 (1.18)	3.400
Heart content	0.316 (0.99)	0.369 (1.15)	0.370 (1.16)	0.320
Heart	0.325 (1.08)	0.280 (0.93)	0.250 (0.83)	0.300
Kidney	0.271 (0.97)	0.213 (0.76)	0.275 (0.98)	0.280
Liver	1.311 (0.94)	1.179 (0.84)	1.400 (1.00)	1.400
Lung	0.978 (1.07)	1.093 (1.20)	0.950 (1.04)	0.910
Lymphatic tissue	0.173 (1.02)	- (-)	0.079 (0.47)	0.170
Marrow (active)	0.956 (1.23)	0.913 (1.17)	0.899 (1.15)	0.780
Marrow (inactive)	1.911 (1.93)	1.827 (1.85)	1.800 (1.82)	0.990
Muscle	20.212 (0.97)	17.830 (0.86)	17.500 (0.84)	20.790
Oral_mucosa	0.008 (-)	- (-)	0.004 (-)	-
Ovary	0.012 (1.09)	0.007 (0.61)	0.011 (1.00)	0.011
Pancreas	0.113 (1.02)	0.095 (0.86)	0.120 (1.09)	0.110
Salivary gland	0.063 (1.02)	- (-)	0.070 (1.14)	0.062
Skin	1.898 (1.05)	1.730 (0.96)	2.721 (1.51)	1.800
Small intestine content	0.283 (1.05)	0.169 (0.62)	0.280 (1.04)	0.270
Small intestine	0.467 (1.04)	0.373 (0.43)	0.600 (1.33)	0.450
Spleen	0.110 (0.92)	0.056 (0.47)	0.130 (1.08)	0.120
Stomach content	0.180 (1.00)	0.411 (2.28)	0.230 (1.28)	0.180
Stomach	0.106 (0.97)	0.104 (0.95)	0.140 (1.27)	0.110
Tooth	0.046 (1.35)	0.056 (1.64)	0.040 (1.18)	0.034
Thymus	0.028 (0.96)	0.019 (0.66)	0.020 (0.69)	0.029
Thyroid	0.017 (0.99)	0.007 (0.43)	0.017 (1.00)	0.017
Tongue	0.051 (1.01)	- (-)	0.060 (1.18)	0.051
Trachea	0.007 (0.97)	0.017 (2.52)	0.008 (1.18)	0.007
Uterus	0.067 (0.96)	0.046 (0.66)	0.080 (1.14)	0.070

Values in parenthesis are the ratios of masses of JF-103, JF-60 and AF to averages of adult Japanese female, respectively

Table 3-4 Masses of skeletal system in JM-103 and JM-60, along with the averages[41)] of Japanese adult male and the reference values of ICRP Publication 89.[3)]

Tissue	Mass (kg)			
	JM-103	JM-60	Japanese average (adult male)	ICRP Publ. 89 (adult male)
Total bone marrow	3.718	3.733	3.900	4.750
Active marrow	1.192	1.197	1.000	1.170
Inactive marrow	2.526	2.536	1.300	2.480
Cartilage	-	-	0.900	1.100
Periarticular tissue	-	-	0.700	-
Total hard bone	7.304	7.320	7.000	5.700
Cortical bone	-	-	3.600	4.400
Trabecular bone	-	-	0.900	1.100
Miscellaneous tissue	-	-	2.500	0.200
Tooth	0.061	0.061	0.045	0.050
Total skeletal system	11.083	11.114	10.945	10.500

Table 3-5 Masses of skeletal sysytem in JF-103 and JF-60, along with the averages[41)] of Japanese adult female and the reference values of ICRP Publication 89.[3)]

Tissue	Mass (kg)			
	JF-103	JF-60	Japanese average (adult female)	ICRP Publ. 89 (adult female)
Total bone marrow	2.867	2.740	3.000	3.600
Active marrow	0.956	0.913	0.780	0.900
Inactive marrow	1.911	1.827	0.990	1.800
Cartilage	-	-	0.700	0.900
Periarticular tissue	-	-	0.530	-
Total hard bone	4.866	4.639	4.190	4.160
Cortical bone	-	-	2.700	3.200
Trabecular bone	-	-	0.700	0.800
Miscellaneous tissue	-	-	0.790	0.160
Tooth	0.046	0.056	0.034	0.040
Total skeletal system	7.779	7.435	7.224	7.800

3.2 Distances between organs (Organ distances)

It was expected that the distances between the centers of gravities in some organs and tissues (hereafter referred to as 'organ distance') are widely varied by modifying the masses and shapes of contents, organs and tissues. In particular, since the SAF is high sensitive to the organ distance, the phantom modification might influence the organ doses due to internal exposures. In addition, the body sizes of the JM-103 and JF-103 phantoms were smaller than those of the AM and AF phantoms; the differences in the body size might also influence the organ distances. Thus, it is important to confirm whether the modifications of the phantoms change the organ distances or not.

Figure 3-1 shows the distributions of the ratios (JM-103/JM-60 or JF-103/JF-60) of the organ distances. The organ distances were calculated by using the centers of gravities in organs and tissues presented in Tables B-1, B-2, B-3 and B-4 (see, Appendix B). In most cases, the organ distances in JF-103 agreed with those in JF-60 within 5%, although the height and weight of JF-103 were larger than those of JF-60 about 2% and 18%, respectively. These results demonstrate that body size modifications for JF-103 construction did not considerably influence its organ distances.

The variations in organ distances were dependent on the locations of organs and tissues in the torso. For example, the organ distances from thyroid, uterus, bladder and testes to other organs were similar between JM-103 and JF-60 or JF-103 and JF-60 (Figures 3-1 (a), (f), (g) and (h)). These organs are located in the top or bottom of trunk. On the other hand, the great changes in organ distances were found in the esophagus, heart, gall bladder and colon (Figures 3-1 (b), (c), (d) and (e)). These organs were also distributed in the middle part of trunk. As described in Section 2.3, the enlargements and reductions of organs and tissues toward horizontal direction in phantom body were mainly performed by using image processing functions; the changes of organ mass distributions in a vertical axis were relatively small (see, Appendix E). Thus, the mass modification procedures adopted in this study did not induce the significant variations in organ distances between the organs and tissues, which were shifted in the axis of vertical direction.

As shown in Figure 3-1 (b), the maximum variations in organ distance were found in the combinations of esophagus and other organs, and were about factor of 2. This is due to the long tubular shape of esophagus; even if the enlargement and reduction of esophagus size were minute, these image processing procedures greatly moved the center of gravity of esophagus in the horizontal direction, and changed the organ distances from esophagus to other organs.

The organ distances from heart, gall bladder and colon to other organs were greatly changed by modifying the masses of organs and tissues for JM-103 and JF-103 constructions (Figures 3-1 (c), (d) and (e)). Since the three organs were membranous organs, the masses of their walls and contents had to be simultaneously modified according to the methods described in Sections 2.3 and 2.3.1. The inflation procedures against gall bladder especially affected the organ distances, since the difference in mass of gall bladder content between JF-60 and Japanese average was extremely large, and was about 94% (Table 3-3). Similar difference was also observed in comparison of JM-60 and Japanese average. The modification procedures of the gall bladder content caused the changes in the gall bladder wall geometries, which were responsible for the variations of the organ distances from gall bladder to other organs.

Table 3-6 shows the organ distances from brain to other organs in the JM-103, JF-103, AM and AF phantoms. The organ distances of AM and AF were calculated by using the centre of mass of organs and tissues given in ICRP Publication 110.[2)] While the body sizes of the JM-103 and JF-103 phantoms were smaller than those of the AM and AF phantoms as mentioned in Section 3.1, the organ distances from brain to most organs in JM-103 and JF-103 were longer than those in AM and AF. On the other hand, the organ distances from brain to ovaries, bladder, prostate and testes in JM-103 and JF-103 are not more than those in AM and AF. The trends in organ distances of the two averaged adult Japanese voxel phantoms and the ICRP adult reference voxel phantoms have already been reported by Takahashi et al.[50)] Takahashi et al. revealed that the differences in the organ distances were caused by the differences in lung locations between the JM-103 and AM phantoms. As defined in ICRP Publication 110,[2)] the lung tissues of AM and AF were compressed by gravity action, since the CT images used to create these phantoms were acquired in supine posture; the abdomen organs and tissues were also shifted toward the lungs. In addition, the lung locations of AM and AF moved toward the neck. On the other hand, the JM-103 and JF-103 phantoms were based on the JM-60 and JF-60 phantoms, which were constructed from the CT images in supine posture. Thus, there was no difference in the postures between the two averaged adult Japanese voxel phantoms and the ICRP adult reference voxel phantoms.

In our previous research,[33,35,36)] the authors clarified that the organ distance from brain to lungs in supine posture was shorter than that in upright posture only about 3.3 mm. On the other hand, the difference in organ distances from brain to lungs between the JM-103 and AM phantoms was about 27 mm as shown in Table 3-6. Similar difference (21 mm) was also found in comparison of the JF-103 and AF phantoms. The differences in organ distances were greater than those expected from the differences in body sizes between the two averaged adult Japanese voxel phantoms and the ICRP adult reference voxel phantoms. This is because the mass ratios of adipose tissue to body weight in the ICRP adult reference voxel phantoms were larger than those in the two averaged adult Japanese voxel phantoms (see, Section 3.1). Generally, the excess adipose tissues in abdomen influence lung function, since there is the case that the abdominal adipose tissues restrict the descent of the diaphragm and the expansion of the lungs. Thus, it was suggested that the differences in the mass and distribution of adipose tissues in trunk between adult Japanese and Caucasian also influenced the differences in the lung positions and the organ distances.

In this study, it was found that there were some differences in the anatomical characteristics such as body sizes, organ masses and organ distances between the two averaged Japanese voxel phantoms and ICRP adult reference voxel phantoms. Thus, the anatomical characteristics between adult Japanese and Caucasian would influence the SAFs and organ doses.

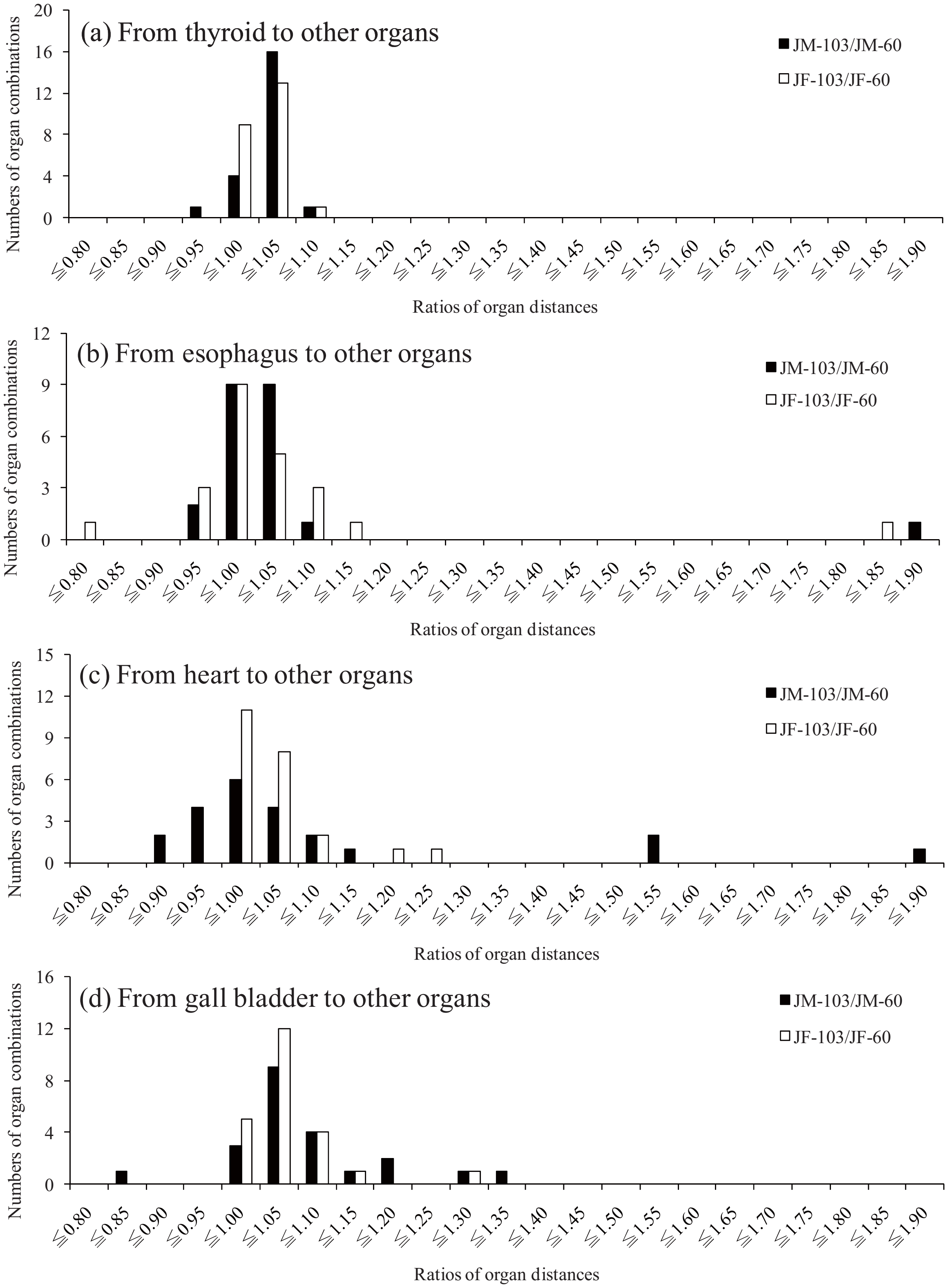

Figure 3-1 Distributions of organ distance ratios between the modified phantoms (JM-103 and JF-103) and the original phantoms (JM-60 and JF-60).

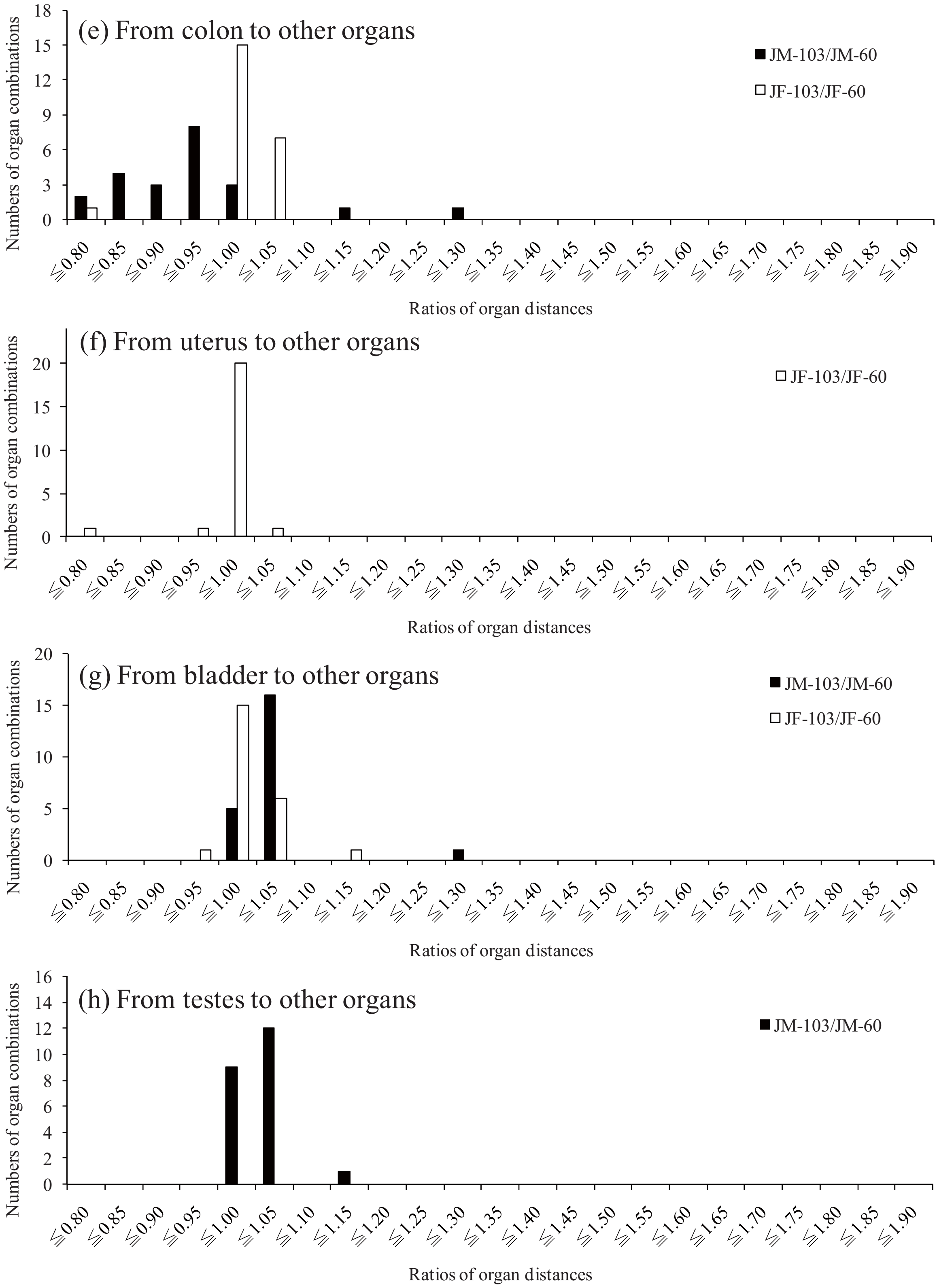

Figure 3-1 (Continued)

Table 3-6 Comparison of organ distances from brain to other organs in the averaged adult Japanese voxel phantoms and those in the ICRP adult reference voxel phantoms.

Organs and tissues	Organ distances (mm)		JM-103/AM	Organ distances (mm)		JF-103/AF
	JM-103	AM		JF-103	AF	
Thyroid	207	206	1.00	173	177	0.97
Trachea	243	226	1.08	219	201	1.08
Thymus	297	252	1.18	282	228	1.24
Bronchi	333	321	1.04	306	287	1.07
Esophagus	345	297	1.16	324	262	1.24
Lungs	353	326	1.08	320	299	1.07
Breast	358	382	0.94	354	305	1.16
Heart	361	351	1.03	337	318	1.06
Liver	480	444	1.08	447	416	1.07
Adrenals	491	462	1.06	477	439	1.09
Spleen	509	440	1.16	474	421	1.13
Stomach	512	451	1.14	516	440	1.17
Pancreas	516	485	1.06	513	473	1.09
Gall bladder	518	477	1.09	514	443	1.16
Kidneys	545	501	1.09	498	496	1.00
Colon	617	574	1.08	640	612	1.05
Small intestine	630	597	1.06	629	582	1.08
Ovaries	-	-	-	708	722	0.98
Bladder	749	750	1.00	712	717	0.99
Uterus	-	-	-	717	722	0.99
Prostate	769	795	0.97	-	-	-
Testes	838	897	0.93	-	-	-

4. Characteristics relevant to internal and external dose assessments of the JM-103 and JF-103 phantoms

4.1 SAFs for internal dose assessment

The specific absorbed fraction (SAF) is basic dosimetric quantity for internal dose assessment, and is calculated by dividing the absorbed fraction by the unit mass (kg) of the target organ. The absorbed fraction is defined as the fraction of energy absorbed by a target as a result of nuclear transformation of radionuclides in a source region. The SAFs are generally sensitive to the shapes and locations of both source and target regions. In this study, the photon and electron SAFs containing the self-specific absorbed fractions (Self-SAFs) for some organs and tissues in JM-103 and JF-103 were calculated, and were compared with those in JM-60 and JF-60 to examine the effects of phantom modifications on internal dosimetry. Furthermore, the SAFs for some organs and tissues in the ICRP adult reference male (the AM phantom) and female (the AF phantom) voxel phantoms[2)] were also calculated to investigate the differences in the SAFs between adult Japanese and Caucasian.

4.1.1 Code system and calculation conditions of SAFs for photons and electrons

A code system, which consists of a SAF calculation system, UCSAF[27,29)] and the electromagnetic cascade Monte Carlo code, EGS4,[51)] was used for calculations of SAFs and Self-SAFs for photons or electrons. UCSAF is one of user codes of EGS4. The code system was installed on commercial personal computers, PowerEdge 600SC and Inspiron 530 (Dell Inc, USA). All male and female phantoms were incorporated into UCSAF. The materials and elemental composition data in Tables 2-4 and 2-5 were applied to the JM-103 and JF-103 phantoms. The organ segmented data and other data containing materials, their elemental compositions and organ ID lists of the AM and AF phantoms were acquired from the data files on the CD-ROM that accompanies the ICRP Publication 110.[2)] As described in a previous report,[36)] the code system requires two phantom data such as the organ segmented data and the bone density data. However, the JM-103, JF-103, AM and AF phantoms consist of only the organ segmented data. Therefore, the dummies of bone density data for these voxel phantoms were created, and were used.

The organ segmented data and the dummies of bone density data of the JM-103, JF-103, AM and AF phantoms were converted to the compressed format developed by the National Research Center for Environment and Health (GSF, now the German Research Center for Environmental Health)[5,6)] and modified by Saito et al.[24,26)] The GSF compressed format data of these voxel phantoms were incorporated into UCSAF.

In the photon transport, photoelectric effect, coherent scattering, Compton scattering and pair production were considered. The primary and secondary photons were followed until their energy fell to 1 keV. The cross-section data for photons were obtained from PHOTX.[52,53)] Mϕller scattering, Bhabha scattering, bremsstrahlung emission and elastic multiple scattering were taken into account for the electron transport. The primary and secondary electrons produced from photon interactions were tracked until their kinetic energy fell to 5 keV; the kerma approximation was not applied. The

Parameter Reduced Electron-Step Transport Algorithm (PRESTA) was adopted to optimize the step size of the electron transport model. The stopping power of electrons was taken from the ICRU Report 37.[54)]

Monoenergetic photon or electron sources were assumed to be distributed uniformly in the source region. The number of primary photons or electrons was set to achieve fraction standard deviations of less than 5% in the deposited energy of each target organ. The calculations of SAFs for photons were performed for 6 energies from 0.02 MeV to 1 MeV and for combinations of 22 targets and 6 sources. The photon and electron Self-SAFs for 10 organs and tissues were calculated at 12 energies from 0.01 MeV to 4 MeV. Some examples of the photon SAFs calculated using the JM-103, JF-103, JM-60 and JF-60 phantoms were also shown in Appendix F.

4.1.2 Validation of SAFs in the JM-103 and JF-103 phantoms by comparison with those in the JM-60 and JF-60 phantoms

Table 4-1 shows photon SAFs and organ distances for the combinations of the liver and adrenals as the target organs, and the lungs and gall bladder content as the source regions in the JM-103, JM-60, JF-103 and JF-60 phantoms. The differences in the SAFs for the liver between JM-103 and JM-60 were within 5% at all calculated energies. Similarly, the SAFs for liver in JF-103 also agreed well with those in JF-60. This is due to the following reasons. Since the lungs directly contact with the liver and their sizes are relatively great, the mass modifications did not affect organ distances between lungs and liver; there are little differences in the SAFs.

On the other hand, the differences in SAFs for adrenals between the JM-103 and JM-60 phantoms were relatively large in the six photon energies. The differences in SAFs were dependent on the photon energy. The maximum difference was about 75% at 0.02 MeV. Similar tendencies of SAFs were also found in the JF-103 and JF-60 phantoms. As shown in Table 4-1, the mass modifications lengthened the organ distances between gall bladder and adrenals in JM-103 and JF-103 about 20 and 6 mm, respectively. Therefore, it was considered that the changes in the organ distances decreased the SAFs for 0.02 MeV photon with short mean free path (about 1.15 cm) in ICRU soft tissue.[47)]

Table 4-1 SAFs calculated using the JM-103, JM-60, JF-103 and JF-60 phantoms for sources in lungs and gall bladder content and for targets in liver and adrenals.

Source → target	Phantom	Organ distances (mm)	SAFs (kg^{-1}) Photon Energy (MeV) 0.02	0.03	0.05	0.1	0.5	1
Lungs → Liver	JM-103	139	1.61E-2	2.36E-2	1.99E-2	1.40E-2	1.21E-2	1.11E-2
	JM-60	138	1.61E-2	2.34E-2	1.96E-2	1.40E-2	1.24E-2	1.14E-2
	(JM-103/JM-60)	(1.01)	(1.00)	(1.01)	(1.01)	(1.00)	(0.97)	(0.97)
	JF-103	133	1.72E-2	2.48E-2	2.08E-2	1.43E-2	1.26E-2	1.16E-2
	JF-60	131	1.83E-2	2.53E-2	2.01E-2	1.43E-2	1.33E-2	1.23E-2
	(JF-103/JF-60)	(1.02)	(0.94)	(0.98)	(1.03)	(1.00)	(0.95)	(0.94)
Gall bladder content → Adrenals	JM-103	97	9.78E-3	4.43E-2	5.09E-2	3.70E-2	3.02E-2	2.73E-2
	JM-60	77	3.85E-2	1.06E-1	9.29E-2	6.01E-2	5.00E-2	4.51E-2
	(JM-103/JM-60)	(1.26)	(0.25)	(0.42)	(0.55)	(0.62)	(0.61)	(0.60)
	JF-103	63	5.64E-2	1.52E-1	1.24E-1	7.90E-2	6.88E-2	6.26E-2
	JF-60	57	1.07E-1	2.29E-1	1.65E-1	1.00E-1	8.81E-2	8.03E-2
	(JF-103/JF-60)	(1.10)	(0.53)	(0.66)	(0.75)	(0.79)	(0.78)	(0.78)

Figure 4-1 shows the distributions of ratios (JM-103/JM-60 or JF-103/JF-60) of photon SAFs for 22 organs and tissues as targets, and the thyroid, esophagus, heart content and bladder content as sources at energies of 0.03 MeV and 0.5 MeV. These source regions were selected, in view of the organ positions as described below. Although the thyroid and bladder content are located in the top and bottom of trunk, respectively, the esophagus and heart content are distributed in the middle part of trunk. At an energy of 0.03 MeV, the differences of SAFs for 22 targets between JM-103 and JM-60 were relatively great, and were within a factor of 3 (Figure 4-1 (a)). As shown in Figure 4-1 (c), similar differences were also found in SAF comparisons of JF-103 and JF-60. On the other hand, the differences in SAFs for 0.5 MeV photon between JM-103 and JM-60 were within 20% in most cases, and were similar to those between JF-103 and JF-60.

As described in Section 3.2, the positions of organs and tissues influenced the variations in organ distances due to the phantom modifications. Since the organ distance was one of determination factors of SAFs,[25,35,36] it was expected from Figure 3.1 that the variations in the SAFs were also relevant to the organ positions. However, the distributions of ratios of SAFs for 22 target organs and tissues were similar between thyroid, esophagus, heart content and bladder content, where the positions were different each other (Figure 4-1). The discrepancies in effects of phantom modifications on organ distances and SAFs were mainly attributed to the image processing methods. In this study, the enlargements and reductions toward horizontal direction of phantom body were mainly performed under considerations of human anatomy (see, Section 2.3). These procedures also induced changes in the minimum distances between source and target, since the organ masses were modified by adding or deleting voxel layers at outer surface of organs and tissues. Generally, the SAFs for low energy photon are more sensitive to the minimum distances rather than the organ distances, because of its short mean free path. Therefore, it was considered that the dependences of organ distance variations on the organ positions seen in Figure 3-1 were offset by the changes in minimum distances, and did not affect the SAFs.

In this study, there were some cases that the SAFs for several organs and tissues in the JM-103 and JF-103 phantoms were considerably different from those in the JM-60 and JF-60 phantoms. These results indicate that the averaging of body sizes and organ masses influence the SAFs. Thus, it can be concluded that the averaging of anatomical characteristics is necessary for the SAF evaluations of average adult Japanese.

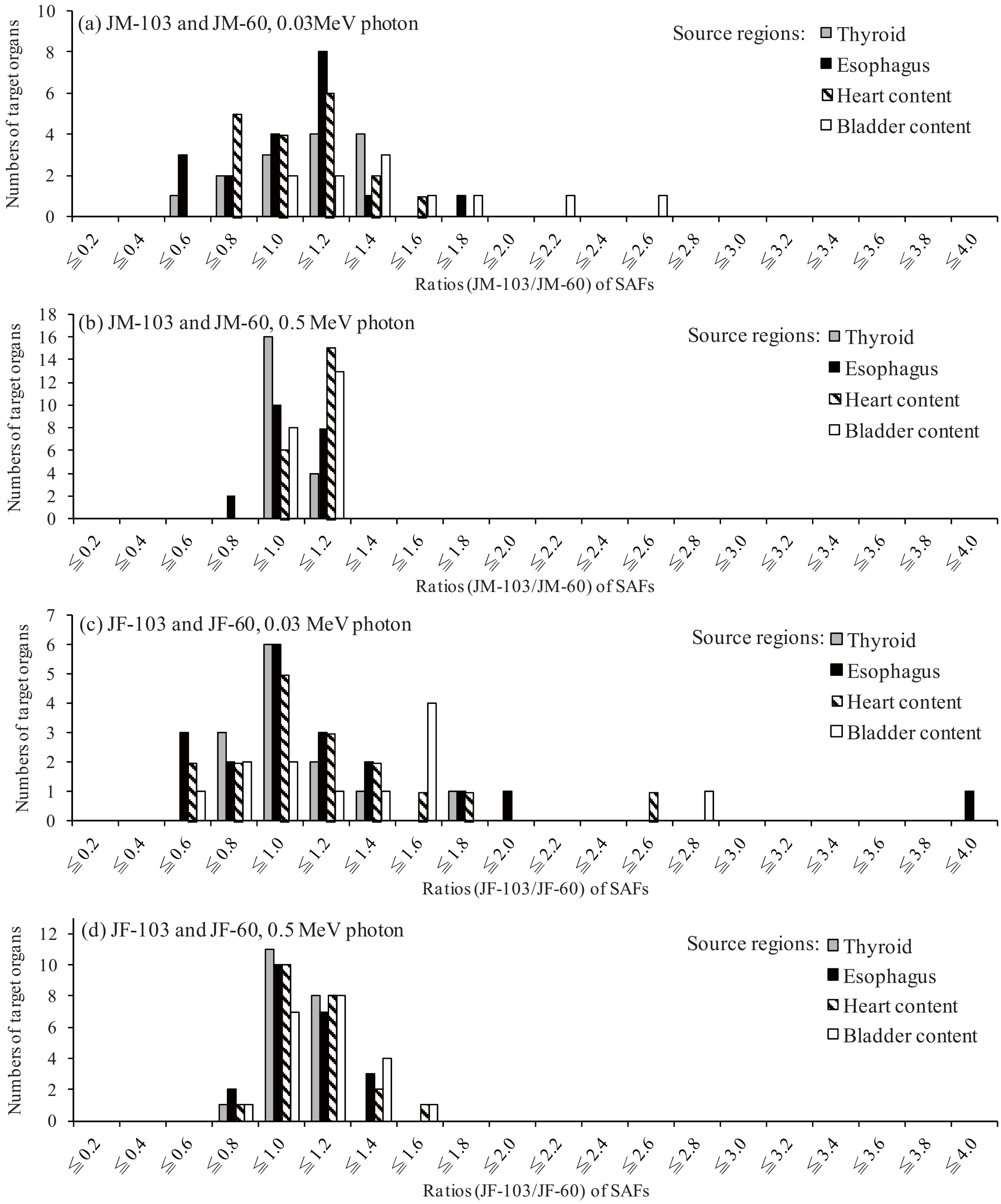

Figure 4-1 Distributions of SAF ratios between the JM-103 and JM-60 or JF-103 and JF-60, when the selected four organs are source.

Figure 4-2 demonstrates photon and electron Self-SAFs for several organs of the JM-103 and JM-60 phantoms. Overall, the photon and electron Self-SAFs decreased with increasing energy. Photon and electron Self-SAFs over energy range of 0.01 MeV to 4 MeV for thymus, spleen and testes of JM-103 agreed with those of JM-60 within 10% (Figures 4-2 (a), (d) and (f)). On the other hand, the differences in photon and electron Self-SAFs for kidneys over energy range of 0.01 MeV to 4.0 MeV between JM-103 and JM-60 were about within 20%, and were larger than those for thymus, spleen and testes. The cause of these results was the differences in organ masses between JM-103 and JM-60; the kidney mass of JM-103 was heavier than that of JM-60 about 26%, although the masses of thymus, spleen and testes in JM-103 were almost the same as those in JM-60 (Table 3-2). The dependences of Self-SAFs for photons and electrons on organ masses have already been reported in previous reports.[23,27,28,36] The results obtained from this study support the conclusions of previous reports.[23,27,28,36]

As shown in Figures 4-2 (b) and (c), the great differences were found in the photon and electron Self-SAFs for membranous organs such as heart and gall bladder. At the energy ranges from 0.01 MeV to 4.0 MeV, the differences in the photon and electron Self-SAFs for heart between JM-103 and JM-60 varied from 18% to 41% and 34% to 37%, respectively (Figure 4-2 (b)). Similar differences in photon and electron Self-SAFs were also found in gall-bladder. The differences in photon and electron Self-SAFs for these membranous organs were greater than the differences in Self-SAFs for kidneys. The authors also changed the boundaries between walls and contents in these organs for the mass modifications. In particular, the wall geometry of gall bladder was extremely altered by the image processing, because the mass of gall bladder content in the JM-60 phantom was significantly different from the Japanese average[41] about 81% (Table 3-2). Therefore, it was considered that the large change in the wall geometry due to the mass modifications also strongly affected the photon and electron Self-SAFs for gall bladder.

Figure 4-3 shows photon and electron Self-SAFs in the energy range from 0.01 MeV to 4.0 MeV for brain, gall bladder, stomach, spleen, adrenals and ovaries of the JF-103 and JF-60 phantoms. The organ masses of JF-60 were generally smaller than those of JF-103 (Table 3-3). Therefore, the Self-SAFs in JF-103 as a whole were smaller than those in JF-60. The maximum differences in photon and electron Self-SAFs between the JF-103 and JF-60 phantoms were found in gall bladder, and were about 62% and 68%, respectively. Similarly to the comparisons of JM-103 and JM-60, it was considered that marked changes in mass of gall bladder content induced the differences in Self-SAFs for gall bladder wall. In internal dose assessment against electron sources, the contributions of Self-SAFs to organ absorbed doses were generally large. The masses of organs, tissues and contents in the JM-103 and JF-103 phantoms agreed well with the averages of adult Japanese male and female, respectively. Therefore, it was concluded that the JM-103 and JF-103 phantoms were useful for internal dose assessments of adult Japanese with average masses of organs and tissues.

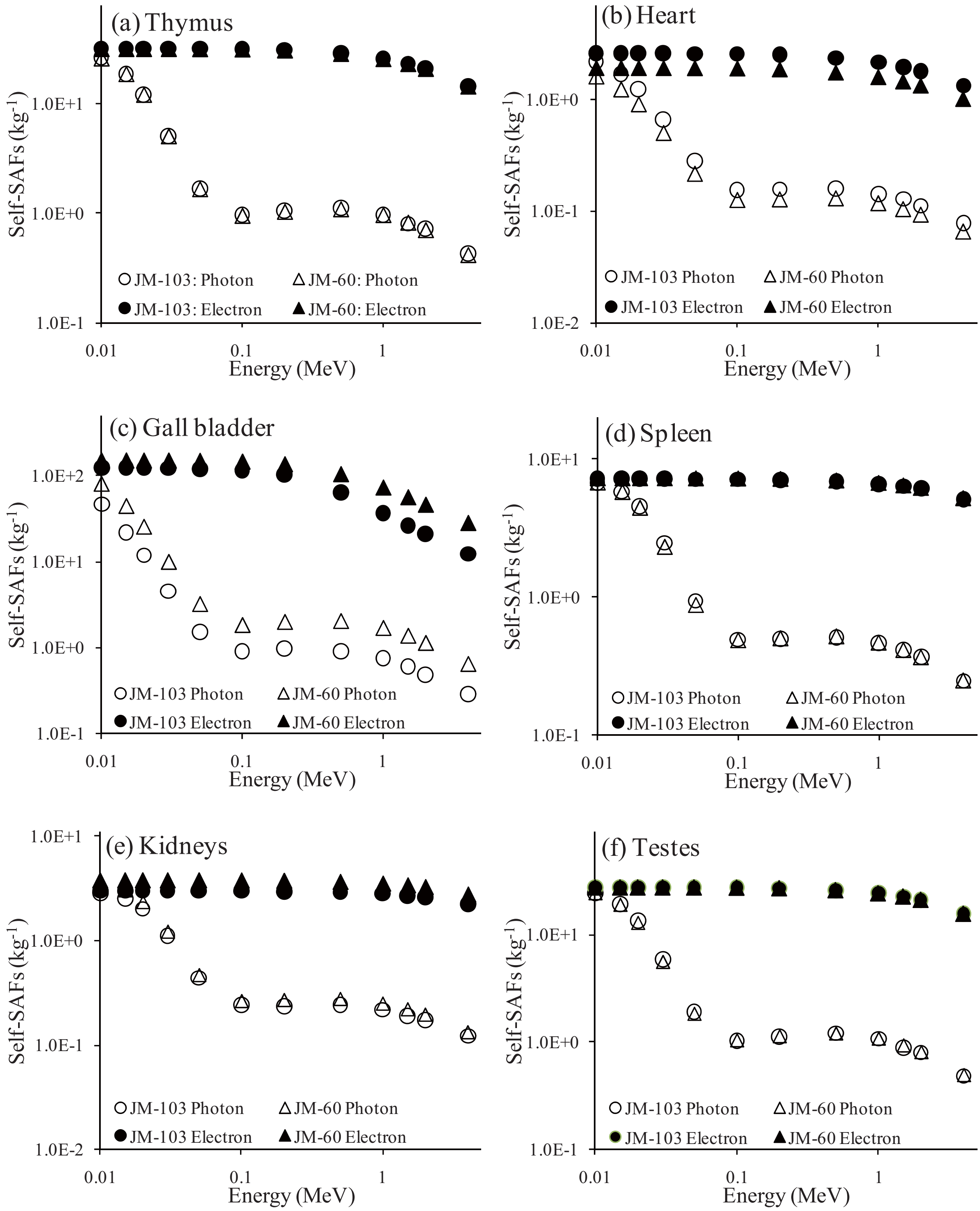

Figure 4-2 Self-SAFs for photons or electrons in selected organs of the JM-103 and JM-60 phantoms. (a) Thymus, (b) Heart, (c) Gall bladder, (d) Spleen, (e) Kidneys and (f) Testes.

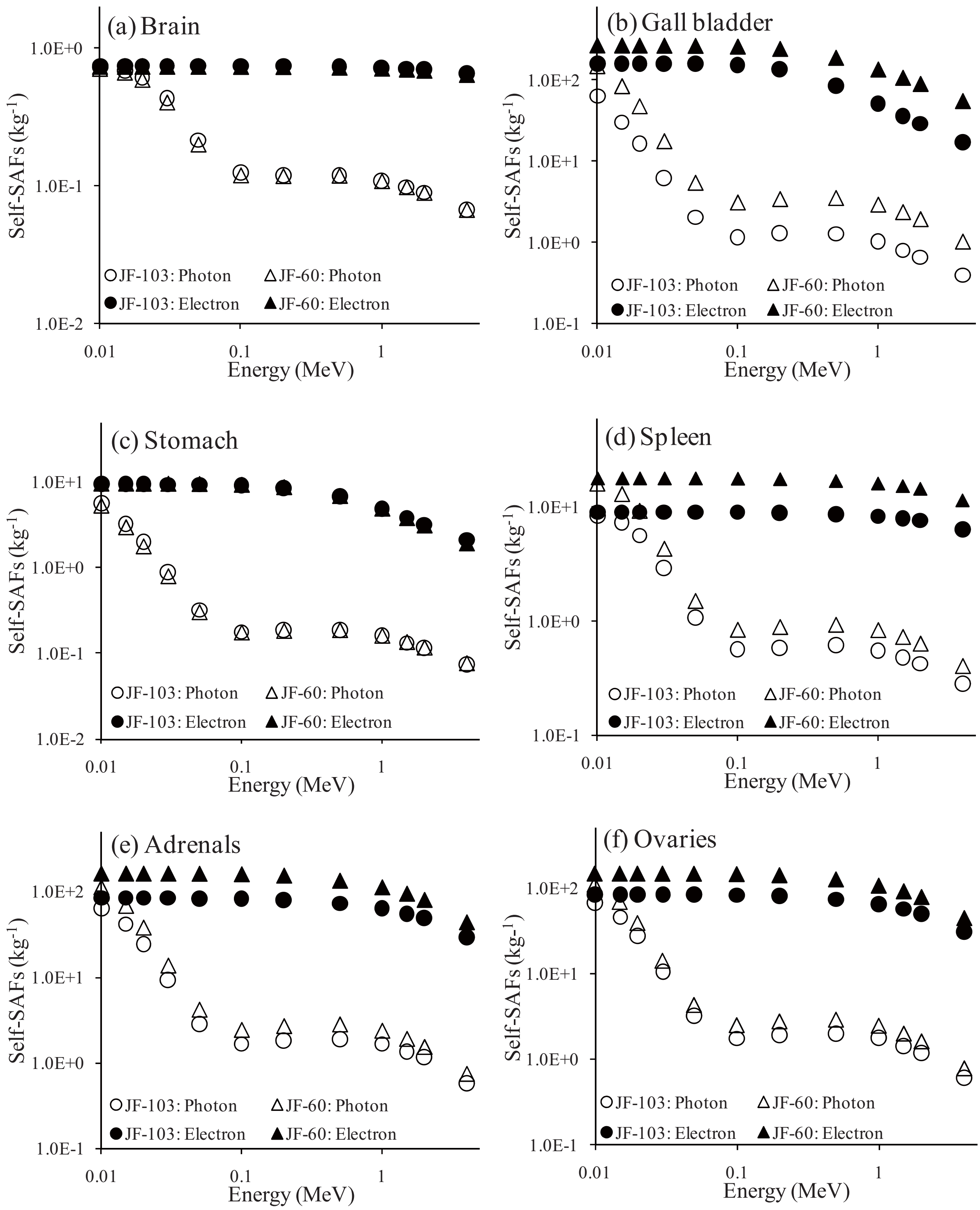

Figure 4-3 Self-SAFs for photons or electrons in selected organs of the JF-103 and JF-60 phantoms. (a) Brain, (b) Gall bladder, (c) Stomach, (d) Spleen, (e) Adrenals and (f) Ovaries.

4.1.3 Comparison of SAFs in the JM-103 and JF-103 phantoms and those in the ICRP adult reference voxel phantoms

In order to compare the SAFs and Self-SAFs in the JM-103 and JF-103 phantoms with those in the AM and AF phantoms, the thyroid, liver and bladder content were selected as the source regions under consideration of anatomical positions. The thyroid and bladder content are located in the top and bottom of trunk, respectively. The liver lies to the middle parts of the trunk.

Table 4-2 shows the SAFs and organ distances for the selected combinations of source regions and target organs in the JM-103, JF-103, AM and AF phantoms. At all calculated energies, SAFs for lungs as a target organ and for thyroid as a source region in JF-103 were lower than those in AF. The lung SAF of JF-103 at an energy of 1 MeV was about 72% of that of AF. The differences in SAFs between JF-103 and AF increased with decrease in the photon energy. Similar trend was also seen in the SAFs of the JM-103 and AM phantoms. As shown in Table 4-2, the organ distances from thyroid to lungs in JM-103 and JF-103 were considerably longer than those in AM and AF, respectively; the positions of lungs in JM-103 and JF-103 shifted toward the abdomen compared with those in AM and AF. As explained in Section 3.1, there were the differences in the adipose tissue masses between JM-103 and AM or JF-103 and AF; the excess adipose tissues in abdomen affected the lung capacity. Thus, it was suggested that the differences in masses of the adipose tissues induced the differences in lung SAFs between the two averaged adult Japanese voxel phantoms and the ICRP adult reference voxel phantoms.

On the other hand, the opposite trend was found in the SAFs for stomach as a target organ and for bladder content as a source region (Table 4-2). The SAFs for stomach in the JM-103 and JF-103 phantoms were considerably higher than those in the AM and AF phantoms, respectively. These results were caused by the differences in the distances from bladder to stomach between JM-103 and AM or JF-103 and AF (Table 4-2). The differences in distances between stomach and bladder were attributed to the following reasons: while the bladder position was not easily changed, the positions of stomach in the JM-103 and JF-103 phantoms were changed by the extension of lungs, and moved in a leg direction compared with those in the AM and AF phantoms.

The SAFs for kidneys as a target organ and for liver as a source region were closely dependent on organ distances, since the SAFs for kidneys increased with the decrease in the organ distances (Table 4-2). In addition, the organ distances increased with increasing body sizes; the liver is located on the front side of body. On the other hand, the kidneys is opposite the liver. Therefore, the organ distances between kidneys and liver are relevant to the diameter of body. The above results suggest that the differences in SAFs for a combination of kidneys and liver were caused by the differences in the body sizes between adult Japanese and Caucasian.

When a source region was the bladder content, the SAFs for bladder in the JM-103 and JF-103 phantoms were relatively greater than those in the AM and AF phantoms. The maximum difference was found in comparison of JF-103 and AF, and was about 116% at 0.02 MeV. As shown in Table 3-3, the mass differences in bladder and bladder content between JF-103 and AF were about 20% and 55%, respectively. The masses of bladder content directly influence the thickness and shape of bladder. Therefore, the mass differences of bladder content were responsible for the differences in bladder SAFs between the JF-103 and AF phantoms. The similar relationship between SAFs and organ content masses was also found in comparison of JM-103 and AM. These results demonstrate that the mass of organ content was also one of determination factors for SAFs of average adult Japanese.

Table 4-3 presents the photon Self-SAFs for thyroid and liver in the JM-103, AM, JF-103 and AF phantoms. At all calculate energies, the difference in the Self-SAFs for thyroid between JM-103 and AM was within 5%. In Self-SAF comparison of JF-103 and AF, the maximum difference was found in the energy of 1 MeV, and was about 6%. On the other hand, the ratios (JM-103/JF-103 or AM/AF) of the thyroid Self-SAFs between adult male and female phantoms were greater than those (JM-103/AM or JF-103/AF) between adult Japanese and Caucasian phantoms, and varied from 14% to 16%. As reported in previous studies,[23,27,28,36)] the Self-SAF is highly dependent on the mass of a target organ. As shown in Tables 3-2 and 3-3, the difference in thyroid masses between JM-103 and JF-103 was about 20%. Similar difference (18%) in thyroid masses was also found in AM and AF. Thus, the above results were mainly caused by the gender differences in thyroid masses.

There is little difference in the Self-SAFs for liver between the JF-103 and AF phantoms (Table 4-3). This is because the mass difference in the liver between JF-103 and AF is relatively small, and is only about 7% (Table 3-3). The different trend in liver Self-SAFs was seen in comparison of the JM-103 and AM phantoms. The differences in the liver Self-SAFs between JM-103 and AM increased with the decreasing the photon energy, and varied from 5% to 17% at all calculated energies. As shown in Table 3-2, the liver mass of JM-103 was lighter than that of AM about 19%. Thus, it was thought that the differences in the liver Self-SAFs between JM-103 and AM were attributed to the differences in liver masses between adult male Japanese and Caucasian.

In conclusion, it can be explained that the differences in the SAFs and Self-SAFs between the JM-103 and AM phantoms or the JF-103 and AF phantoms were caused by the differences in anatomical characteristics such as organ distances and organ masses between adult Japanese and Caucasian.

Table 4-2 SAFs and organ distances for selected combinations of source regions and target organs in the JM-103, AM, JF-103 and AF phantoms.

Source → Target	Phantoms	Organ distances (mm)	SAFs (kg^{-1}) Photon energy (MeV) 0.02	0.03	0.05	0.1	0.5	1
Thyroid → Lungs	JM-103	149	6.75E-3	1.87E-2	1.75E-2	1.29E-2	1.17E-2	1.08E-2
	AM	124	0.00E+0	2.18E-2	2.17E-2	1.63E-2	1.46E-2	1.34E-2
	JF-103	155	5.59E-3	1.70E-2	1.65E-2	1.22E-2	1.16E-2	1.07E-2
	AF	124	9.58E-3	2.62E-2	2.52E-2	1.80E-2	1.61E-2	1.48E-2
Liver →Kidneys	JM-103	94	2.73E-2	4.76E-2	4.30E-2	2.96E-2	2.45E-2	2.24E-2
	AM	102	1.90E-2	3.68E-2	3.67E-2	2.60E-2	2.08E-2	1.90E-2
	JF-103	77	5.21E-2	7.48E-2	5.87E-2	3.81E-2	3.31E-2	3.03E-2
	AF	82	2.97E-2	4.99E-2	4.64E-2	3.23E-2	2.69E-2	2.47E-2
Bladder-content → Stomach	JM-103	248	6.10E-7	1.47E-4	1.14E-3	1.71E-3	1.92E-3	2.07E-3
	AM	306	0.00E+0	1.53E-5	2.45E-4	5.67E-4	8.61E-4	9.81E-4
	JF-103	209	1.44E-5	1.13E-3	3.80E-3	4.07E-3	4.00E-3	4.03E-3
	AF	283	0.00E+0	2.26E-5	3.69E-4	7.39E-4	1.10E-3	1.25E-3
Bladder-content → Bladder	JM-103	1	2.50E+0	1.53E+0	6.23E-1	3.31E-1	3.25E-1	2.98E-1
	AM	5	1.38E+0	1.06E+0	4.94E-1	2.63E-1	2.47E-1	2.26E-1
	JF-103	4	3.11E+0	1.84E+0	7.36E-1	3.89E-1	3.86E-1	3.53E-1
	AF	5	1.44E+0	1.04E+0	4.75E-1	2.55E-1	2.47E-1	2.27E-1

Table 4-3 Self-SAFs for thyroid and liver in the JM-103, AM, JF-103 and AF phantoms.

Organs (Source = Target)	Phantoms	Self-SAFs (kg^{-1}) Photon energy (MeV) 0.02	0.03	0.05	0.1	0.5	1
Thyroid	JM-103	1.92E+1	7.91E+0	3.06E+0	1.45E+0	1.53E+0	1.34E+0
	AM	1.88E+1	7.67E+0	2.96E+0	1.41E+0	1.48E+0	1.29E+0
	JF-103	2.30E+1	9.39E+0	3.62E+0	1.72E+0	1.82E+0	1.60E+0
	AF	2.20E+1	8.99E+0	3.46E+0	1.64E+0	1.73E+0	1.51E+0
Liver	JM-103	5.36E-1	3.68E-1	1.85E-1	1.06E-1	1.01E-1	9.16E-2
	AM	4.56E-1	3.30E-1	1.75E-1	1.01E-1	9.24E-2	8.39E-2
	JF-103	5.86E-1	3.96E-1	1.93E-1	1.10E-1	1.06E-1	9.68E-2
	AF	5.70E-1	3.96E-1	1.99E-1	1.13E-1	1.06E-1	9.67E-2

4.2 Organ doses due to external photon exposure

4.2.1 Code system and calculation conditions of organ doses for photons

Organ dose is fundamental quantity in estimating the risk to radiation exposure. Since the organ doses cannot be measured directly, dose conversion coefficients that relate a specified dosimetric quantity to organ doses have been used for external dose assessment. The dose conversion coefficients were calculated by using an organ dose calculation system, which consists of EGS4[51)] and EGS4 user code named 'UCPIXEL'.[24,26,29)] The organ dose calculation system can simulate the transport of photon and electron in voxel phantoms, and calculate the organ doses due to the external photon and electron exposures under the idealized irradiation conditions.

The organ dose calculation system uses the GSF compressed format organ segmented data and bone density data. As described in Section 4.1.1, the JM-103, JF-103, AM and AF phantoms consist of only the organ segmented data. Therefore, the organ segmented data together with the dummies of bone density data were compressed by previous methods,[5,6,24,26)] and were incorporated into UCPIXEL code. The transport simulations of the photon and electron in voxel phantom were performed under the same conditions mentioned in Section 4.1.1.

The dose conversion coefficients were given as absorbed dose per unit air-kerma free-in-air, and were calculated for 8 incident photon energies (0.03, 0.06, 0.08, 0.1, 0.15, 0.5, 1.0 and 5.0 MeV) for six idealized irradiation geometries (AP: anterior to posterior, PA: posterior to anterior, LLAT: left lateral, RLAT: right lateral, ROT: rotational and ISO: isotropic).[55)] Some examples of dose conversion coefficients of the JM-103, JF-103, JM-60 and JF-60 phantoms were shown in Appendix G.

4.2.2 Validation of organ doses in the JM-103 and JF-103 phantoms by comparison with those in the JM-60 and JF-60 phantoms

Figure 4-4 shows the absorbed doses in brain, thyroid, lungs, liver, stomach and bladder of JM-103, JM-60, JF-103 and JF-60 on selected incident photon energies for the AP irradiation geometry. These organs were chosen under consideration of anatomical location. At energies of more than 0.06 MeV, the absorbed doses of the brain, lungs and liver with heavy masses in the JM-103 phantom agreed with those of the JM-60 phantom within 10%. The differences of the absorbed doses in these organs increased with decreasing photon energy. Similar trends in organ doses were also found in comparison of the JF-103 and JF-60 phantoms. On the other hand, the great differences in absorbed doses were found in the thyroid, stomach and bladder with small masses. At 0.03 MeV, the differences in bladder doses between JM-103 and JM-60 or JF-103 and JF-60 were about 35% and 33%, respectively. These differences were due to the difference in the elemental compositions of bladder. The thyroid doses at less than 0.1 MeV in the JM-103 were higher than those in JM-60 about 11-32%. Similar results were also obtained from the comparison of JF-103 and JF-60. As shown in Tables 2-4 and 2-5, the thyroid of JM-103 and JF-103 contained the iodine. Therefore, it was considered that the interaction of iodine in thyroid with photons strongly influenced the thyroid doses.

Above results indicate that the organ dose conversions of selected organs except bladder and thyroid in JM-103 and JF-103 agreed well with those in JM-60 and JF-60. The little differences in dose conversion coefficients suggest that there are no anatomical problems in constructing the JM-103 and JF-103 phantoms. Therefore, it can be concluded that there is no practical problem in using JM-103 and JF-103 for the calculation of organ doses due to external exposures.

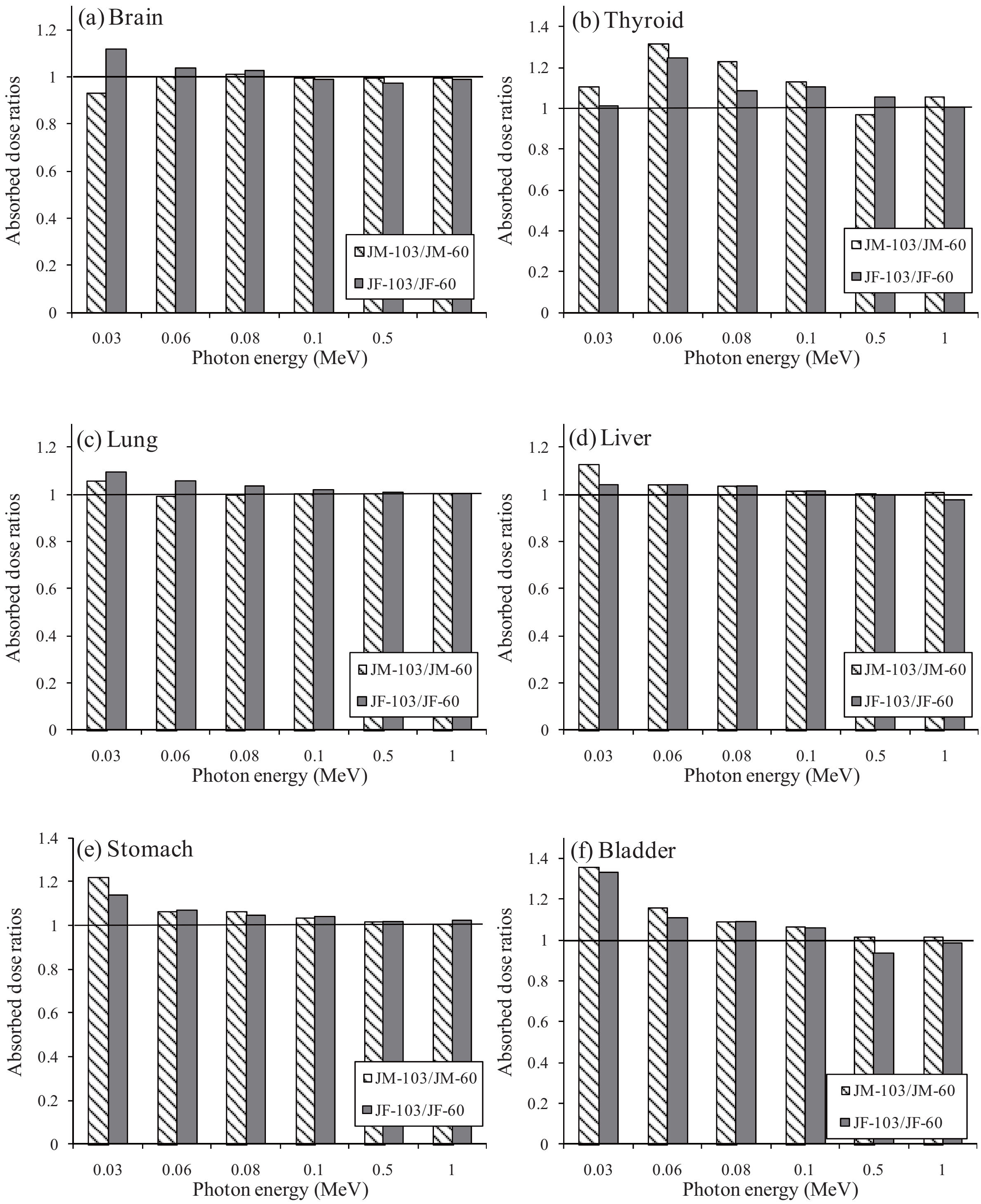

Figure 4-4 The ratios (JM-103/JM-60 or JF-103/JF-60) of absorbed doses for the AP irradiation geometry. (a) Brain, (b) Thyroid, (c) Lung, (d) Liver, (e) Stomach and (f) Bladder.

4.2.3 Comparison of organ doses in the JM-103 and JF-103 phantoms and those in the ICRP adult reference voxel phantoms

Table 4-4 shows examples of the absorbed doses of selected organs and tissues of the JM-103, AM, JF-103 and AF phantoms for the AP irradiation geometry at energy of 0.1 MeV. The differences of the absorbed doses in the thyroid, thymus, lungs, breast and heart between JM-103 and AM were relatively small, and were within 10%. Similar results were also found in comparison of JF-103 and AF. As described in Section 3.2, it was found that the lungs of the AM and AF phantoms shifted toward the neck compared with those of the JM-103 and JF-103 phantoms; the lungs of the ICRP adult reference voxel phantoms were compressed by the gravity actions as described in ICRP Publication 110.[2)] These facts mean that the thoracic parts of AM and AF were relatively small for their body sizes; there is little difference in the size of thoracic part between JM-103 and AM or JF-103 and AF. Thus, it was considered that the trends in absorbed doses of the thyroid, thymus, lungs, breast and heart were attributed to the differences in the lung volumes between the two averaged adult Japanese voxel phantoms and the ICRP adult reference voxel phantoms.

On the other hand, the absorbed doses in the adrenals, stomach, pancreas and gall bladder of the JM-103 and JF-103 phantoms were higher than those of the AM and AF phantoms about more 10%. The maximum differences (38%) in organ doses between JM-103 and AM were found in the adrenals. Similar difference (39%) in absorbed doses of the adrenals was also found in comparison of JF-103 and AF. The adrenals, stomach, pancreas and gall bladder was situated in the abdomen. As discussed in Section 3.1, the adipose masses of the AM and AF phantoms were heavier than those of the JM-103 and JF-103 phantoms. The mass differences in the adipose tissue influence the shapes, positions and distributions of internal organs and tissues. For example, the excess adipose tissue increases the thickness of the subcutaneous soft tissues; the distances from body surface to each organ and tissue in the AM and AF phantoms were generally longer than those in the JM-103 and JF-103 phantoms. Thus, the differences in absorbed doses in the adrenals, stomach, pancreas and gall bladder were caused by the differences in the distances from body surface to each organ and tissue. The adipose tissue mass was also important for the determination of organ doses due to external exposures, while the tissue weighting factor was not specified for the adipose tissue.[1,37)]

The contrary trend in the absorbed doses was seen in the bladder, ovaries, uterus and prostate. The absorbed doses in these organs of the JM-103 and JF-103 phantoms were smaller than those of the AM and AF phantoms. The ovaries, uterus and prostate located around the bladder. As shown in Table 3-3, the mass of bladder contents in the JF-103 phantom was only about 45% of the AF phantom. The mass difference in bladder content between the JM-103 and AM phantoms was also relatively large, and was about 49% (Table 3-2). The mass differences in bladder content induced the differences in the absorbed doses of bladder, ovaries, uterus and prostate, since the locations of these organs were easily moved by the changes in volume of bladder content; the volume of bladder content influence the distances from body surface to bladder, ovaries, uterus and prostate. These results suggest that the organ content mass was also one of important factors for organ dose determinations.

In conclusion, the differences in the anatomical characteristics such as the masses of organ and organ content were major causes of the differences in the absorbed doses of organs and tissues between the two averaged adult Japanese voxel phantoms and the ICRP adult reference voxel phantoms. Thus, the human phantoms, which have the anatomical characteristics of adult Japanese, should be used for the dose assessment.

Table 4-4 Organ absorbed dose per unit air-kerma for the AP irradiation geometry at energy of 0.1 MeV.

Organs and tissues	Organ doses (Gy Gy^{-1})			
	JM-103	AM	JF-103	AF
Brain	0.788	0.748 (1.05)[a]	0.792	0.784 (1.01)[b]
ET regions	1.352	1.239 (1.09)	1.284	1.096 (1.17)
Salivary glands	1.128	1.076 (1.05)	1.155	1.007 (1.15)
Tongue	1.108	1.154 (0.96)	1.111	1.093 (1.02)
Oral mucosa	1.175	1.041 (1.13)	1.191	1.200 (0.99)
Teeth	3.745	3.350 (1.12)	3.638	3.464 (1.05)
Thyroid	1.933	1.992 (0.97)	1.884	1.996 (0.94)
Trachea	1.489	1.688 (0.88)	1.450	1.537 (0.94)
Thymus	1.606	1.663 (0.97)	1.547	1.704 (0.91)
Esophagus	1.158	1.133 (1.02)	1.141	1.276 (0.89)
Lungs	1.295	1.273 (1.02)	1.255	1.231 (1.02)
Breast	1.503	1.538 (0.98)	1.474	1.564 (0.94)
Heart	1.433	1.416 (1.01)	1.431	1.453 (0.98)
Liver	1.372	1.259 (1.09)	1.404	1.390 (1.01)
Adrenals	0.965	0.701 (1.38)	1.189	0.857 (1.39)
Spleen	0.888	0.802 (1.11)	1.029	0.942 (1.09)
Stomach	1.568	1.418 (1.11)	1.615	1.474 (1.10)
Pancreas	1.444	1.294 (1.12)	1.680	1.471 (1.14)
Gall bladder	1.509	1.294 (1.17)	1.508	1.348 (1.12)
Kidneys	0.966	0.787 (1.23)	1.125	1.037 (1.08)
Colon	1.430	1.404 (1.02)	1.418	1.539 (0.92)
Small intestine	1.524	1.462 (1.04)	1.549	1.485 (1.04)
Bladder	1.471	1.511 (0.97)	1.399	1.670 (0.84)
Ovaries	-	- (-)	1.001	1.159 (0.86)
Uterus	-	- (-)	1.089	1.270 (0.86)
Prostate	1.114	1.253 (0.89)	-	- (-)
Testes	1.803	1.817 (0.99)	-	- (-)
Skin	1.160	1.131 (1.03)	1.160	1.163 (1.00)
Lymphatic tissues	1.261	1.390 (0.91)	1.327	1.421 (0.93)

[a]Values in parenthesis are the ratios of the organ doses of JM-103 to those of AM.

[b]Values in parenthesis are the ratios of the organ doses of JF-103 to those of AF.

5. Conclusions

The two averaged adult Japanese male and female voxel phantoms, which were constructed by modifying the JM[23] and JF[25] phantoms previously developed at JAEA, named 'the JM-103 phantom' and 'the JF-103 phantom', respectively. For convenience, the previously developed JM and JF were called 'the JM-60 phantom' and 'the JF-60 phantom', respectively. The heights and weights of JM-103 and JF-103 were in excellent agreement with the Japanese averages. The JM-103 and JF-103 phantoms can use in the calculations of the absorbed doses in the organs and tissues with the tissue weighing factors, which were defined by ICRP Publication 103. Except for the skeleton tissue, ET region and oral mucosa, the masses of organs and tissues in JM-103 and JF-103 were adjusted to the Japanese averages within 10%.

To validate the anatomical characteristics of JM-103 and JF-103, their organ distances and organ mass distributions were compared with those of JM-60 and JF-60. The differences in the organ distances between female phantoms were within 5% in most cases, although the height and weight of JF-103 were larger than those of JF-60 about 2% and 18%, respectively (see, Section 3.2). Similar differences were also observed in analysis of organ distances and organ mass distributions in male phantoms, which have almost the same body size. These results indicate that there are no problems for the anatomical structures in the JM-103 and JF-103 phantoms, since JM-103 and JF-103 fully reflected those in the JM-60 and JF-60 phantoms, which were exactly developed on the basis of CT images of actual living persons.

In photon SAF comparisons of male or female phantoms, the significant differences were mainly found in low energy region, and were attributed to the differences in the organ geometries (see, Section 4.1.2). On the other hand, the photon and electron Self-SAFs for selected organs in the male and female phantoms were strongly dependent on the masses of organs and tissues (see, Section 4.1.2). As described above, the masses of organs and tissues in JM-103 and JF-103 were in agreement with Japanese averages within 10%. Therefore, these results indicate that JM-103 and JF-103 can utilize for accurate evaluations of photon and electron Self-SAFs of average adult Japanese, and are useful for the internal dose assessment in average adult Japanese. With regards to this point, the JM-103 and JF-103 phantoms have the excellent characteristics as compared with the existing voxel phantoms containing the JM-60 and JF-60 phantoms. In external photon exposures, the absorbed doses in selected organs of the JM-103 and JF-103 phantoms agreed well with those of the JM-60 and JF-60 phantoms in most cases (see, Section 4.2.2). In conclusion, there are no problems in applying JM-103 and JF-103 to the assessment of organ doses due to diverse radiation exposures.

In some case, the SAFs, Self-SAFs and dose conversion coefficients of the JM-103 and JF-103 phantoms were different from those of the ICRP adult reference voxel phantoms. These differences were highly relevant to anatomical characteristics such as the organ masses and organ distances. Thus, while the ICRP adult reference voxel phantoms can provide the reasonable dose coefficients and dose conversion coefficients for the radiation protection purposes, there are some cases that the anatomical characteristics of the subjects should be considered for the evaluations of SAFs and organ doses. In this respect, the human phantoms, which have anatomical characteristics of average adult Japanese, will be needed for various dose assessment fields containing the medical treatments and radiation accidents.

In the fields of medical treatment and radiation accident, there are some cases that the individual differences in the postures, and the locations and shapes of organ influence the organ doses. These facts suggest that the dose assessment considering individual characteristics in body is of great importance to radiation accident and medical treatment. Recently, the highly flexible and deformable human phantoms (NURBS and polygon phantoms) have become available for calculating the organ doses under consideration of various body sizes and postures. In future, the authors will apply the deformation techniques to the JM-103 and JF-103 phantoms in order to analyze the effects of body sizes of individual subjects on the dose assessment in the CT examination.

Acknowledgment

The authors would like to express their gratitude to Dr K Saito of Japan Atomic Energy Agency for his valuable and technical advices on the development of JM-103 and JF-103.

References

1) International Commission on Radiological Protection (ICRP): “The 2007 Recommendations of the International Commission on Radiological Protection. Approved by the Commission in March 2007”, ICRP Publication 103 (2007).
2) International Commission on Radiological Protection (ICRP): “Adult reference computational phantoms. Approved by ICRP in October 2007 and adopted by ICRU in October 2008”, ICRP Publication 110 (2009).
3) International Commission on Radiological Protection (ICRP): “Basic anatomical and physiological data for use in radiological protection: Reference values”, ICRP Publication 89 (2002).
4) S. J. Gibbs, A. Pujol, T. S. Chen, A. W. Malcolm and A. E. James: “Patient risk from interproximal radiography”, Oral. Surg. Oral. Med. Oral. Pathol. 58, p.347-354 (1984).
5) M. Zankl, R. Veit, G. Williams, K. Schneider, H. Fendel, N. Petoussi and G. Drexler:“The construction of computer tomographic phantoms and their application in radiobiology and radiation protection“, Radiat. Environ. Biophys. 27, p.153-164 (1988).
6) R. Veit, M. Zankl, N. Petoussi, E. Mannweiler, G. Williams and G. Drexler: “Tomographic anthropomorphic models. Part I: Construction technique and description of models of an 8-week-old baby and a 7-year-old child”, GSF-Bericht 3/89 (1989).
7) P. J. Dimbylow: “FDTD calculations of the whole body averaged SAR in an anatomically realistic voxel model of the human body from 1MHz to 1 GHz”, Phys. Med. Biol. 42, p.479-490 (1997).
8) M. Zankl and A. Wittmann: “The adult male voxel model “Golem” segmented from whole-body CT patient data”, Radiat. Environ. Biophys. 40, p.153-162 (2001).
9) X. G. Xu, T. C. Chao and A. Bozkurt: “A VIP-Man: An image-based whole-body adult male model constructed from color photographs of the visible human project for multi-particle Monte

Carlo calculations", Health Phys. 78, p.476-486 (2000).
10) R. Kramer, J. W. Vieira, H. J. Khoury, F. R. A. Lima and D. Fuelle: 2003 "All about max: a male adult voxel phantom for Monte Carlo calculations in radiation protection dosimetry", Phys. Med. Biol. 48, p.1239-1262 (2003).
11) R. Kramer, J. W. Vieira, H. J. Khoury, F. R. A. Lima, E. CM. Loureiro, V. JM. Lima and G. Hoff G: "All about fax: a female adult voxel phantom for Monte Carlo calculation in radiation protection dosimetry", Phys .Med. Biol. 49, p.5203-5216 (2004).
12) U.A. Fill, M. Zankl, N. Petoussi-Henss, M. Siebert and D. Regulla: "Adult female voxel models of different stature and photon conversion coefficients for radiation protection", Health Phys. 86, p.253-272 (2004).
13) R. Veit and M. Zankl: "Influence of patient size on organ doses in diagnostic radiology", Radiat. Prot. Dosim. 43, p.241-243 (1992).
14) R. Veit and M. Zankl: "Variation of organ doses in pediatric radiology due to patient diameter calculated with phantoms of varying voxel size", Radiat. Prot. Dosim. 49, p.353-356 (1993).
15) C. Lee, C. Lee, J. L. Williams and W. E. Bolch: "Whole-body voxel phantoms of paediatric patients—UF Series B", Phys. Med. Biol. 51, p.4649–4661 (2006).
16) V. F. Cassola, V. J. de. Melo. Lima, R. Kramer and H J Khoury: "FASH and MASH: female and male adult human phantoms based on polygon mesh surfaces: I. Development of the anatomy", Phys. Med. Biol. 55, p.133-162 (2010).
17) R. Kramer, V. F. Cassola, H. J. Khoury, J. W. Vieira, V. J. de. Melo. Lima and K. R. Brown: "FASH and MASH: female and male adult human phantoms based on polygon mesh surfaces: II. Dosimetric calculations", Phys. Med. Biol. 55, p.163-189 (2010).
18) C. Lee, D. Lodwick, J. Hurtado, D. Pafundi, J. L. Williams and W. E. Bolch: "The UF family of reference hybrid phantoms for computational radiation dosimetry", Phys. Med. Biol. 55, p.339-363 (2010).
19) V. F. Cassola, R. Kramer, C. Brayner and H. J. Khoury: "Posture-specific phantoms representing female and male adults in Monte Carlo-based simulations for radiological protection", Phys. Med. Biol. 55, p.4399-4430 (2010).
20) J. Zhang, Y. H. Na, P. F. Caracappa and X. G. Xu: "RPI-AM and RPI-AF, a pair of mesh-based, size-adjustable adult male and female computational phantoms using ICRP-89 parameters and their calculations for organ doses from monoenergetic photon beams", Phys. Med. Biol. 54, p.5885-5908 (2009).
21) L. Liu, Z. Zeng, J. Li, R. Qiu, B. Zhang, J. Ma, R. Li, W. Li and L. Bi: "Organ dose conversion coefficients on an ICRP-based Chinese adult male voxel model from idealized external photons exposures", Phys. Med. Biol. 54, p.6645-6673 (2009).
22) L. Liu, Z. Zeng, J. Li, B. Zhang, R. Qiu and J. Ma: "An ICRP-based Chinese adult male voxel model and its absorbed dose for idealized photon exposures—the skeleton", Phys. Med. Biol. 54, p.6675-6690 (2009).
23) K. Sato, H. Noguchi, Y. Emoto, S. Koga and K Saito: "Japanese adult male voxel phantom constructed on the basis of CT-images", Radiat. Protect. Dosim. 123, p.337-344 (2007).

24) K. Saito, A. Wittmann, S. Koga, Y. Ida, J. Kamei, J. Funabiki and M. Zankl: "Construction of a computed tomographic phantom for a Japanese male adult and dose calculation system", Radiat. Environ. Biophys. 40, p.69-76 (2001).
25) K. Sato, H. Noguchi, Y. Emoto, S. Koga and K. Saito: "Development of a Japanese adult female voxel phantom", J. Nucl. Sci. Tech. 46, p.907-913 (2009).
26) K. Saito, S. Koga, Y. Ida, T. Kamei and J. Funabiki: "Construction of a voxel phantom based on CT data for a Japanese female adult and its use for calculation of organ doses from external electrons", Jpn. J. Health Phys. 43, p.122-130 (2008).
27) S. Kinase, M. Zankl, J. Kuwabara, K. Sato, H. Noguchi, J. Funabiki and K. Saito: "Evaluation of specific absorbed fraction in voxel phantoms using Monte Carlo calculation", Radiat. Prot. Dosim. 105, p.557-563 (2003).
28) S. Kinase, M. Zankl, J. Funabiki, H. Noguchi and K. Saito: "Evaluation of S values for beta-ray emitters within the urinary bladder", J. Nucl. Sci. Tech. Suppl. 4, p.136-139 (2004).
29) K. Saito, K. Sato, S. Kinase, H. Noguchi, J. Funabiki, S. Takagi, O. Sato, Y. Emoto and S. Koga: "Dose calculation using Japanese voxel phantoms for diverse exposures", Proceedings of Monte Carlo 2005 Topical Meeting: The Monte Carlo Method: Versatility Unbounded in a Dynamic Computing World (2005).
30) S. Kinase and K. Saito: "Evaluation of self-dose S values for positron emitters in voxel phantoms", Radiat. Protect. Dosim. 127, p.197-200 (2007).
31) K. Tsuda, S. Kinase M. Fukushi and K. Saito: "Evaluation of the dose coefficient from in vivo counting to organ doses in FDG-PET", Jpn. J. Health Phys. 42, p.349-352 (2007). (in Japanese)
32) S. Kinase, S. Takagi, H. Noguchi and K. Saito: "Application of voxel phantoms and Monte Carlo method to whole-body counter calibrations", Radiat. Protect. Dosim. 125, p.189-193 (2007).
33) K. Sato, H. Noguchi, A. Endo, Y. Emoto, S. Koga and K. Saito: "Development of a voxel phantom of Japanese adult male in upright posture", Radiat. Protect. Dosim. 127, p.205-208 (2007).
34) K. Sato, A. Endo and K. Saito: "Dose conversion coefficients calculated using a series of adult Japanese voxel phantoms against external photon exposure", JAEA-Data/Code 2008-016 (2008).
35) K. Sato and A. Endo: "Analysis of effects of posture on organ doses by internal photon emitters using voxel phantoms", Phys. Med. Biol. 53, p.4555-4572 (2008).
36) K. Sato, F. Takahashi, D. Satoh and A. Endo: "Development of adult Japanese voxel phantoms and their application to evaluation of radiation exposure doses", JAEA-Data/Code 2010-009 (2010).
37) International Commission on Radiological Protection (ICRP): "1990 Recommendations of the International Commission on Radiological Protection. Adopted by the Commission in November 1990", ICRP Publication 60 (1991).
38) F. Takahashi, K. Sato, A. Endo, K. Ono, T. Yoshitake, T. Hasegawa, Y. Katsunuma, N. Ban and M. Kai: "Effects of human model configuration in Monte Carlo calculations on organ doses from CT examinations", Joint International Conference on Supercomputing in Nuclear Applications and Monte Carlo 2010 (SNA+MC2010), "Progress in Nuclear Science and Technology" published by

the Atomic Energy Society of Japan (AESJ), (to be published).

39) F. Takahashi, A. Endo, K. Sato, K. Ono, T. Yoshitake, T. Hasegawa, Y. Katsunuma, N. Ban and M. Kai, "WAZA-ARI: Comupational dosimetry system for x-ray CT examinations, I Radiation transport calculation for organ and tissue doses evaluation using JM phantom," Proc. of the 3rd Asian and Oceanic Congress on Radiation Protection (AOCRP3), Tokyo, Japan, May 24-28, 2010. Radiat. Protect. Dosim. 146, p.241-243 (2011).
40) N. Ban, F. Takahashi, K. Ono, T. Hasegawa, T. Yoshitake, Y. Katsunuma, K. Sato, A. Endo and M. Kai, "WAZA-ARI: Comupational dosimetry system for x-ray CT examinations, II Development of web-based system," Proc. of the 3rd Asian and Oceanic Congress on Radiation Protection (AOCRP3), Tokyo, Japan, May 24-28, 2010. Radiat. Protect. Dosim. 146, p.244-247 (2011).
41) G. Tanaka and H. Kawamura: "Anatomical and physiological characteristics for Asian reference man. Male and female of different ages", NIRS-M-115 (1996).
42) F. S. Nooruddin and G. Turk: "Simplification and repair of polygonal models using volumetric techniques", IEEE. Trans. Visu. Comp. Grap. 9, p.191-205 (2003).
43) International Commission on Radiological Protection (ICRP): "Basic anatomical and physiological data for use in radiological protection: The skeleton. A report of a Task Group of Committee 2 of the International Commission on Radiological Protection", ICRP Publication 70, (1994).
44) International Commission on Radiological Protection (ICRP): "Human respiratory tract model for radiological protection. A report of a Task Group of the International Commission on Radiological Protection ", ICRP Publication 66, (1994).
45) International Commission on Radiological Protection (ICRP): "Human alimentary tract model for radiological protection. Approved by the Commission in March 2005", ICRP Publication 100, (2006).
46) J. Staubesand: "Sobbota Atlas der Anatomie des Menschen 19. Auflage. Fourth Japanese edition", Igaku-Shoin Ltd (1996). (in Japanese)
47) International Commission on Radiation Units and Measurements (ICRU): "Tissue substitute in radiation dosimetry and measurement", ICRU Report 44 (1989).
48) International Commission on Radiation Units and Measurements (ICRU): "Photon, electron, proton and neutron interaction data for body tissues“, ICRU Report 46 (1992).
49) H. Schlattl, M. Zankl and N. Petoussi-Henss: "Organ dose conversion coefficients for voxel models of the reference male and female from idealized photon exposures", Phys. Med. Biol. 52, p.2123-2145 (2007).
50) F. Takahashi, A. Endo, K. Sato, T. Hasegawa, Y. Katsunuma, K. Ono, T. Yoshitake, N. Ban and M. Kai: "Analysis of organ doses from computed tomography (CT) examination by the radiation transport calculation to develop the dosimetry system, WAZA-ARI", Prog. in. Nucl. Sci. Technol. 1, p.517-520 (2011).
51) W. R. Nelson, H. Hirayama and D. W. O. Rogers: "The EGS4 code system", SLAC-265 (1985).
52) ORNL / Radiation Shielding Information Center (RSIC): "DLC-136/PHOTX Photon interaction cross section library (contributed by National Institute of Standards and Technology)", (1993).

53) Y. Sakamoto: “Photon cross section data PHOTX for PEGS4 code”, KEK Proceedings 93-15, p. 77-82 (in Japanese) (1993).
54) International Commission on Radiation Units and Measurements (ICRU): “Stopping power for electrons and positrons”, ICRU Report 37 (1984).
55) International Commission on Radiological Protection (ICRP): “Conversion coefficients for use in radiological protection against external radiation”, ICRP Publication 74 (1996).

Appendix A　Coordinate system of the JM-103 and JF-103 phantoms

The organ segmented data of the JM-103 and JF-103 phantoms are recorded as ASCII text files. The capacity per an ASCII text file is about 1 MB. As described in previous report,[36] the ASCII text files of two phantoms are named in order of CT slice number from top of head to the bottom of feet (Figure A-1).

The three dimensional coordinate system are not common to the JM-103 and JF-103 phantoms. Figure A-2 illustrates the array of ASCII text file. The numbers of pixels per column and pixels per row in the JM-103 phantom are 512 and 512, respectively. On the other hand, the array of ASCII text file in the JF-103 phantom is 526 columns and 526 rows. Each numeral in ASCII text file corresponds to organ ID (see, Appendix C) assigned to each pixel.

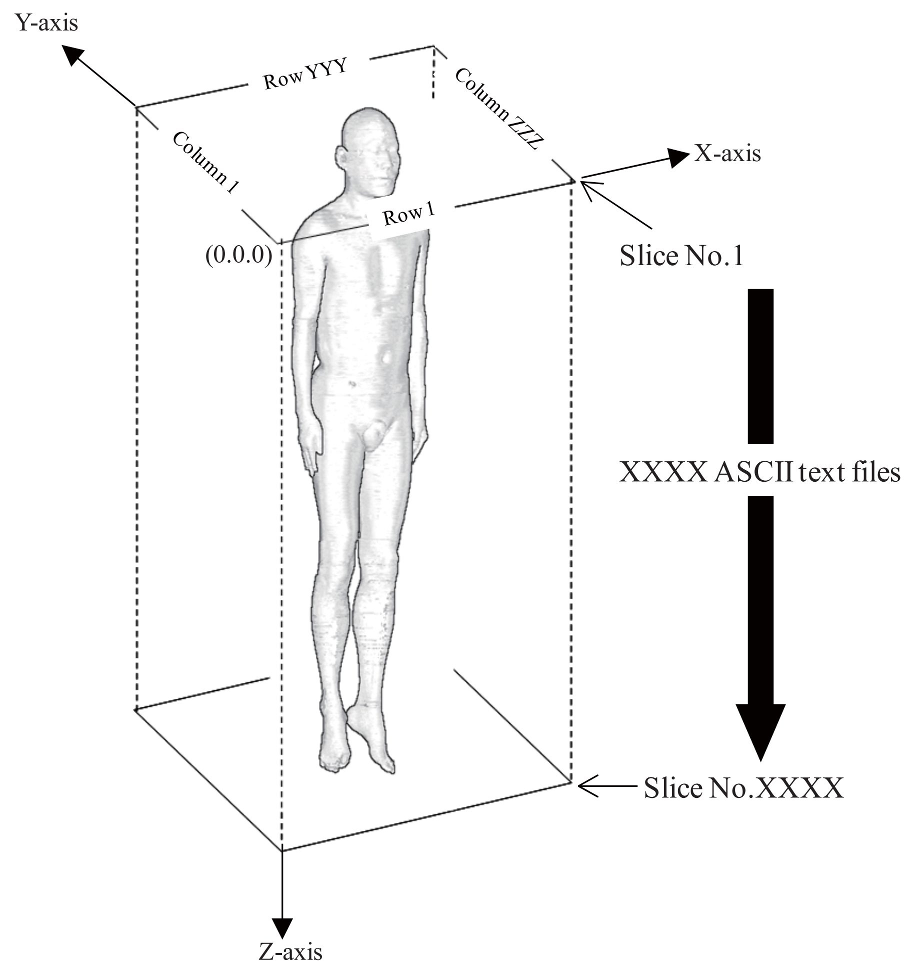

Figure A-1　Example of three dimensional coordinate system of the JM-103 and JF-103 phantoms.

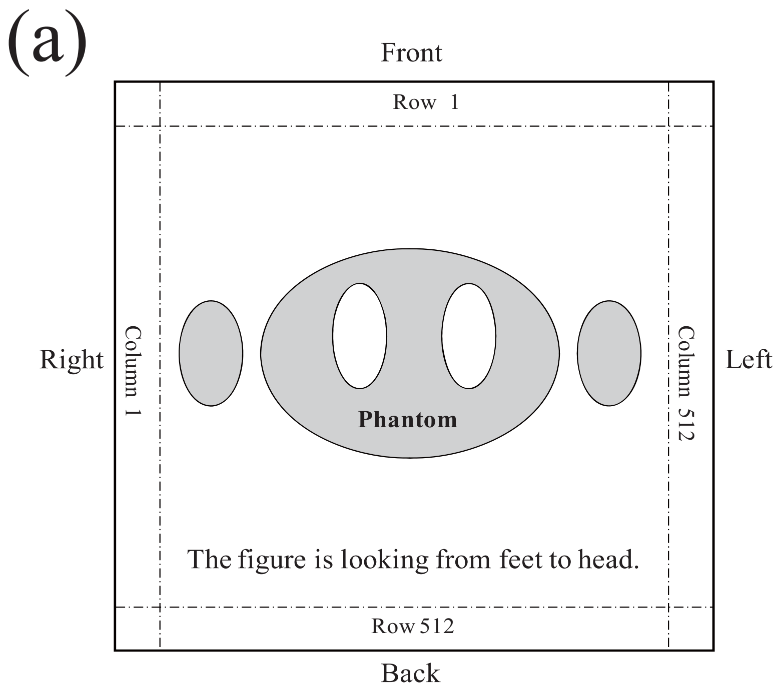

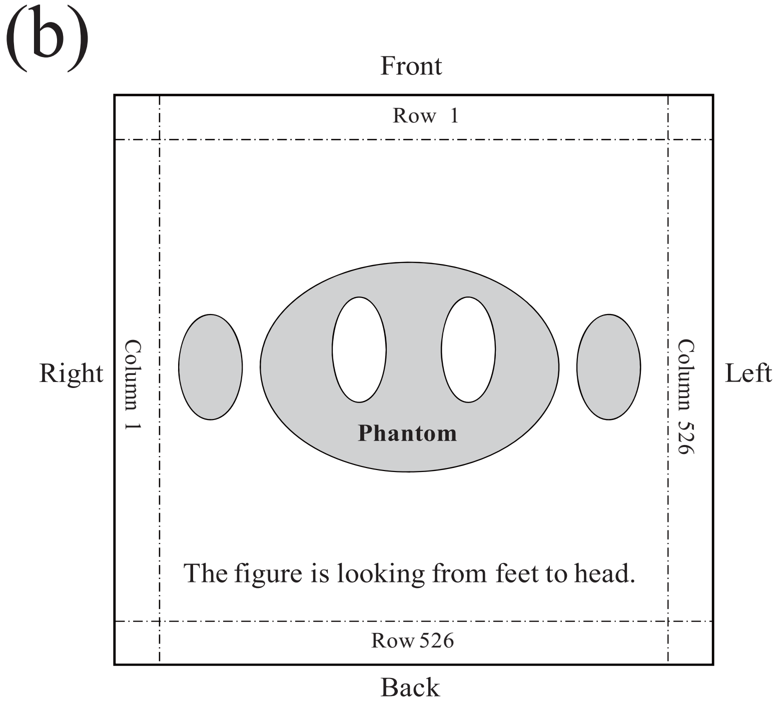

Figure A-2 Examples of the phantom geometry in ASCII text file.
(a) JM-103 and (b) JF-103.

Appendix B Centroids of organs in the JM-103, JM-60, JF-103 and JF-60 phantoms

This appendix presents the centers of masses in some organs and tissues of the male and female phantoms. The centroids of active marrow, adipose, hard bone, inactive marrow, lymphatic tissues, muscle and skin are not shown, since these organs and tissues are widely distributed in whole body.

In the tables, the centroid coordinates (x, y, z) of organs and tissues in each phantom are based on the coordinate system depicted in Figure A-1, and are given by unit of millimeters.

Table B-1 Centroids of some organs and tissues in the JM-60 phantom.

Organs and tissues	Centroid coordinate (mm)			Numbers of voxel
	X	Y	Z	
Adrenals	263.12	270.57	571.50	11832
Bladder	250.43	246.03	830.50	37386
Brain	259.06	237.30	82.50	1690003
Breast	259.87	166.31	428.00	98520
Bronchi	261.64	268.81	413.50	9129
Esophagus	269.24	262.65	426.00	36792
Eyes	261.89	152.49	111.00	13421
Eye lenses	261.71	144.57	110.00	369
Gall bladder	202.58	224.17	589.50	6644
Heart	272.59	243.73	431.00	524123
Left kidney	313.49	286.32	617.50	126359
Left lung	336.70	263.08	433.00	2633261
Liver	200.07	235.28	558.50	1293582
Lower large intestine	295.64	263.90	792.00	117083
Pancreas	277.75	229.63	597.50	117804
Right kidney	191.28	277.47	632.00	136484
Right lung	187.08	260.16	439.00	2816695
Small intestine	267.17	224.24	712.50	427738
Spleen	352.61	298.00	579.50	136957
Stomach	304.27	213.46	591.50	123347
Teeth	260.92	151.60	185.00	22948
Testes	253.02	204.65	919.50	36494
Thymus	261.26	208.43	378.00	31382
Thyroid	255.96	227.66	289.00	21628
Trachea	255.90	247.71	324.00	10122
Upper large intestine	218.63	221.11	669.50	133632

Table B-2 Centroids of some organs and tissues in the JM-103 phantom.

Organs and tissues	Centroid coordinate (mm)			Numbers of voxel
	X	Y	Z	
Adrenals	266.29	271.50	571.50	14775
Bladder	250.37	246.06	831.00	38916
Brain	259.13	237.29	82.00	1530778
Breast	261.57	162.09	432.00	24935
Bronchi	261.63	268.80	413.50	9128
Esophagus	269.24	262.65	426.00	36790
ET-region	261.28	169.09	134.00	43006
Eyes	261.89	152.49	110.50	13421
Eye lenses	261.71	144.57	110.00	369
Gall bladder	189.34	214.63	595.00	8211
Heart	271.05	230.05	443.00	385389
Left colon	331.00	223.95	667.00	129341
Left kidney	313.15	286.33	617.50	161004
Left lung	336.84	263.62	431.00	2340189
Liver	202.12	235.27	558.50	1449372
Oral mucosa	260.52	172.30	186.00	9915
Pancreas	278.12	229.79	597.50	136457
Parotid	257.03	213.02	178.00	51582
Prostate	256.50	276.96	850.50	11402
Right colon	182.11	227.11	680.00	138693
Right kidney	191.72	277.49	633.00	169408
Right lung	186.95	260.38	436.50	2526712
Salivary lingual	259.52	174.55	213.50	10412
Salivary maxillary	258.49	213.33	190.50	25037
Sigmoid colon	255.28	289.56	811.50	61177
Small intestine	267.01	224.48	711.50	562653
Spleen	352.61	298.00	579.00	136957
Stomach	304.47	213.56	591.50	142425
Teeth	260.92	151.60	185.00	22943
Testes	253.02	204.65	919.50	36491
Thymus	261.26	208.43	377.50	31382
Thyroid	255.83	227.71	288.50	19981
Tongue	260.18	177.71	183.50	61283
Trachea	255.86	248.12	325.00	8964

Table B-3 Centroids of some organs and tissues in the JF-60 phantom.

Organs and tissues	Centroid coordinate (mm)			Numbers of
	X	Y	Z	voxel
Adrenals	244.21	240.97	547.00	6188
Bladder	250.93	264.91	786.50	20046
Brain	256.55	250.05	74.50	1343908
Bronchi	258.65	243.27	380.00	14092
Esophagus	261.55	241.23	389.50	49134
Eyes	256.38	173.85	92.00	14607
Eye lenses	257.33	164.92	91.50	814
Gall bladder	207.90	211.24	580.50	3767
Heart	263.16	212.77	403.00	277992
Left breast	360.39	177.26	417.00	306661
Left kidney	296.18	267.06	567.50	108132
Left lung	318.23	244.35	399.50	2229886
Liver	214.91	219.61	517.50	1169240
Lower large intestine	279.26	269.71	745.50	114697
Ovaries	248.13	289.97	780.50	6694
Pancreas	252.29	220.33	588.50	95109
Right-breast	163.13	164.00	417.50	337242
Right kidney	188.05	266.37	576.50	102951
Right lung	196.29	238.35	392.00	2148342
Small intestine	248.94	226.61	696.50	377407
Spleen	326.23	280.38	544.50	55074
Stomach	286.82	214.73	587.00	105455
Teeth	258.06	167.28	157.00	21065
Thymus	258.21	192.14	351.00	19217
Thyroid	259.09	211.31	242.00	7269
Trachea	257.42	220.22	289.50	17319
Upper large intestine	228.32	217.55	685.50	120142
Uterus	251.28	285.48	793.50	47125

Table B-4 Centroids of some organs and tissues in the JF-103 phantom.

Organs and tissues	Centroid coordinate (mm)			Numbers of
	X	Y	Z	voxel
Adrenals	250.47	248.35	551.00	12032
Bladder	258.74	270.29	786.50	31920
Brain	263.55	256.81	74.50	1336112
Breast-adipose	264.68	172.07	418.00	212233
Bronchi	265.51	250.12	380.50	20629
Esophagus	268.46	248.43	398.50	31696
ET-region	264.20	187.24	120.00	30391
Eyes	263.76	176.00	92.50	11588
Eye lenses	263.82	165.30	93.00	273
Gall bladder	204.77	219.37	584.00	6259
Heart	271.27	215.56	408.50	322639
Left colon	315.41	246.06	717.00	99765
Left kidney	303.77	274.85	566.50	137664
Left lung	327.34	251.90	398.00	1983202
Liver	221.19	225.83	518.50	1300148
Mammary gland	264.14	178.20	420.50	128110
Oral mucosa	264.11	186.77	164.50	8417
Ovaries	254.48	298.07	781.50	11891
Pancreas	263.59	225.89	587.00	112849
Parotid	263.99	216.56	128.00	37141
Right colon	198.96	219.71	694.50	97671
Right kidney	194.19	274.36	577.00	131073
Right lung	200.99	245.31	391.00	1932966
Salivary lingual	266.52	188.63	191.50	7842
Salivary maxillary	265.46	225.18	169.00	18380
Sigmoid colon	255.04	317.10	749.00	49676
Small intestine	253.23	235.93	703.50	472161
Spleen	334.87	284.89	543.00	108221
Stomach	294.63	220.02	588.00	107618
Teeth	265.34	171.58	158.50	17420
Thymus	265.99	196.35	350.50	28127
Thyroid	266.08	216.84	242.50	16663
Tongue	264.01	192.02	162.00	51015
Trachea	264.27	226.61	291.00	6676
Uterus	258.24	292.44	790.50	68832

Appendix C Organ ID, material ID, density, volume and mass of each organ, tissue and content in the JM-103 and JF-103 phantoms

In this appendix, the organ ID, material ID, density, volume and mass of each organ, tissue and content in the JM-103 and JF-103 phantoms are presented. The organ ID numbers are assigned to voxels belonging to each organ, tissue and content in order to identify the segmented regions in the phantoms. The elemental compositions corresponding to each material ID of JM-103 and JF-103 are given in Tables 2-2 and 2-3. “None” means that there is no organ segmented region, which the organ ID is assigned.

Table C-1 Organ ID, material ID, density, volume and mass of each organ, tissue and content in the JM-103 phantom.

Organ ID	Organ/tissue/content	Material ID	Density (g/cm^3)	Volume (cc)	Mass (g)
1	None				
2	Adipose_head	m34	9.500E-1	6.1942E+2	5.8845E+2
3	None				
4	Adipose_trunk	m34	9.500E-1	9.7612E+3	9.2731E+3
5	None				
6	Adipose_left_arm	m34	9.500E-1	5.8325E+2	5.5409E+2
7	None				
8	Adipose_right_arm	m34	9.500E-1	5.8223E+2	5.5312E+2
9	None				
10	Adipose_left_leg	m34	9.500E-1	1.7313E+3	1.6447E+3
11	None				
12	Adipose_right_leg	m34	9.500E-1	1.6612E+3	1.5781E+3
13	None				
14	Adrenals	m31	1.030E+0	1.4190E+1	1.4616E+1
15	None				
16	Bladder_wall	m41	1.040E+0	3.7375E+1	3.8870E+1
17	Bladder_content	m31	1.030E+0	9.9359E+1	1.0234E+2
18	Brain	m42	1.040E+0	1.4702E+3	1.5290E+3
19	Meninges	m31	1.030E+0	1.5291E+2	1.5750E+2
20	Breast_adipose	m35	9.500E-1	2.3948E+1	2.2751E+1
21	Parotid	m31	1.030E+0	4.9539E+1	5.1025E+1
22	Submaxillary	m31	1.030E+0	2.4046E+1	2.4767E+1
23	Sublingual	m31	1.030E+0	9.9997E+0	1.0300E+1
24	Air in nose or air duct	m99	1.204E-3	1.3602E+2	1.6377E-1
25	Oral_mucosa	m32	1.050E+0	9.5224E+0	9.9985E+0
26	Tongue	m32	1.050E+0	5.8856E+1	6.1799E+1
27	ET regions	m31	1.030E+0	4.1303E+1	4.2542E+1
28	Bronchi	m31	1.030E+0	8.7665E+0	9.0295E+0
29	None				
30	Eye	m43	1.070E+0	1.2890E+1	1.3792E+1
31	None				
32	Eye_lens	m43	1.070E+0	3.5439E-1	3.7920E-1
33	Vena Cava	m44	1.050E+0	3.1196E+1	3.2756E+1
34	Heart_wall	m44	1.050E+0	3.7013E+2	3.8864E+2
35	Aorta	m44	1.050E+0	9.8510E+1	1.0344E+2
36	Left_kidney	m45	1.050E+0	1.5463E+2	1.6236E+2
37	None				
38	Rifgt_kidney	m45	1.050E+0	1.6270E+2	1.7084E+2
39	None				
40	Liver	m46	1.050E+0	1.3920E+3	1.4616E+3
41	None				
42	Left_lung	m36	2.600E-1	2.2475E+3	5.8435E+2
43	Left_Pleura	m31	1.030E+0	3.0491E+2	3.1406E+2
44	Right_lung	m36	2.600E-1	2.4267E+3	6.3094E+2
45	Right_Pleura	m31	1.030E+0	3.0618E+2	3.1537E+2

Table C-1 (Continued).

Organ ID	Organ/tissue/content	Material ID	Density (g/cm^3)	Volume (cc)	Mass (g)
46	Muscle_head	m32	1.050E+0	1.4491E+3	1.5216E+3
47	None				
48	Muscle_trunk	m32	1.050E+0	1.2868E+4	1.3511E+4
49	None				
50	Muscle_left_arm	m32	1.050E+0	9.8096E+2	1.0300E+3
51	None				
52	Muscle_right_arm	m32	1.050E+0	1.0408E+3	1.0928E+3
53	None				
54	Muscle_Left_leg	m32	1.050E+0	5.1926E+3	5.4522E+3
55	None				
56	Muscle_right_leg	m32	1.050E+0	5.3242E+3	5.5904E+3
57	None				
58	Esophagus	m31	1.030E+0	3.5333E+1	3.6393E+1
59	None				
60	Gall_bladder_wall	m31	1.030E+0	7.8858E+0	8.1224E+0
61	Gall_bladder_content	m31	1.030E+0	4.7601E+1	4.9029E+1
62	Pancreas	m47	1.040E+0	1.3105E+2	1.3629E+2
63	Vena Cava_content	m51	1.060E+0	3.1481E+1	3.3370E+1
64	Heart_content	m51	1.060E+0	3.4172E+2	3.6222E+2
65	Aorta_content	m51	1.060E+0	1.3752E+2	1.4577E+2
66	Small_int_wall	m49	1.030E+0	5.4037E+2	5.5658E+2
67	Small_int_content	m31	1.030E+0	3.4060E+2	3.5082E+2
68	None				
69	None				
70	None				
71	None				
72	Skin_head	m33	1.090E+0	1.7330E+2	1.8890E+2
73	None				
74	Skin_trunk	m33	1.090E+0	7.4671E+2	8.1391E+2
75	None				
76	Skin_left_arm	m33	1.090E+0	1.5998E+2	1.7438E+2
77	None				
78	Skin_right_arm	m33	1.090E+0	1.6203E+2	1.7661E+2
79	None				
80	Skin_left_leg	m33	1.090E+0	3.8526E+2	4.1993E+2
81	None				
82	Skin_right_leg	m33	1.090E+0	3.8063E+2	4.1489E+2
83	None				
84	None				
85	None				
86	None				
87	None				
88	Spleen	m48	1.060E+0	1.3153E+2	1.3942E+2
89	None				
90	Stomach_wall	m49	1.030E+0	1.3678E+2	1.4088E+2
91	Stomach_content	m81	6.790E-1	3.5338E+2	2.3995E+2

Table C-1 (Continued).

Organ ID	Organ/tissue/content	Material ID	Density (g/cm^3)	Volume (cc)	Mass (g)
92	Teeth	m37	2.750E+0	2.2034E+1	6.0594E+1
93	None				
94	Testes	m52	1.040E+0	3.5046E+1	3.6448E+1
95	Prostate	m54	1.030E+0	1.0950E+1	1.1279E+1
96	Thymus	m31	1.030E+0	3.0139E+1	3.1043E+1
97	None				
98	Thyroid	m50	1.050E+0	1.9190E+1	2.0150E+1
99	None				
100	Trachea	m31	1.030E+0	8.6090E+0	8.8673E+0
101	None				
102	Right_colon_wall	m49	1.030E+0	1.3320E+2	1.3720E+2
103	Right_colon_content	m82	7.210E-1	2.2249E+2	1.6042E+2
104	Left_colon_wall	m49	1.030E+0	1.2422E+2	1.2795E+2
105	Left_colon_content	m82	7.210E-1	1.3856E+2	9.9902E+1
106	Sigmoid_colon_wall	m49	1.030E+0	5.8754E+1	6.0517E+1
107	Sigmoid_colon_content	m82	7.210E-1	1.3855E+2	9.9895E+1
108	None				
109	None				
110	Lymphatic_nodes_extrath	m53	1.030E+0	9.4993E+0	9.7843E+0
111	Lymphatic_nodes_thoraci	m53	1.030E+0	8.9087E+0	9.1760E+0
112	Lymphatic_nodes_head	m53	1.030E+0	4.3737E+0	4.5049E+0
113	Lymphatic_nodes_trunk	m53	1.030E+0	1.6425E+2	1.6918E+2
114	Lymphatic_nodes_arms	m53	1.030E+0	1.2693E+1	1.3074E+1
115	Lymphatic_nodes_legs	m53	1.030E+0	1.7707E+1	1.8238E+1
116	None				
117	None				
118	None				
119	None				
120	Cranium01	m11	1.155E+0	3.9086E+1	4.5144E+1
121	Cranium02	m12	1.254E+0	3.8862E+1	4.8733E+1
122	Cranium03	m13	1.318E+0	9.9472E+1	1.3110E+2
123	Cranium04	m14	1.388E+0	1.4166E+2	1.9662E+2
124	Cranium05	m15	1.494E+0	1.2482E+2	1.8648E+2
125	Cranium06	m16	1.641E+0	1.9356E+2	3.1763E+2
126	Cranium07	m17	1.765E+0	2.3820E+2	4.2042E+2
127	None				
128	None				
129	None				
130	Mandible01	m11	1.155E+0	2.9888E+0	3.4521E+0
131	Mandible02	m12	1.254E+0	8.1259E+0	1.0190E+1
132	Mandible03	m13	1.318E+0	1.5673E+1	2.0657E+1
133	Mandible04	m14	1.388E+0	1.5877E+1	2.2037E+1
134	Mandible05	m15	1.494E+0	1.3088E+1	1.9553E+1
135	Mandible06	m16	1.641E+0	1.7283E+1	2.8361E+1
136	Mandible07	m17	1.765E+0	3.4354E+1	6.0635E+1

Table C-1 (Continued).

Organ ID	Organ/tissue/content	Material ID	Density (g/cm^3)	Volume (cc)	Mass (g)
137	None				
138	None				
139	None				
140	Cer.-vertebra01	m11	1.155E+0	6.9245E-1	7.9978E-1
141	Cer.-vertebra02	m12	1.254E+0	5.6942E+0	7.1405E+0
142	Cer.-vertebra03	m13	1.318E+0	3.0842E+1	4.0650E+1
143	Cer.-vertebra04	m14	1.388E+0	4.5060E+1	6.2543E+1
144	Cer.-vertebra05	m15	1.494E+0	3.1801E+1	4.7511E+1
145	Cer.-vertebra06	m16	1.641E+0	2.4091E+1	3.9533E+1
146	Cer.-vertebra07	m17	1.765E+0	4.8798E+0	8.6128E+0
147	None				
148	None				
149	None				
150	Thor.-vertebra01	m11	1.155E+0	1.9467E+1	2.2484E+1
151	Thor.-vertebra02	m12	1.254E+0	1.1079E+2	1.3893E+2
152	Thor.-vertebra03	m13	1.318E+0	1.5345E+2	2.0225E+2
153	Thor.-vertebra04	m14	1.388E+0	1.1518E+2	1.5987E+2
154	Thor.-vertebra05	m15	1.494E+0	4.8839E+1	7.2965E+1
155	Thor.-vertebra06	m16	1.641E+0	3.0158E+1	4.9489E+1
156	Thor.-vertebra07	m17	1.765E+0	4.3746E+0	7.7212E+0
157	None				
158	None				
159	None				
160	Lumb.-vertebra01	m11	1.155E+0	3.1764E+1	3.6687E+1
161	Lumb.-vertebra02	m12	1.254E+0	1.7009E+2	2.1329E+2
162	Lumb.-vertebra03	m13	1.318E+0	9.3480E+1	1.2321E+2
163	Lumb.-vertebra04	m14	1.388E+0	6.9781E+1	9.6856E+1
164	Lumb.-vertebra05	m15	1.494E+0	3.6478E+1	5.4498E+1
165	Lumb.-vertebra06	m16	1.641E+0	2.9865E+1	4.9008E+1
166	Lumb.-vertebra07	m17	1.765E+0	9.0086E+0	1.5900E+1
167	None				
168	None				
169	None				
170	Sacrum01	m11	1.155E+0	4.7612E+1	5.4992E+1
171	Sacrum02	m12	1.254E+0	5.3054E+1	6.6530E+1
172	Sacrum03	m13	1.318E+0	4.0112E+1	5.2868E+1
173	Sacrum04	m14	1.388E+0	3.0119E+1	4.1805E+1
174	Sacrum05	m15	1.494E+0	1.5179E+1	2.2677E+1
175	Sacrum06	m16	1.641E+0	1.0564E+1	1.7336E+1
176	Sacrum07	m17	1.765E+0	2.5210E+0	4.4496E+0
177	None				
178	None				
179	None				
180	Clavicles01	m11	1.155E+0	4.0539E+0	4.6823E+0
181	Clavicles02	m12	1.254E+0	9.6847E+0	1.2145E+1
182	Clavicles03	m13	1.318E+0	1.4396E+1	1.8974E+1

Table C-1 (Continued).

Organ ID	Organ/tissue/content	Material ID	Density (g/cm^3)	Volume (cc)	Mass (g)
183	Clavicles04	m14	1.388E+0	1.4007E+1	1.9442E+1
184	Clavicles05	m15	1.494E+0	1.0874E+1	1.6246E+1
185	Clavicles06	m16	1.641E+0	1.4573E+1	2.3914E+1
186	Clavicles07	m17	1.765E+0	9.1372E+0	1.6127E+1
187	None				
188	None				
189	None				
190	Scapulae01	m11	1.155E+0	1.8027E+0	2.0821E+0
191	Scapulae02	m12	1.254E+0	2.0493E+1	2.5698E+1
192	Scapulae03	m13	1.318E+0	5.5541E+1	7.3203E+1
193	Scapulae04	m14	1.388E+0	5.8765E+1	8.1566E+1
194	Scapulae05	m15	1.494E+0	3.9926E+1	5.9649E+1
195	Scapulae06	m16	1.641E+0	3.1350E+1	5.1445E+1
196	Scapulae07	m17	1.765E+0	9.3975E+0	1.6587E+1
197	None				
198	None				
199	None				
200	Sternum01	m11	1.155E+0	1.1312E+1	1.3065E+1
201	Sternum02	m12	1.254E+0	2.4162E+1	3.0299E+1
202	Sternum03	m13	1.318E+0	1.7193E+1	2.2660E+1
203	Sternum04	m14	1.388E+0	1.5134E+1	2.1006E+1
204	Sternum05	m15	1.494E+0	9.1891E+0	1.3729E+1
205	Sternum06	m16	1.641E+0	3.8646E+0	6.3418E+0
206	Sternum07	m17	1.765E+0	8.8357E-2	1.5595E-1
207	None				
208	None				
209	None				
210	Ribs01	m11	1.155E+0	4.1094E+1	4.7464E+1
211	Ribs02	m12	1.254E+0	2.3855E+2	2.9914E+2
212	Ribs03	m13	1.318E+0	1.6571E+2	2.1841E+2
213	Ribs04	m14	1.388E+0	1.3386E+2	1.8580E+2
214	Ribs05	m15	1.494E+0	7.4520E+1	1.1133E+2
215	Ribs06	m16	1.641E+0	4.7138E+1	7.7353E+1
216	Ribs07	m17	1.765E+0	3.1655E+0	5.5871E+0
217	None				
218	None				
219	None				
220	Os-coxae01	m11	1.155E+0	9.9661E+1	1.1511E+2
221	Os-coxae02	m12	1.254E+0	1.9827E+2	2.4863E+2
222	Os-coxae03	m13	1.318E+0	1.4570E+2	1.9203E+2
223	Os-coxae04	m14	1.388E+0	1.2673E+2	1.7590E+2
224	Os-coxae05	m15	1.494E+0	8.8653E+1	1.3245E+2
225	Os-coxae06	m16	1.641E+0	9.1130E+1	1.4954E+2
226	Os-coxae07	m17	1.765E+0	2.4644E+1	4.3497E+1
227	None				
228	None				
229	None				

Table C-1 (Continued).

Organ ID	Organ/tissue/content	Material ID	Density (g/cm^3)	Volume (cc)	Mass (g)
230	Hum.-upper01	m11	1.155E+0	5.6716E+1	6.5507E+1
231	Hum.-upper02	m12	1.254E+0	3.7115E+1	4.6542E+1
232	Hum.-upper03	m13	1.318E+0	3.8647E+1	5.0937E+1
233	Hum.-upper04	m14	1.388E+0	2.5780E+1	3.5783E+1
234	Hum.-upper05	m15	1.494E+0	1.3565E+1	2.0266E+1
235	Hum.-upper06	m16	1.641E+0	1.5786E+1	2.5905E+1
236	Hum.-upper07	m17	1.765E+0	3.5320E+1	6.2340E+1
237	None				
238	None				
239	None				
240	Hum.-lower01	m11	1.155E+0	1.7082E+1	1.9730E+1
241	Hum.-lower02	m12	1.254E+0	2.6611E+1	3.3370E+1
242	Hum.-lower03	m13	1.318E+0	3.2212E+1	4.2455E+1
243	Hum.-lower04	m14	1.388E+0	3.2194E+1	4.4685E+1
244	Hum.-lower05	m15	1.494E+0	2.0648E+1	3.0848E+1
245	Hum.-lower06	m16	1.641E+0	2.3173E+1	3.8027E+1
246	Hum.-lower07	m17	1.765E+0	4.5459E+1	8.0235E+1
247	None				
248	None				
249	None				
250	Forearm01	m11	1.155E+0	2.6333E+1	3.0415E+1
251	Forearm02	m12	1.254E+0	3.2773E+1	4.1097E+1
252	Forearm03	m13	1.318E+0	3.5370E+1	4.6618E+1
253	Forearm04	m14	1.388E+0	3.9452E+1	5.4759E+1
254	Forearm05	m15	1.494E+0	2.7517E+1	4.1110E+1
255	Forearm06	m16	1.641E+0	3.7531E+1	6.1588E+1
256	Forearm07	m17	1.765E+0	4.8186E+1	8.5048E+1
257	None				
258	None				
259	None				
260	Wrist-hand01	m11	1.155E+0	7.2202E+0	8.3393E+0
261	Wrist-hand02	m12	1.254E+0	8.7329E+0	1.0951E+1
262	Wrist-hand03	m13	1.318E+0	2.9510E+1	3.8894E+1
263	Wrist-hand04	m14	1.388E+0	5.0936E+1	7.0699E+1
264	Wrist-hand05	m15	1.494E+0	3.0845E+1	4.6082E+1
265	Wrist-hand06	m16	1.641E+0	2.0554E+1	3.3729E+1
266	Wrist-hand07	m17	1.765E+0	6.4942E+0	1.1462E+1
267	None				
268	None				
269	None				
270	Fem.-upper01	m11	1.155E+0	9.1918E+1	1.0617E+2
271	Fem.-upper02	m12	1.254E+0	7.9155E+1	9.9260E+1
272	Fem.-upper03	m13	1.318E+0	7.4118E+1	9.7688E+1
273	Fem.-upper04	m14	1.388E+0	6.6803E+1	9.2723E+1
274	Fem.-upper05	m15	1.494E+0	3.2454E+1	4.8486E+1
275	Fem.-upper06	m16	1.641E+0	3.5859E+1	5.8845E+1

Table C-1 (Continued).

Organ ID	Organ/tissue/content	Material ID	Density (g/cm^3)	Volume (cc)	Mass (g)
276	Fem.-upper07	m17	1.765E+0	1.2609E+2	2.2255E+2
277	None				
278	None				
279	None				
280	Fem.-lower01	m11	1.155E+0	1.1606E+2	1.3405E+2
281	Fem.-lower02	m12	1.254E+0	1.3408E+2	1.6814E+2
282	Fem.-lower03	m13	1.318E+0	1.2373E+2	1.6308E+2
283	Fem.-lower04	m14	1.388E+0	9.1685E+1	1.2726E+2
284	Fem.-lower05	m15	1.494E+0	4.1684E+1	6.2276E+1
285	Fem.-lower06	m16	1.641E+0	3.3991E+1	5.5779E+1
286	Fem.-lower07	m17	1.765E+0	1.2252E+2	2.1625E+2
287	None				
288	None				
289	None				
290	Tib.-fib.-pate01	m11	1.155E+0	1.8719E+2	2.1620E+2
291	Tib.-fib.-pate02	m12	1.254E+0	2.5961E+2	3.2555E+2
292	Tib.-fib.-pate03	m13	1.318E+0	1.7068E+2	2.2496E+2
293	Tib.-fib.-pate04	m14	1.388E+0	1.1812E+2	1.6395E+2
294	Tib.-fib.-pate05	m15	1.494E+0	7.1860E+1	1.0736E+2
295	Tib.-fib.-pate06	m16	1.641E+0	8.2539E+1	1.3545E+2
296	Tib.-fib.-pate07	m17	1.765E+0	2.2071E+2	3.8955E+2
297	None				
298	None				
299	None				
300	Ankle-foot01	m11	1.155E+0	4.3702E+1	5.0476E+1
301	Ankle-foot02	m12	1.254E+0	1.2659E+2	1.5874E+2
302	Ankle-foot03	m13	1.318E+0	1.1673E+2	1.5385E+2
303	Ankle-foot04	m14	1.388E+0	1.3850E+2	1.9224E+2
304	Ankle-foot05	m15	1.494E+0	1.0863E+2	1.6229E+2
305	Ankle-foot06	m16	1.641E+0	7.2204E+1	1.1849E+2
306	Ankle-foot07	m17	1.765E+0	2.0247E+1	3.5736E+1
307	None				
308	None				
309	None				
310	Os-hyoideum01	m11	1.155E+0	9.6040E-4	1.1093E-3
311	Os-hyoideum02	m12	1.254E+0	1.7288E-2	2.1679E-2
312	Os-hyoideum03	m13	1.318E+0	6.7324E-1	8.8733E-1
313	Os-hyoideum04	m14	1.388E+0	7.4143E-1	1.0291E+0
314	Os-hyoideum05	m15	1.494E+0	7.1262E-1	1.0647E+0
315	Os-hyoideum06	m16	1.641E+0	4.6195E-1	7.5806E-1
316	Os-hyoideum07	m17	1.765E+0	3.6495E-2	6.4414E-2
317	None				
318	None				
319	None				

Table C-2 Organ ID, material ID, density, volume and mass of each organ, tissue and content in the JF-103 phantom.

Organ ID	Organ/tissue/content	Material ID	Density (g/cm^3)	Volume (cc)	Mass (g)
1	None				
2	Adipose_head	m34	9.500E-1	8.2633E+2	7.8501E+2
3	None				
4	Adipose_trunk	m34	9.500E-1	6.8923E+3	6.5477E+3
5	None				
6	Adipose_left_arm	m34	9.500E-1	6.6443E+2	6.3121E+2
7	None				
8	Adipose_right_arm	m34	9.500E-1	6.5061E+2	6.1808E+2
9	None				
10	Adipose_left_leg	m34	9.500E-1	2.8223E+3	2.6812E+3
11	Breast_adipose	m34	9.500E-1	2.0383E+2	1.9364E+2
12	Adipose_right_leg	m34	9.500E-1	2.6861E+3	2.5518E+3
13	None				
14	Adrenals	m31	1.030E+0	1.1556E+1	1.1903E+1
15	None				
16	Bladder_wall	m41	1.040E+0	3.0656E+1	3.1882E+1
17	Bladder_content	m31	1.030E+0	8.7448E+1	9.0071E+1
18	Brain	m42	1.040E+0	1.2832E+3	1.3345E+3
19	Meninges	m31	1.030E+0	6.3640E+1	6.5549E+1
20	Mammary_gland	m35	9.400E-1	1.2304E+2	1.1566E+2
21	Parotid	m31	1.030E+0	3.5670E+1	3.6740E+1
22	Submaxillary	m31	1.030E+0	1.7652E+1	1.8182E+1
23	Sublingual	m31	1.030E+0	7.5315E+0	7.7574E+0
24	Air in nose or air duct	m99	1.204E-3	7.9888E+1	9.6185E-2
25	Oral_mucosa	m32	1.050E+0	8.0837E+0	8.4879E+0
26	Tongue	m32	1.050E+0	4.8995E+1	5.1445E+1
27	ET regions	m31	1.030E+0	2.9188E+1	3.0064E+1
28	Bronchi	m31	1.030E+0	1.9812E+1	2.0406E+1
29	None				
30	Eye	m43	1.070E+0	1.1129E+1	1.1908E+1
31	None				
32	Eye_lens	m43	1.070E+0	2.6219E-1	2.8054E-1
33	Vena Cava	m44	1.050E+0	2.9841E+1	3.1333E+1
34	Heart_wall	m44	1.050E+0	3.0986E+2	3.2535E+2
35	Aorta	m44	1.050E+0	5.9359E+1	6.2327E+1
36	Left_kidney	m45	1.050E+0	1.3221E+2	1.3882E+2
37	None				
38	Rifgt_kidney	m45	1.050E+0	1.2588E+2	1.3217E+2
39	None				
40	Liver	m46	1.050E+0	1.2487E+3	1.3111E+3
41	None				
42	Left_lung	m36	2.600E-1	1.9047E+3	4.9522E+2
43	Left_Pleura	m31	1.030E+0	3.5555E+2	3.6622E+2
44	Right_lung	m36	2.600E-1	1.8564E+3	4.8266E+2
45	Right_Pleura	m31	1.030E+0	3.2079E+2	3.3041E+2

Table C-2 (Continued).

Organ ID	Organ/tissue/content	Material ID	Density (g/cm^3)	Volume (cc)	Mass (g)
46	Muscle_head	m32	1.050E+0	7.4725E+2	7.8461E+2
47	None				
48	Muscle_trunk	m32	1.050E+0	9.3977E+3	9.8676E+3
49	None				
50	Muscle_left_arm	m32	1.050E+0	8.4393E+2	8.8613E+2
51	None				
52	Muscle_right_arm	m32	1.050E+0	7.8767E+2	8.2705E+2
53	None				
54	Muscle_Left_leg	m32	1.050E+0	3.6819E+3	3.8660E+3
55	None				
56	Muscle_right_leg	m32	1.050E+0	3.7906E+3	3.9801E+3
57	None				
58	Esophagus	m31	1.030E+0	3.0441E+1	3.1354E+1
59	None				
60	Gall_bladder_wall	m31	1.030E+0	6.0111E+0	6.1914E+0
61	Gall_bladder_content	m31	1.030E+0	3.3870E+1	3.4886E+1
62	Pancreas	m47	1.040E+0	1.0838E+2	1.1272E+2
63	Vena Cava_content	m51	1.060E+0	2.3836E+1	2.5266E+1
64	Heart_content	m51	1.060E+0	2.9804E+2	3.1592E+2
65	Aorta_content	m51	1.060E+0	8.1913E+1	8.6828E+1
66	Small_int_wall	m49	1.030E+0	4.5346E+2	4.6706E+2
67	Small_int_content	m31	1.030E+0	2.7492E+2	2.8317E+2
68	None				
69	None				
70	None				
71	None				
72	Skin_head	m33	1.090E+0	1.3659E+2	1.4888E+2
73	None				
74	Skin_trunk	m33	1.090E+0	6.3846E+2	6.9592E+2
75	None				
76	Skin_left_arm	m33	1.090E+0	1.4108E+2	1.5378E+2
77	None				
78	Skin_right_arm	m33	1.090E+0	1.3708E+2	1.4942E+2
79	None				
80	Skin_left_leg	m33	1.090E+0	3.4285E+2	3.7371E+2
81	None				
82	Skin_right_leg	m33	1.090E+0	3.4531E+2	3.7639E+2
83	None				
84	None				
85	None				
86	None				
87	None				
88	Spleen	m48	1.060E+0	1.0394E+2	1.1018E+2
89	None				
90	Stomach_wall	m49	1.030E+0	1.0336E+2	1.0646E+2
91	Stomach_content	m38	4.349E-1	4.1389E+2	1.8000E+2

Table C-2 (Continued).

Organ ID	Organ/tissue/content	Material ID	Density (g/cm^3)	Volume (cc)	Mass (g)
92	Teeth	m37	2.750E+0	1.6730E+1	4.6008E+1
93	None				
94	Ovary	m52	1.050E+0	1.1420E+1	1.1991E+1
95	Uterus	m53	1.020E+0	6.6106E+1	6.7428E+1
96	Thymus	m31	1.030E+0	2.7013E+1	2.7823E+1
97	None				
98	Thyroid	m50	1.050E+0	1.6003E+1	1.6803E+1
99	None				
100	Trachea	m31	1.030E+0	6.4116E+0	6.6039E+0
101	None				
102	Right_colon_wall	m49	1.030E+0	9.3803E+1	9.6617E+1
103	Right_colon_content	m31	1.030E+0	1.3429E+2	1.3832E+2
104	Left_colon_wall	m49	1.030E+0	9.5814E+1	9.8688E+1
105	Left_colon_content	m31	1.030E+0	6.9676E+1	7.1766E+1
106	Sigmoid_colon_wall	m49	1.030E+0	4.7709E+1	4.9140E+1
107	Sigmoid_colon_content	m31	1.030E+0	7.6555E+1	7.8852E+1
108	None				
109	None				
110	Lymphatic_nodes_extrath	m54	1.030E+0	7.6918E+0	7.9226E+0
111	Lymphatic_nodes_thoraci	m54	1.030E+0	7.2587E+0	7.4765E+0
112	Lymphatic_nodes_head	m54	1.030E+0	2.6891E+0	2.7698E+0
113	Lymphatic_nodes_trunk	m54	1.030E+0	1.2752E+2	1.3135E+2
114	Lymphatic_nodes_arms	m54	1.030E+0	9.3572E+0	9.6379E+0
115	Lymphatic_nodes_legs	m54	1.030E+0	1.3699E+1	1.4110E+1
116	None				
117	None				
118	None				
119	None				
120	Cranium01	m11	1.155E+0	6.7324E+1	7.7759E+1
121	Cranium02	m12	1.261E+0	7.3325E+1	9.2463E+1
122	Cranium03	m13	1.318E+0	6.8747E+1	9.0609E+1
123	Cranium04	m14	1.388E+0	7.8299E+1	1.0868E+2
124	Cranium05	m15	1.485E+0	8.1706E+1	1.2133E+2
125	Cranium06	m16	1.641E+0	1.5596E+2	2.5593E+2
126	Cranium07	m17	1.765E+0	1.9694E+2	3.4760E+2
127	None				
128	None				
129	None				
130	Mandible01	m11	1.155E+0	8.1730E-1	9.4398E-1
131	Mandible02	m12	1.261E+0	6.0832E+0	7.6709E+0
132	Mandible03	m13	1.318E+0	7.0532E+0	9.2961E+0
133	Mandible04	m14	1.388E+0	8.0702E+0	1.1201E+1
134	Mandible05	m15	1.485E+0	8.1932E+0	1.2167E+1
135	Mandible06	m16	1.641E+0	1.3824E+1	2.2685E+1
136	Mandible07	m17	1.765E+0	2.8235E+1	4.9835E+1
137	None				

Table C-2 (Continued).

Organ ID	Organ/tissue/content	Material ID	Density (g/cm^3)	Volume (cc)	Mass (g)
138	None				
139	None				
140	Cer.-vertebra01	m11	1.155E+0	5.2822E-1	6.1009E-1
141	Cer.-vertebra02	m12	1.261E+0	1.2765E+1	1.6097E+1
142	Cer.-vertebra03	m13	1.318E+0	2.4368E+1	3.2117E+1
143	Cer.-vertebra04	m14	1.388E+0	2.8828E+1	4.0013E+1
144	Cer.-vertebra05	m15	1.485E+0	1.6628E+1	2.4693E+1
145	Cer.-vertebra06	m16	1.641E+0	1.1234E+1	1.8435E+1
146	Cer.-vertebra07	m17	1.765E+0	2.2752E+0	4.0157E+0
147	None				
148	None				
149	None				
150	Thor.-vertebra01	m11	1.155E+0	1.2313E+1	1.4222E+1
151	Thor.-vertebra02	m12	1.261E+0	1.3239E+2	1.6694E+2
152	Thor.-vertebra03	m13	1.318E+0	1.1811E+2	1.5567E+2
153	Thor.-vertebra04	m14	1.388E+0	5.6754E+1	7.8775E+1
154	Thor.-vertebra05	m15	1.485E+0	2.4160E+1	3.5878E+1
155	Thor.-vertebra06	m16	1.641E+0	1.4951E+1	2.4535E+1
156	Thor.-vertebra07	m17	1.765E+0	1.5146E+0	2.6733E+0
157	None				
158	None				
159	None				
160	Lumb.-vertebra01	m11	1.155E+0	3.1650E+1	3.6556E+1
161	Lumb.-vertebra02	m12	1.261E+0	1.6049E+2	2.0238E+2
162	Lumb.-vertebra03	m13	1.318E+0	7.7911E+1	1.0269E+2
163	Lumb.-vertebra04	m14	1.388E+0	4.3911E+1	6.0948E+1
164	Lumb.-vertebra05	m15	1.485E+0	2.0250E+1	3.0071E+1
165	Lumb.-vertebra06	m16	1.641E+0	1.9734E+1	3.2383E+1
166	Lumb.-vertebra07	m17	1.765E+0	5.1324E+0	9.0587E+0
167	None				
168	None				
169	None				
170	Sacrum01	m11	1.155E+0	6.7788E+1	7.8295E+1
171	Sacrum02	m12	1.261E+0	6.4592E+1	8.1451E+1
172	Sacrum03	m13	1.318E+0	4.0670E+1	5.3603E+1
173	Sacrum04	m14	1.388E+0	1.6524E+1	2.2935E+1
174	Sacrum05	m15	1.485E+0	6.4356E+0	9.5569E+0
175	Sacrum06	m16	1.641E+0	3.4334E+0	5.6342E+0
176	Sacrum07	m17	1.765E+0	3.4286E-1	6.0515E-1
177	None				
178	None				
179	None				
180	Clavicles01	m11	1.155E+0	4.5907E+0	5.3023E+0
181	Clavicles02	m12	1.261E+0	1.0064E+1	1.2691E+1
182	Clavicles03	m13	1.318E+0	9.5176E+0	1.2544E+1
183	Clavicles04	m14	1.388E+0	7.1031E+0	9.8591E+0

Table C-2 (Continued).

Organ ID	Organ/tissue/content	Material ID	Density (g/cm^3)	Volume (cc)	Mass (g)
184	Clavicles05	m15	1.485E+0	5.1862E+0	7.7015E+0
185	Clavicles06	m16	1.641E+0	7.8657E+0	1.2908E+1
186	Clavicles07	m17	1.765E+0	6.0630E+0	1.0701E+1
187	None				
188	None				
189	None				
190	Scapulae01	m11	1.155E+0	8.7396E-1	1.0094E+0
191	Scapulae02	m12	1.261E+0	2.6314E+1	3.3182E+1
192	Scapulae03	m13	1.318E+0	3.8470E+1	5.0703E+1
193	Scapulae04	m14	1.388E+0	3.3837E+1	4.6966E+1
194	Scapulae05	m15	1.485E+0	2.2935E+1	3.4058E+1
195	Scapulae06	m16	1.641E+0	1.7168E+1	2.8173E+1
196	Scapulae07	m17	1.765E+0	4.9653E+0	8.7638E+0
197	None				
198	None				
199	None				
200	Sternum01	m11	1.155E+0	1.6684E+1	1.9270E+1
201	Sternum02	m12	1.261E+0	1.6154E+1	2.0370E+1
202	Sternum03	m13	1.318E+0	1.1710E+1	1.5434E+1
203	Sternum04	m14	1.388E+0	5.7960E+0	8.0448E+0
204	Sternum05	m15	1.485E+0	6.7228E-1	9.9834E-1
205	Sternum06	m16	1.641E+0	8.9317E-2	1.4657E-1
206	Sternum07	m17	1.765E+0	0.0000E+0	0.0000E+0
207	None				
208	None				
209	None				
210	Ribs01	m11	1.155E+0	3.4805E+1	4.0200E+1
211	Ribs02	m12	1.261E+0	1.6736E+2	2.1104E+2
212	Ribs03	m13	1.318E+0	9.1244E+1	1.2026E+2
213	Ribs04	m14	1.388E+0	7.5013E+1	1.0412E+2
214	Ribs05	m15	1.485E+0	4.0202E+1	5.9700E+1
215	Ribs06	m16	1.641E+0	1.8371E+1	3.0147E+1
216	Ribs07	m17	1.765E+0	5.6856E-1	1.0035E+0
217	None				
218	None				
219	None				
220	Os-coxae01	m11	1.155E+0	6.5122E+1	7.5216E+1
221	Os-coxae02	m12	1.261E+0	1.5806E+2	1.9931E+2
222	Os-coxae03	m13	1.318E+0	1.1904E+2	1.5689E+2
223	Os-coxae04	m14	1.388E+0	9.7568E+1	1.3542E+2
224	Os-coxae05	m15	1.485E+0	6.6806E+1	9.9207E+1
225	Os-coxae06	m16	1.641E+0	5.4714E+1	8.9786E+1
226	Os-coxae07	m17	1.765E+0	1.2615E+1	2.2265E+1
227	None				
228	None				
229	None				

Table C-2 (Continued).

Organ ID	Organ/tissue/content	Material ID	Density (g/cm^3)	Volume (cc)	Mass (g)
230	Hum.-upper01	m11	1.155E+0	3.9516E+1	4.5641E+1
231	Hum.-upper02	m12	1.261E+0	3.4881E+1	4.3985E+1
232	Hum.-upper03	m13	1.318E+0	2.1961E+1	2.8945E+1
233	Hum.-upper04	m14	1.388E+0	1.3355E+1	1.8537E+1
234	Hum.-upper05	m15	1.485E+0	8.0040E+0	1.1886E+1
235	Hum.-upper06	m16	1.641E+0	1.1522E+1	1.8908E+1
236	Hum.-upper07	m17	1.765E+0	1.7623E+1	3.1105E+1
237	None				
238	None				
239	None				
240	Hum.-lower01	m11	1.155E+0	9.9584E+0	1.1502E+1
241	Hum.-lower02	m12	1.261E+0	1.8000E+1	2.2698E+1
242	Hum.-lower03	m13	1.318E+0	1.3672E+1	1.8020E+1
243	Hum.-lower04	m14	1.388E+0	1.3053E+1	1.8118E+1
244	Hum.-lower05	m15	1.485E+0	8.9701E+0	1.3321E+1
245	Hum.-lower06	m16	1.641E+0	1.2501E+1	2.0514E+1
246	Hum.-lower07	m17	1.765E+0	2.2856E+1	4.0341E+1
247	None				
248	None				
249	None				
250	Forearm01	m11	1.155E+0	1.7829E+1	2.0592E+1
251	Forearm02	m12	1.261E+0	3.7250E+1	4.6972E+1
252	Forearm03	m13	1.318E+0	3.2288E+1	4.2556E+1
253	Forearm04	m14	1.388E+0	2.8467E+1	3.9512E+1
254	Forearm05	m15	1.485E+0	1.8146E+1	2.6947E+1
255	Forearm06	m16	1.641E+0	2.4676E+1	4.0493E+1
256	Forearm07	m17	1.765E+0	1.7629E+1	3.1115E+1
257	None				
258	None				
259	None				
260	Wrist-hand01	m11	1.155E+0	6.9571E+0	8.0355E+0
261	Wrist-hand02	m12	1.261E+0	3.8888E+1	4.9038E+1
262	Wrist-hand03	m13	1.318E+0	4.5256E+1	5.9647E+1
263	Wrist-hand04	m14	1.388E+0	2.6447E+1	3.6708E+1
264	Wrist-hand05	m15	1.485E+0	1.0039E+1	1.4908E+1
265	Wrist-hand06	m16	1.641E+0	6.8265E+0	1.1202E+1
266	Wrist-hand07	m17	1.765E+0	7.5872E-2	1.3391E-1
267	None				
268	None				
269	None				
270	Fem.-upper01	m11	1.155E+0	4.6761E+1	5.4009E+1
271	Fem.-upper02	m12	1.261E+0	7.9885E+1	1.0073E+2
272	Fem.-upper03	m13	1.318E+0	5.7115E+1	7.5278E+1
273	Fem.-upper04	m14	1.388E+0	4.5953E+1	6.3783E+1
274	Fem.-upper05	m15	1.485E+0	2.3085E+1	3.4281E+1
275	Fem.-upper06	m16	1.641E+0	2.4972E+1	4.0979E+1

Table C-2 (Continued).

Organ ID	Organ/tissue/content	Material ID	Density (g/cm^3)	Volume (cc)	Mass (g)
276	Fem.-upper07	ml7	1.765E+0	6.6455E+1	1.1729E+2
277	None				
278	None				
279	None				
280	Fem.-lower01	ml1	1.155E+0	1.1365E+2	1.3127E+2
281	Fem.-lower02	ml2	1.261E+0	1.1436E+2	1.4421E+2
282	Fem.-lower03	ml3	1.318E+0	7.5173E+1	9.9078E+1
283	Fem.-lower04	ml4	1.388E+0	4.2648E+1	5.9195E+1
284	Fem.-lower05	ml5	1.485E+0	2.2385E+1	3.3242E+1
285	Fem.-lower06	ml6	1.641E+0	2.3320E+1	3.8268E+1
286	Fem.-lower07	ml7	1.765E+0	7.7957E+1	1.3759E+2
287	None				
288	None				
289	None				
290	Tib.-fib.-pate01	ml1	1.155E+0	1.8114E+2	2.0922E+2
291	Tib.-fib.-pate02	ml2	1.261E+0	2.0138E+2	2.5394E+2
292	Tib.-fib.-pate03	ml3	1.318E+0	1.2113E+2	1.5965E+2
293	Tib.-fib.-pate04	ml4	1.388E+0	6.8951E+1	9.5704E+1
294	Tib.-fib.-pate05	ml5	1.485E+0	4.4004E+1	6.5346E+1
295	Tib.-fib.-pate06	ml6	1.641E+0	5.0315E+1	8.2567E+1
296	Tib.-fib.-pate07	ml7	1.765E+0	1.1019E+2	1.9449E+2
297	None				
298	None				
299	None				
300	Ankle-foot01	ml1	1.155E+0	3.5217E+1	4.0676E+1
301	Ankle-foot02	ml2	1.261E+0	8.9074E+1	1.1232E+2
302	Ankle-foot03	ml3	1.318E+0	1.1272E+2	1.4856E+2
303	Ankle-foot04	ml4	1.388E+0	9.9644E+1	1.3831E+2
304	Ankle-foot05	ml5	1.485E+0	3.9890E+1	5.9237E+1
305	Ankle-foot06	ml6	1.641E+0	1.6142E+1	2.6489E+1
306	Ankle-foot07	ml7	1.765E+0	5.3091E+0	9.3706E+0
307	None				
308	None				
309	None				
310	Os-hyoideum01	ml1	1.155E+0	3.8416E-3	4.4370E-3
311	Os-hyoideum02	ml2	1.261E+0	7.4527E-1	9.3979E-1
312	Os-hyoideum03	ml3	1.318E+0	8.3075E-1	1.0949E+0
313	Os-hyoideum04	ml4	1.388E+0	7.2606E-1	1.0078E+0
314	Os-hyoideum05	ml5	1.485E+0	2.9004E-1	4.3071E-1
315	Os-hyoideum06	ml6	1.641E+0	1.6423E-1	2.6950E-1
316	Os-hyoideum07	ml7	1.765E+0	7.6832E-3	1.3561E-2
317	None				
318	None				
319	None				

Appendix D Total mass, and mass fraction of active and inactive marrows, and hard bone in each skeletal segmented region except teeth of the JM-103 and JF-103 phantoms

In this appendix, total masses, and mass fractions of active and inactive marrows, and hard bone in each skeletal segmented region of the JM-103 and JF-103 phantoms are presented. The masses of active and inactive marrows and hard bone in each skeletal segmented were based on the previous reports.[36)]

Table D-1 Organ ID, total mass and mass fraction of active and inactive marrows and hard bone in the JM-103 phantom.

Organ ID	Skeletal segmented region	Total mass of skeleton except teeth (g)	Mass fraction		
			Active marrow	Inactive marrow	Hard bone
120	Cranium01	4.5144E+1	0.242	0.458	0.300
121	Cranium02	4.8733E+1	0.187	0.353	0.460
122	Cranium03	1.3110E+2	0.155	0.295	0.550
123	Cranium04	1.9662E+2	0.124	0.236	0.640
124	Cranium05	1.8648E+2	0.083	0.157	0.760
125	Cranium06	3.1763E+2	0.035	0.065	0.900
126	Cranium07	4.2042E+2	0.000	0.000	1.000
130	Mandible01	3.4521E+0	0.197	0.503	0.300
131	Mandible02	1.0190E+1	0.152	0.388	0.460
132	Mandible03	2.0657E+1	0.126	0.324	0.550
133	Mandible04	2.2037E+1	0.101	0.259	0.640
134	Mandible05	1.9553E+1	0.067	0.173	0.760
135	Mandible06	2.8361E+1	0.028	0.072	0.900
136	Mandible07	6.0635E+1	0.000	0.000	1.000
140	Cer.-vertebra01	7.9978E-1	0.523	0.177	0.300
141	Cer.-vertebra02	7.1405E+0	0.404	0.136	0.460
142	Cer.-vertebra03	4.0650E+1	0.336	0.114	0.550
143	Cer.-vertebra04	6.2543E+1	0.269	0.091	0.640
144	Cer.-vertebra05	4.7511E+1	0.179	0.061	0.760
145	Cer.-vertebra06	3.9533E+1	0.075	0.025	0.900
146	Cer.-vertebra07	8.6128E+0	0.000	0.000	1.000
150	Thor.-vertebra01	2.2484E+1	0.501	0.199	0.300
151	Thor.-vertebra02	1.3893E+2	0.386	0.154	0.460
152	Thor.-vertebra03	2.0225E+2	0.322	0.128	0.550
153	Thor.-vertebra04	1.5987E+2	0.258	0.102	0.640
154	Thor.-vertebra05	7.2965E+1	0.172	0.068	0.760
155	Thor.-vertebra06	4.9489E+1	0.072	0.028	0.900
156	Thor.-vertebra07	7.7212E+0	0.000	0.000	1.000
160	Lumb.-vertebra01	3.6687E+1	0.402	0.298	0.300
161	Lumb.-vertebra02	2.1329E+2	0.310	0.230	0.460
162	Lumb.-vertebra03	1.2321E+2	0.258	0.192	0.550
163	Lumb.-vertebra04	9.6856E+1	0.207	0.153	0.640
164	Lumb.-vertebra05	5.4498E+1	0.138	0.102	0.760
165	Lumb.-vertebra06	4.9008E+1	0.057	0.043	0.900
166	Lumb.-vertebra07	1.5900E+1	0.000	0.000	1.000
170	Sacrum01	5.4992E+1	0.669	0.031	0.300
171	Sacrum02	6.6530E+1	0.516	0.024	0.460
172	Sacrum03	5.2868E+1	0.430	0.020	0.550
173	Sacrum04	4.1805E+1	0.344	0.016	0.640
174	Sacrum05	2.2677E+1	0.229	0.011	0.760
175	Sacrum06	1.7336E+1	0.096	0.004	0.900
176	Sacrum07	4.4496E+0	0.000	0.000	1.000
180	Clavicles01	4.6823E+0	0.211	0.489	0.300
181	Clavicles02	1.2145E+1	0.163	0.377	0.460
182	Clavicles03	1.8974E+1	0.135	0.315	0.550
183	Clavicles04	1.9442E+1	0.108	0.252	0.640

Table D-1 (Continued).

Organ ID	Skeletal segmented region	Total mass of skeleton except teeth (g)	Mass fraction: Active marrow	Mass fraction: Inactive marrow	Mass fraction: Hard bone
184	Clavicles05	1.6246E+1	0.072	0.168	0.760
185	Clavicles06	2.3914E+1	0.030	0.070	0.900
186	Clavicles07	1.6127E+1	0.000	0.000	1.000
190	Scapulae01	2.0821E+0	0.245	0.455	0.300
191	Scapulae02	2.5698E+1	0.189	0.351	0.460
192	Scapulae03	7.3203E+1	0.157	0.293	0.550
193	Scapulae04	8.1566E+1	0.126	0.234	0.640
194	Scapulae05	5.9649E+1	0.084	0.156	0.760
195	Scapulae06	5.1445E+1	0.035	0.065	0.900
196	Scapulae07	1.6587E+1	0.000	0.000	1.000
200	Sternum01	1.3065E+1	0.539	0.161	0.300
201	Sternum02	3.0299E+1	0.416	0.124	0.460
202	Sternum03	2.2660E+1	0.347	0.103	0.550
203	Sternum04	2.1006E+1	0.277	0.083	0.640
204	Sternum05	1.3729E+1	0.185	0.055	0.760
205	Sternum06	6.3418E+0	0.077	0.023	0.900
206	Sternum07	1.5595E-1	0.000	0.000	1.000
210	Ribs01	4.7464E+1	0.331	0.369	0.300
211	Ribs02	2.9914E+2	0.256	0.284	0.460
212	Ribs03	2.1841E+2	0.213	0.237	0.550
213	Ribs04	1.8580E+2	0.170	0.190	0.640
214	Ribs05	1.1133E+2	0.114	0.126	0.760
215	Ribs06	7.7353E+1	0.047	0.053	0.900
216	Ribs07	5.5871E+0	0.000	0.000	1.000
220	Os-coxae01	1.1511E+2	0.376	0.324	0.300
221	Os-coxae02	2.4863E+2	0.290	0.250	0.460
222	Os-coxae03	1.9203E+2	0.241	0.209	0.550
223	Os-coxae04	1.7590E+2	0.193	0.167	0.640
224	Os-coxae05	1.3245E+2	0.129	0.111	0.760
225	Os-coxae06	1.4954E+2	0.054	0.046	0.900
226	Os-coxae07	4.3497E+1	0.000	0.000	1.000
230	Hum.-upper01	6.5507E+1	0.175	0.525	0.300
231	Hum.-upper02	4.6542E+1	0.135	0.405	0.460
232	Hum.-upper03	5.0937E+1	0.113	0.337	0.550
233	Hum.-upper04	3.5783E+1	0.090	0.270	0.640
234	Hum.-upper05	2.0266E+1	0.060	0.180	0.760
235	Hum.-upper06	2.5905E+1	0.025	0.075	0.900
236	Hum.-upper07	6.2340E+1	0.000	0.000	1.000
240	Hum.-lower01	1.9730E+1	0.000	0.700	0.300
241	Hum.-lower02	3.3370E+1	0.000	0.540	0.460
242	Hum.-lower03	4.2455E+1	0.000	0.450	0.550
243	Hum.-lower04	4.4685E+1	0.000	0.360	0.640
244	Hum.-lower05	3.0848E+1	0.000	0.240	0.760
245	Hum.-lower06	3.8027E+1	0.000	0.100	0.900
246	Hum.-lower07	8.0235E+1	0.000	0.000	1.000
250	Forearm01	3.0415E+1	0.000	0.700	0.300
251	Forearm02	4.1097E+1	0.000	0.540	0.460

Table D-1 (Continued).

Organ ID	Skeletal segmented region	Total mass of skeleton except teeth (g)	Mass fraction: Active marrow	Mass fraction: Inactive marrow	Mass fraction: Hard bone
252	Forearm03	4.6618E+1	0.000	0.450	0.550
253	Forearm04	5.4759E+1	0.000	0.360	0.640
254	Forearm05	4.1110E+1	0.000	0.240	0.760
255	Forearm06	6.1588E+1	0.000	0.100	0.900
256	Forearm07	8.5048E+1	0.000	0.000	1.000
260	Wrist-hand01	8.3393E+0	0.000	0.700	0.300
261	Wrist-hand02	1.0951E+1	0.000	0.540	0.460
262	Wrist-hand03	3.8894E+1	0.000	0.450	0.550
263	Wrist-hand04	7.0699E+1	0.000	0.360	0.640
264	Wrist-hand05	4.6082E+1	0.000	0.240	0.760
265	Wrist-hand06	3.3729E+1	0.000	0.100	0.900
266	Wrist-hand07	1.1462E+1	0.000	0.000	1.000
270	Fem.-upper01	1.0617E+2	0.264	0.436	0.300
271	Fem.-upper02	9.9260E+1	0.204	0.336	0.460
272	Fem.-upper03	9.7688E+1	0.170	0.280	0.550
273	Fem.-upper04	9.2723E+1	0.136	0.224	0.640
274	Fem.-upper05	4.8486E+1	0.091	0.149	0.760
275	Fem.-upper06	5.8845E+1	0.038	0.062	0.900
276	Fem.-upper07	2.2255E+2	0.000	0.000	1.000
280	Fem.-lower01	1.3405E+2	0.000	0.700	0.300
281	Fem.-lower02	1.6814E+2	0.000	0.540	0.460
282	Fem.-lower03	1.6308E+2	0.000	0.450	0.550
283	Fem.-lower04	1.2726E+2	0.000	0.360	0.640
284	Fem.-lower05	6.2276E+1	0.000	0.240	0.760
285	Fem.-lower06	5.5779E+1	0.000	0.100	0.900
286	Fem.-lower07	2.1625E+2	0.000	0.000	1.000
290	Tib.-fib.-pate01	2.1620E+2	0.000	0.700	0.300
291	Tib.-fib.-pate02	3.2555E+2	0.000	0.540	0.460
292	Tib.-fib.-pate03	2.2496E+2	0.000	0.450	0.550
293	Tib.-fib.-pate04	1.6395E+2	0.000	0.360	0.640
294	Tib.-fib.-pate05	1.0736E+2	0.000	0.240	0.760
295	Tib.-fib.-pate06	1.3545E+2	0.000	0.100	0.900
296	Tib.-fib.-pate07	3.8955E+2	0.000	0.000	1.000
300	Ankle-foot01	5.0476E+1	0.000	0.700	0.300
301	Ankle-foot02	1.5874E+2	0.000	0.540	0.460
302	Ankle-foot03	1.5385E+2	0.000	0.450	0.550
303	Ankle-foot04	1.9224E+2	0.000	0.360	0.640
304	Ankle-foot05	1.6229E+2	0.000	0.240	0.760
305	Ankle-foot06	1.1849E+2	0.000	0.100	0.900
306	Ankle-foot07	3.5736E+1	0.000	0.000	1.000
310	Os-hyoideum01	1.1093E-3	0.225	0.475	0.300
311	Os-hyoideum02	2.1679E-2	0.173	0.367	0.460
312	Os-hyoideum03	8.8733E-1	0.144	0.306	0.550
313	Os-hyoideum04	1.0291E+0	0.116	0.244	0.640
314	Os-hyoideum05	1.0647E+0	0.077	0.163	0.760
315	Os-hyoideum06	7.5806E-1	0.032	0.068	0.900
316	Os-hyoideum07	6.4414E-2	0.000	0.000	1.000

Table D-2 Organ ID, total mass and mass fraction of active and inactive marrows and hard bone in the JF-103 phantom.

Organ ID	Skeletal segmented region	Total mass of skeleton except teeth (g)	Mass fraction: Active marrow	Mass fraction: Inactive marrow	Mass fraction: Hard bone
120	Cranium01	7.7759E+1	0.214	0.486	0.300
121	Cranium02	9.2462E+1	0.162	0.368	0.470
122	Cranium03	9.0609E+1	0.138	0.312	0.550
123	Cranium04	1.0868E+2	0.110	0.250	0.640
124	Cranium05	1.2133E+2	0.076	0.174	0.750
125	Cranium06	2.5593E+2	0.031	0.069	0.900
126	Cranium07	3.4760E+2	0.000	0.000	1.000
130	Mandible01	9.4398E-1	0.271	0.429	0.300
131	Mandible02	7.6709E+0	0.205	0.325	0.470
132	Mandible03	9.2961E+0	0.174	0.276	0.550
133	Mandible04	1.1201E+1	0.139	0.221	0.640
134	Mandible05	1.2167E+1	0.097	0.153	0.750
135	Mandible06	2.2685E+1	0.039	0.061	0.900
136	Mandible07	4.9834E+1	0.000	0.000	1.000
140	Cer.-vertebra01	6.1009E-1	0.555	0.145	0.300
141	Cer.-vertebra02	1.6096E+1	0.420	0.110	0.470
142	Cer.-vertebra03	3.2117E+1	0.357	0.093	0.550
143	Cer.-vertebra04	4.0014E+1	0.285	0.075	0.640
144	Cer.-vertebra05	2.4693E+1	0.198	0.052	0.750
145	Cer.-vertebra06	1.8435E+1	0.079	0.021	0.900
146	Cer.-vertebra07	4.0157E+0	0.000	0.000	1.000
150	Thor.-vertebra01	1.4222E+1	0.505	0.195	0.300
151	Thor.-vertebra02	1.6695E+2	0.382	0.148	0.470
152	Thor.-vertebra03	1.5567E+2	0.325	0.125	0.550
153	Thor.-vertebra04	7.8774E+1	0.260	0.100	0.640
154	Thor.-vertebra05	3.5877E+1	0.180	0.070	0.750
155	Thor.-vertebra06	2.4534E+1	0.072	0.028	0.900
156	Thor.-vertebra07	2.6732E+0	0.000	0.000	1.000
160	Lumb.-vertebra01	3.6556E+1	0.379	0.321	0.300
161	Lumb.-vertebra02	2.0237E+2	0.287	0.243	0.470
162	Lumb.-vertebra03	1.0269E+2	0.244	0.206	0.550
163	Lumb.-vertebra04	6.0949E+1	0.195	0.165	0.640
164	Lumb.-vertebra05	3.0071E+1	0.135	0.115	0.750
165	Lumb.-vertebra06	3.2384E+1	0.054	0.046	0.900
166	Lumb.-vertebra07	9.0586E+0	0.000	0.000	1.000
170	Sacrum01	7.8295E+1	0.485	0.215	0.300
171	Sacrum02	8.1450E+1	0.367	0.163	0.470
172	Sacrum03	5.3603E+1	0.312	0.138	0.550
173	Sacrum04	2.2935E+1	0.249	0.111	0.640
174	Sacrum05	9.5569E+0	0.173	0.077	0.750
175	Sacrum06	5.6343E+0	0.069	0.031	0.900
176	Sacrum07	6.0515E-1	0.000	0.000	1.000
180	Clavicles01	5.3023E+0	0.234	0.466	0.300
181	Clavicles02	1.2691E+1	0.177	0.353	0.470
182	Clavicles03	1.2544E+1	0.151	0.299	0.550
183	Clavicles04	9.8591E+0	0.120	0.240	0.640

Table D-2 (Continued).

Organ ID	Skeletal segmented region	Total mass of skeleton except teeth (g)	Mass fraction: Active marrow	Mass fraction: Inactive marrow	Mass fraction: Hard bone
184	Clavicles05	7.7014E+0	0.084	0.166	0.750
185	Clavicles06	1.2908E+1	0.033	0.067	0.900
186	Clavicles07	1.0701E+1	0.000	0.000	1.000
190	Scapulae01	1.0094E+0	0.275	0.425	0.300
191	Scapulae02	3.3182E+1	0.208	0.322	0.470
192	Scapulae03	5.0703E+1	0.177	0.273	0.550
193	Scapulae04	4.6965E+1	0.141	0.219	0.640
194	Scapulae05	3.4059E+1	0.098	0.152	0.750
195	Scapulae06	2.8173E+1	0.039	0.061	0.900
196	Scapulae07	8.7637E+0	0.000	0.000	1.000
200	Sternum01	1.9270E+1	0.593	0.107	0.300
201	Sternum02	2.0370E+1	0.449	0.081	0.470
202	Sternum03	1.5434E+1	0.381	0.069	0.550
203	Sternum04	8.0449E+0	0.305	0.055	0.640
204	Sternum05	9.9834E-1	0.212	0.038	0.750
205	Sternum06	1.4657E-1	0.085	0.015	0.900
206	Sternum07	0.0000E+0	0.000	0.000	0.000
210	Ribs01	4.0200E+1	0.420	0.280	0.300
211	Ribs02	2.1104E+2	0.318	0.212	0.470
212	Ribs03	1.2026E+2	0.270	0.180	0.550
213	Ribs04	1.0412E+2	0.216	0.144	0.640
214	Ribs05	5.9700E+1	0.150	0.100	0.750
215	Ribs06	3.0146E+1	0.060	0.040	0.900
216	Ribs07	1.0035E+0	0.000	0.000	1.000
220	Os-coxae01	7.5216E+1	0.398	0.302	0.300
221	Os-coxae02	1.9932E+2	0.301	0.229	0.470
222	Os-coxae03	1.5690E+2	0.256	0.194	0.550
223	Os-coxae04	1.3542E+2	0.205	0.155	0.640
224	Os-coxae05	9.9207E+1	0.142	0.108	0.750
225	Os-coxae06	8.9786E+1	0.057	0.043	0.900
226	Os-coxae07	2.2265E+1	0.000	0.000	1.000
230	Hum.-upper01	4.5641E+1	0.201	0.499	0.300
231	Hum.-upper02	4.3985E+1	0.152	0.378	0.470
232	Hum.-upper03	2.8945E+1	0.129	0.321	0.550
233	Hum.-upper04	1.8537E+1	0.103	0.257	0.640
234	Hum.-upper05	1.1886E+1	0.072	0.178	0.750
235	Hum.-upper06	1.8907E+1	0.029	0.071	0.900
236	Hum.-upper07	3.1105E+1	0.000	0.000	1.000
240	Hum.-lower01	1.1502E+1	0.000	0.700	0.300
241	Hum.-lower02	2.2698E+1	0.000	0.530	0.470
242	Hum.-lower03	1.8020E+1	0.000	0.450	0.550
243	Hum.-lower04	1.8117E+1	0.000	0.360	0.640
244	Hum.-lower05	1.3321E+1	0.000	0.250	0.750
245	Hum.-lower06	2.0513E+1	0.000	0.100	0.900
246	Hum.-lower07	4.0340E+1	0.000	0.000	1.000
250	Forearm01	2.0592E+1	0.000	0.700	0.300
251	Forearm02	4.6972E+1	0.000	0.530	0.470

Table D-2 (Continued).

Organ ID	Skeletal segmented region	Total mass of skeleton except teeth (g)	Mass fraction		
			Active marrow	Inactive marrow	Hard bone
252	Forearm03	4.2555E+1	0.000	0.450	0.550
253	Forearm04	3.9512E+1	0.000	0.360	0.640
254	Forearm05	2.6947E+1	0.000	0.250	0.750
255	Forearm06	4.0493E+1	0.000	0.100	0.900
256	Forearm07	3.1115E+1	0.000	0.000	1.000
260	Wrist-hand01	8.0355E+0	0.000	0.700	0.300
261	Wrist-hand02	4.9037E+1	0.000	0.530	0.470
262	Wrist-hand03	5.9647E+1	0.000	0.450	0.550
263	Wrist-hand04	3.6708E+1	0.000	0.360	0.640
264	Wrist-hand05	1.4908E+1	0.000	0.250	0.750
265	Wrist-hand06	1.1202E+1	0.000	0.100	0.900
266	Wrist-hand07	1.3391E-1	0.000	0.000	1.000
270	Fem.-upper01	5.4009E+1	0.294	0.406	0.300
271	Fem.-upper02	1.0074E+2	0.222	0.308	0.470
272	Fem.-upper03	7.5278E+1	0.189	0.261	0.550
273	Fem.-upper04	6.3783E+1	0.151	0.209	0.640
274	Fem.-upper05	3.4281E+1	0.105	0.145	0.750
275	Fem.-upper06	4.0980E+1	0.042	0.058	0.900
276	Fem.-upper07	1.1729E+2	0.000	0.000	1.000
280	Fem.-lower01	1.3127E+2	0.000	0.700	0.300
281	Fem.-lower02	1.4421E+2	0.000	0.530	0.470
282	Fem.-lower03	9.9079E+1	0.000	0.450	0.550
283	Fem.-lower04	5.9195E+1	0.000	0.360	0.640
284	Fem.-lower05	3.3242E+1	0.000	0.250	0.750
285	Fem.-lower06	3.8269E+1	0.000	0.100	0.900
286	Fem.-lower07	1.3759E+2	0.000	0.000	1.000
290	Tib.-fib.-pate01	2.0922E+2	0.000	0.700	0.300
291	Tib.-fib.-pate02	2.5394E+2	0.000	0.530	0.470
292	Tib.-fib.-pate03	1.5964E+2	0.000	0.450	0.550
293	Tib.-fib.-pate04	9.5704E+1	0.000	0.360	0.640
294	Tib.-fib.-pate05	6.5345E+1	0.000	0.250	0.750
295	Tib.-fib.-pate06	8.2567E+1	0.000	0.100	0.900
296	Tib.-fib.-pate07	1.9449E+2	0.000	0.000	1.000
300	Ankle-foot01	4.0676E+1	0.000	0.700	0.300
301	Ankle-foot02	1.1232E+2	0.000	0.530	0.470
302	Ankle-foot03	1.4857E+2	0.000	0.450	0.550
303	Ankle-foot04	1.3831E+2	0.000	0.360	0.640
304	Ankle-foot05	5.9237E+1	0.000	0.250	0.750
305	Ankle-foot06	2.6490E+1	0.000	0.100	0.900
306	Ankle-foot07	9.3705E+0	0.000	0.000	1.000
310	Os-hyoideum01	4.4370E-3	0.269	0.431	0.300
311	Os-hyoideum02	9.3979E-1	0.204	0.326	0.470
312	Os-hyoideum03	1.0949E+0	0.173	0.277	0.550
313	Os-hyoideum04	1.0078E+0	0.138	0.222	0.640
314	Os-hyoideum05	4.3071E-1	0.096	0.154	0.750
315	Os-hyoideum06	2.6950E-1	0.038	0.062	0.900
316	Os-hyoideum07	1.3561E-2	0.000	0.000	1.000

Appendix E　Mass distribution of some organs and tissues in the JM-103, JM-60, JF-103 and JF-60 phantoms

This appendix presents mass distributions of some organs and tissues along the head-leg axis of body in the male and female phantoms. The mass distributions are given as the masses (g) of each organ and tissue every 1mm slice thickness. As shown in Appendix A, the "slices No.1" is the cross sectional image at the top of head.

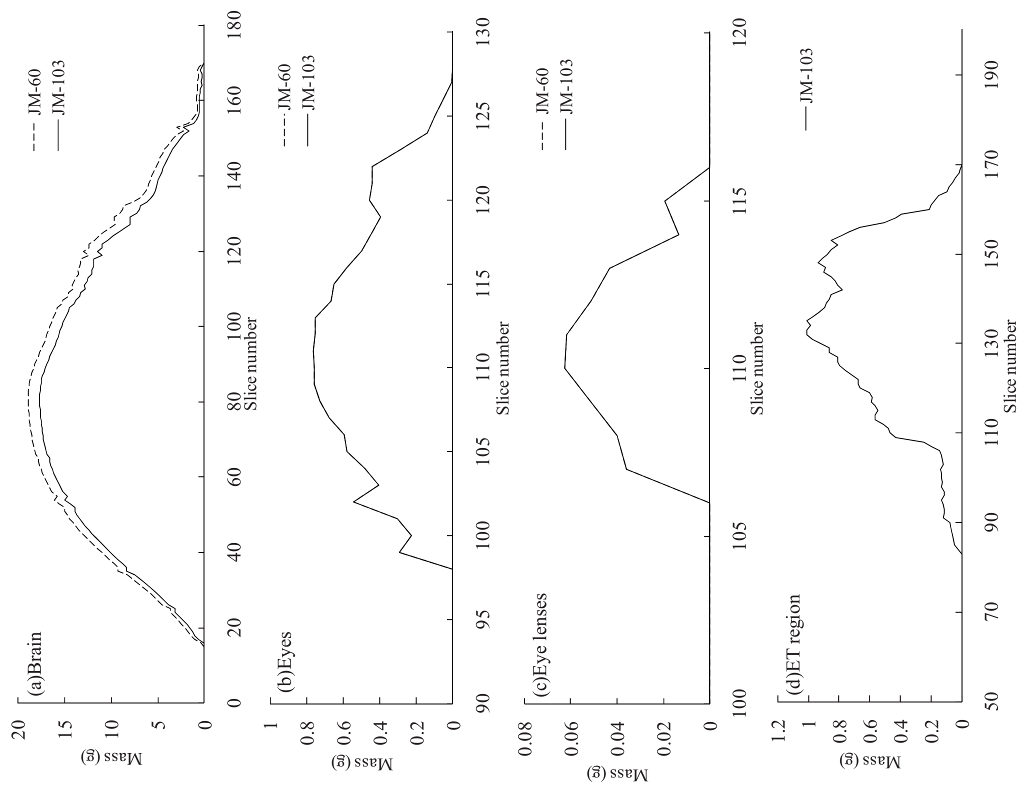

Figure E-1　Mass distribution of some organs and tissues along the head-leg axis of body in the JM-60 and JM-103. (a) Brain, (b) Eyes, (c) Eye lenses and (d) ET region.

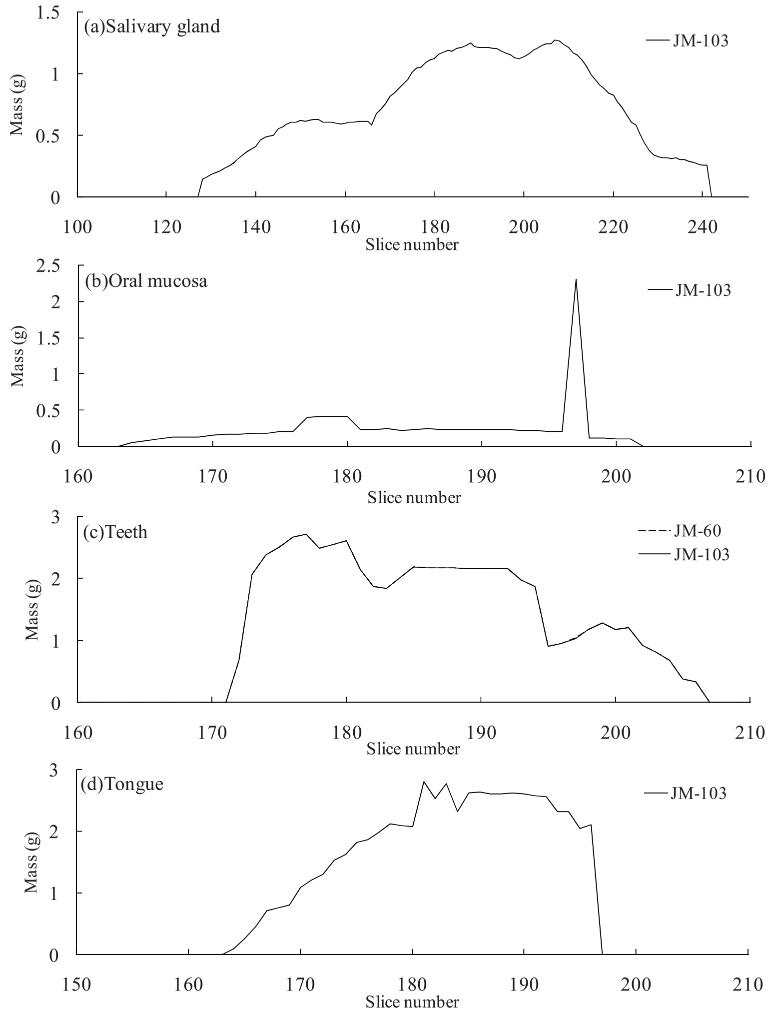

Figure E-2 Mass distribution of some organs and tissues along the head-leg axis of body in the JM-60 and JM-103. (a) Salivary gland, (b) Oral mucosa, (c) Teeth and (d) Tongue.

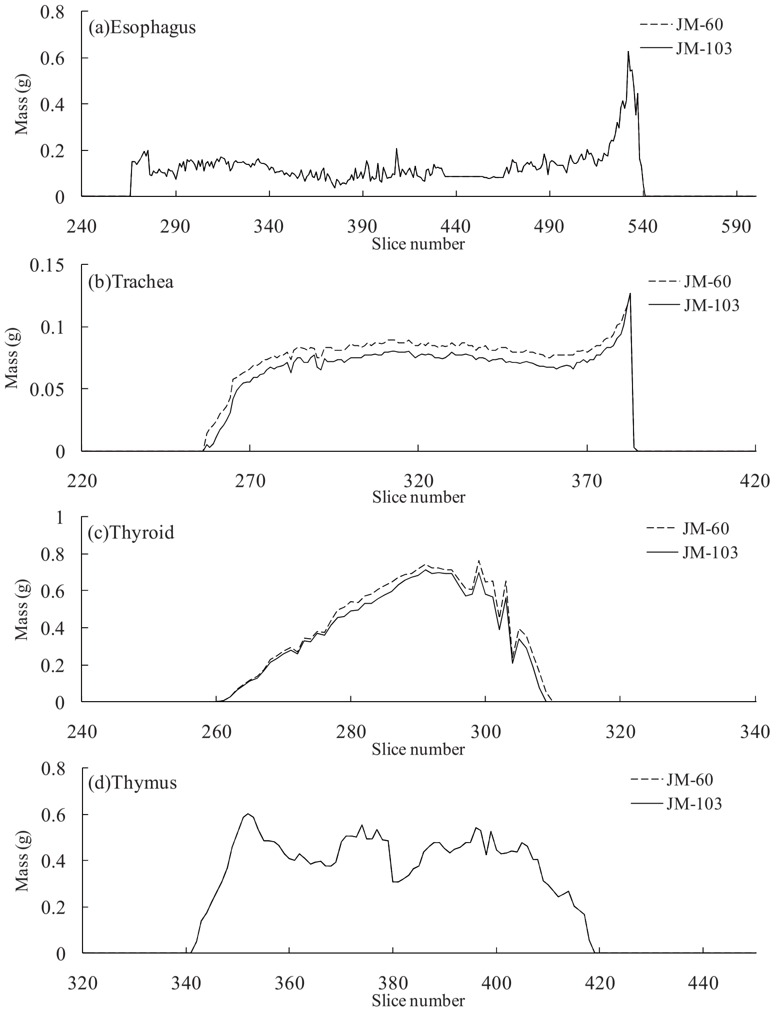

Figure E-3 Mass distribution of some organs and tissues along the head-leg axis of body in the JM-60 and JM-103. (a) Esophagus, (b) Trachea, (c) Thyroid and (d) Thymus.

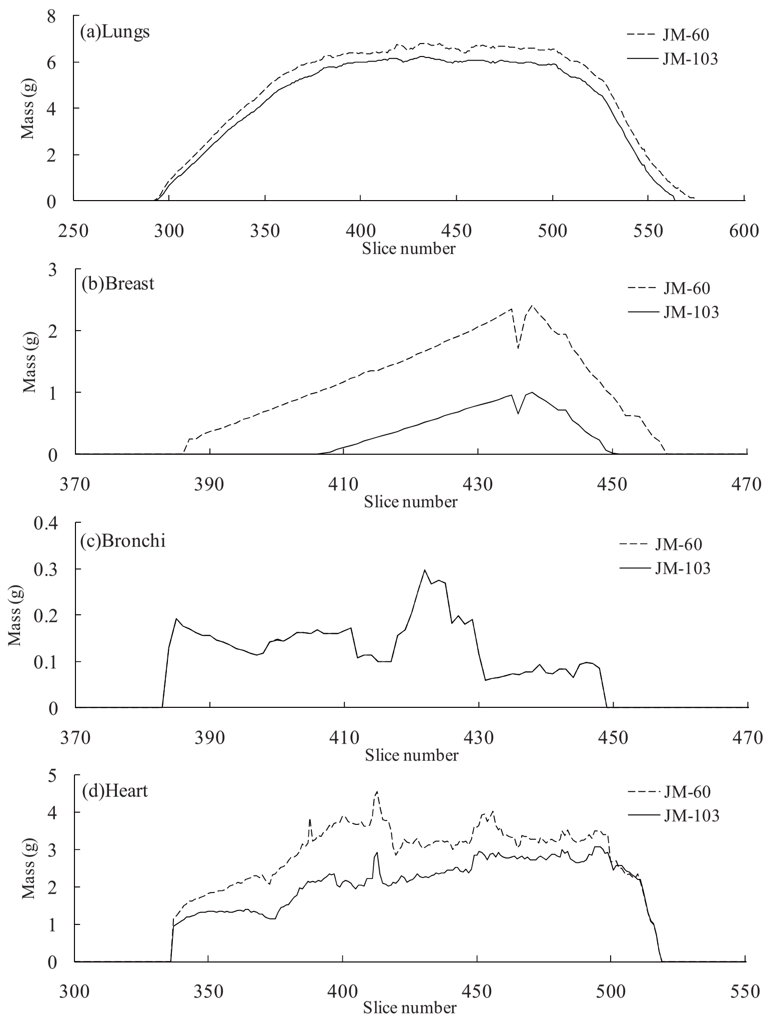

Figure E-4 Mass distribution of some organs and tissues along the head-leg axis of body in the JM-60 and JM-103. (a) Lungs, (b) Breast, (c) Bronchi and (d) Heart.

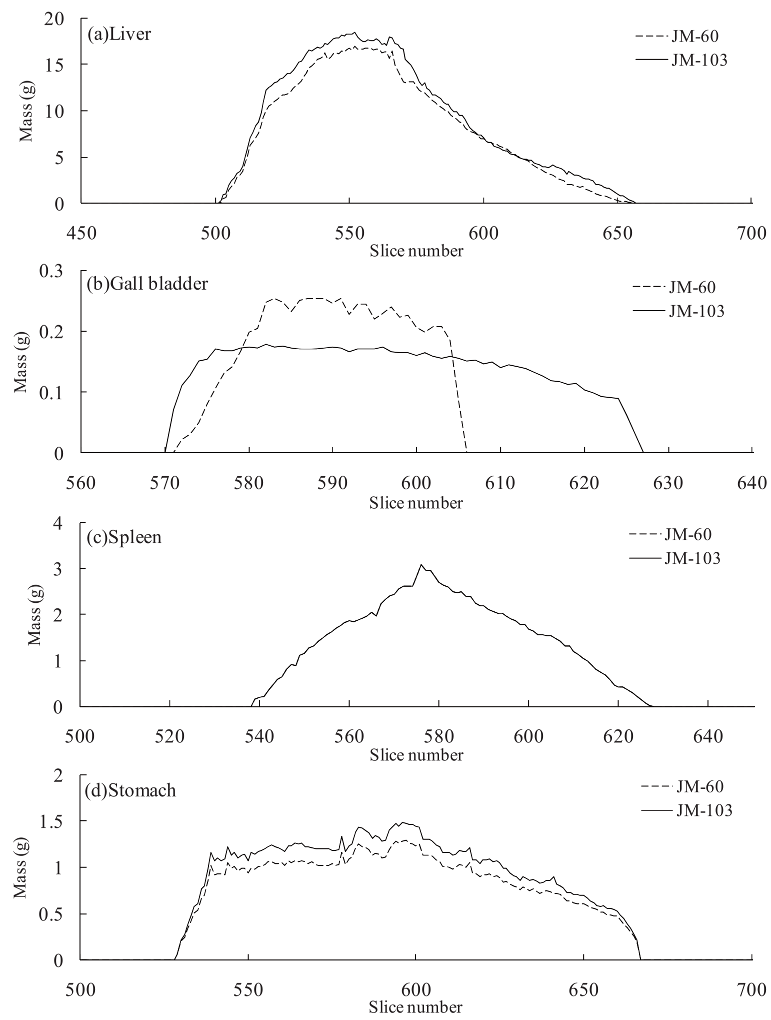

Figure E-5 Mass distribution of some organs and tissues along the head-leg axis of body in the JM-60 and JM-103. (a) Liver, (b) Gall bladder, (c) Spleen and (d) Stomach.

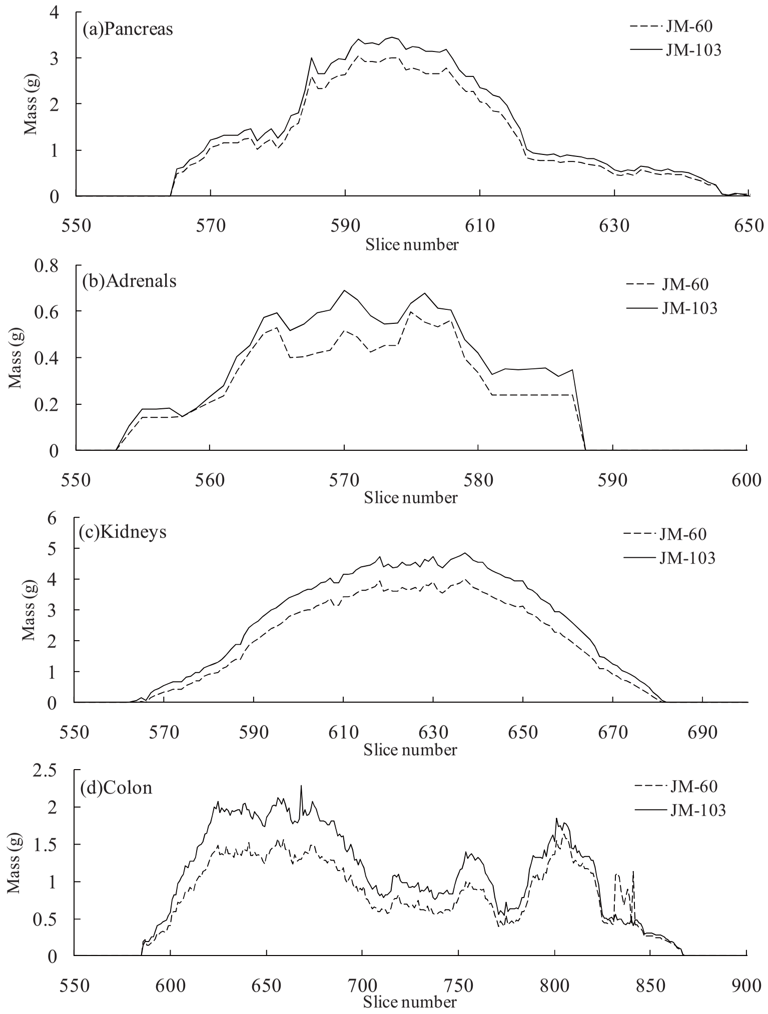

Figure E-6 Mass distribution of some organs and tissues along the head-leg axis of body in the JM-60 and JM-103. (a) Pancreas, (b) Adrenals, (c) Kidneys and (d) Colon.

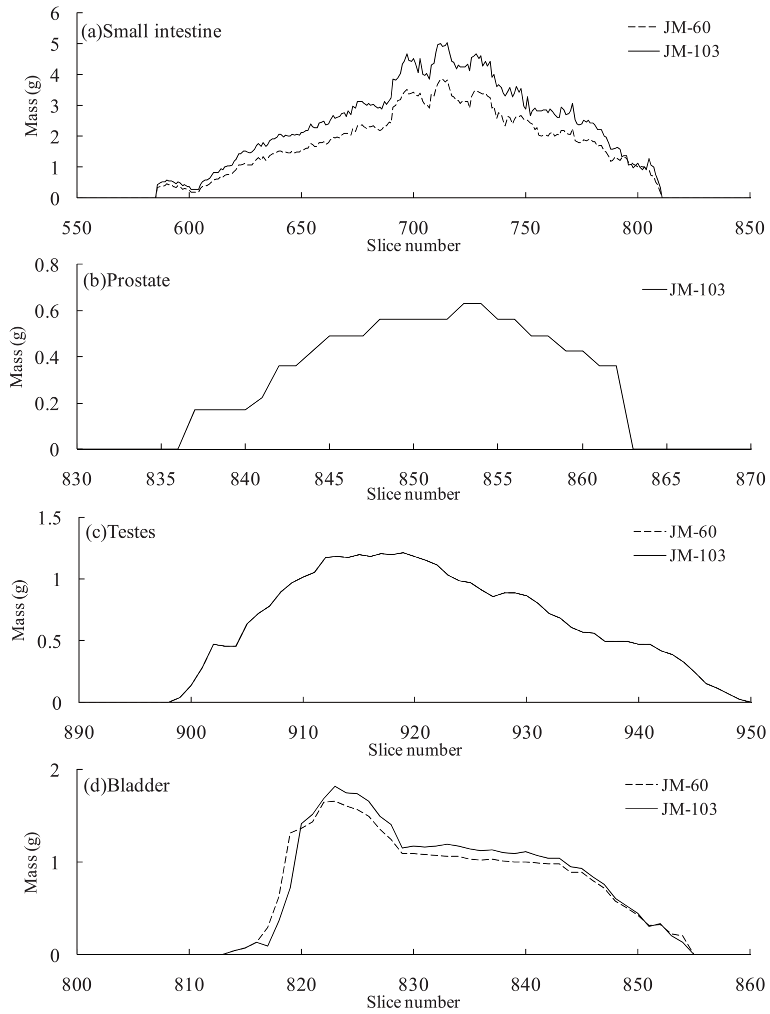

Figure E-7 Mass distribution of some organs and tissues along the head-leg axis of body in the JM-60 and JM-103. (a) Small intestine, (b) Prostate, (c) Testes and (d) Bladder.

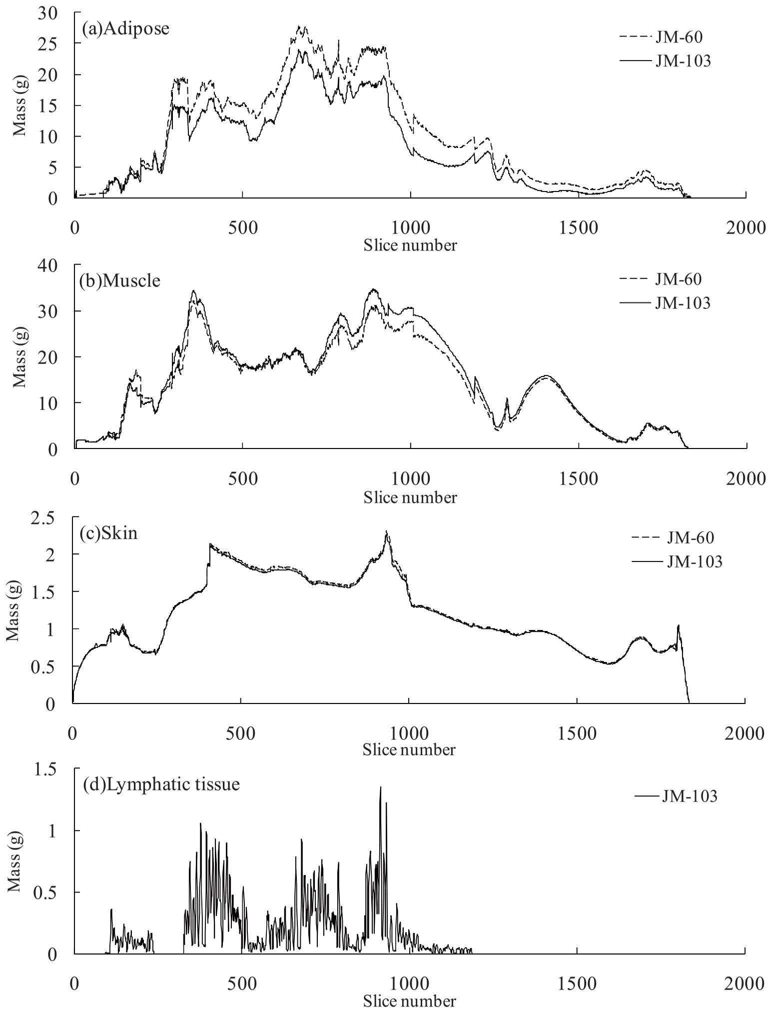

Figure E-8 Mass distribution of some organs and tissues along the head-leg axis of body in the JM-60 and JM-103. (a) Adipose, (b) Muscle, (c) Skin and (d) Lymphatic tissue.

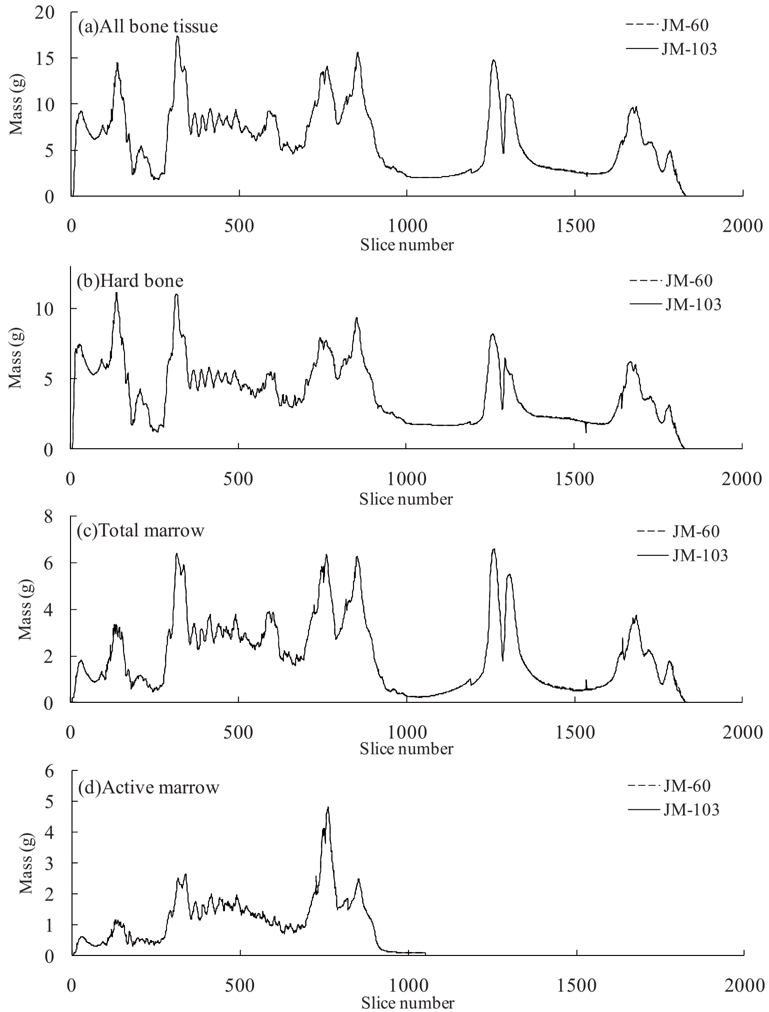

Figure E-9 Mass distribution of some organs and tissues along the head-leg axis of body in the JM-60 and JM-103. (a) All bone tissue, (b) Hard bone, (c) Total marrow and (d) Active marrow.

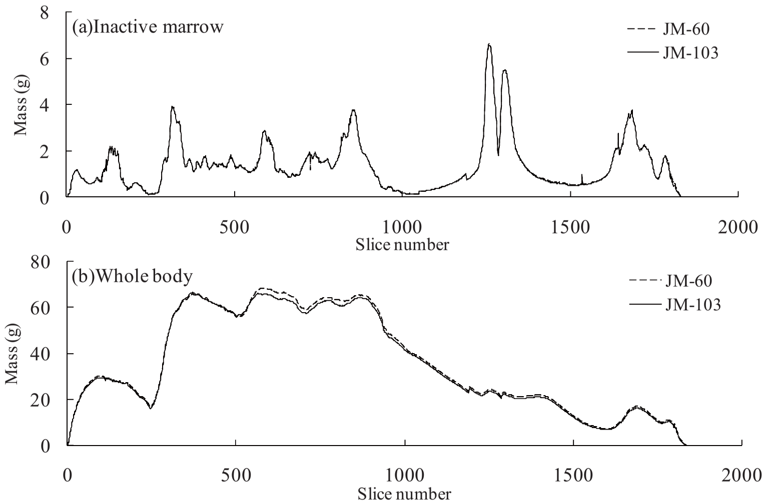

Figure E-10 Mass distribution of some organs and tissues along the head-leg axis of body in the JM-60 and JM-103. (a) Inactive marrow and (b) Whole body.

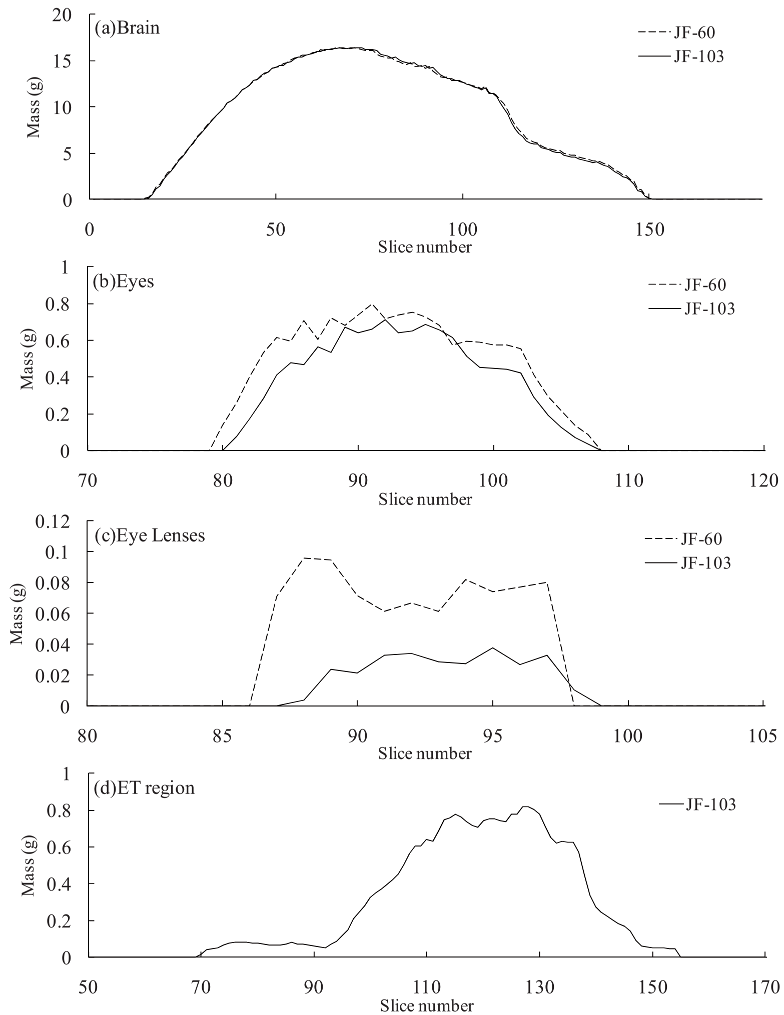

Figure E-11 Mass distribution of some organs and tissues along the head-leg axis of body in the JF-60 and JF-103. (a) Brain, (b) Eyes, (c) Eye lenses and (d) ET region.

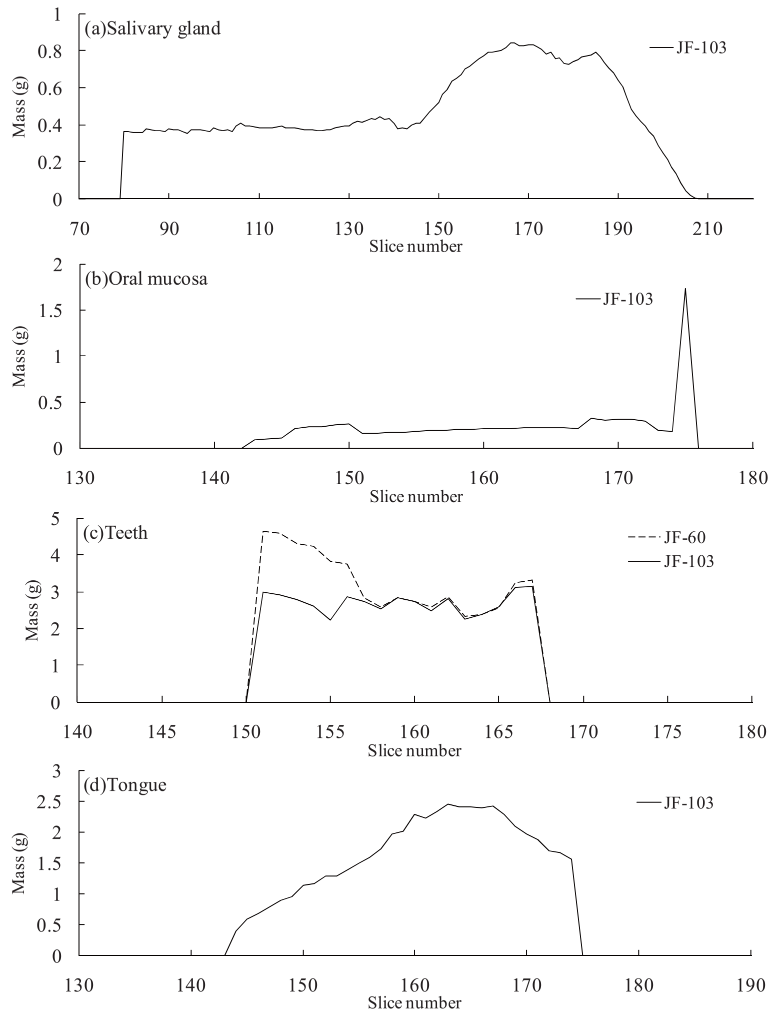

Figure E-12 Mass distribution of some organs and tissues along the head-leg axis of body in the JF-60 and JF-103. (a) Salivary gland, (b) Oral mucosa, (c) Teeth and (d) Tongue.

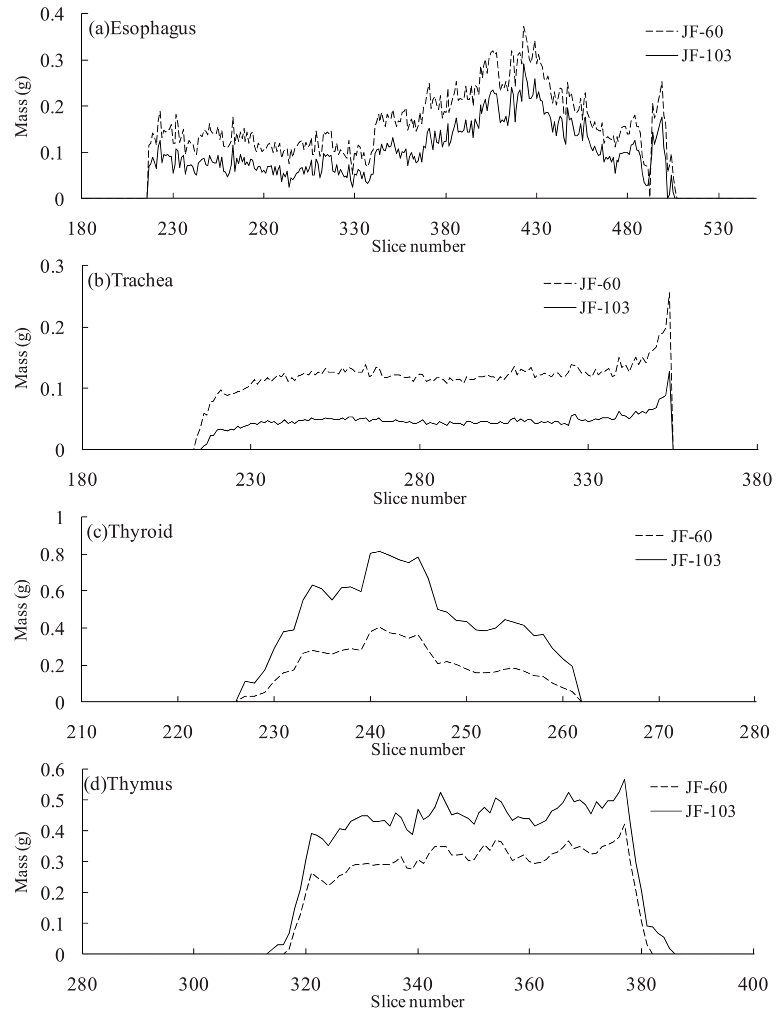

Figure E-13 Mass distribution of some organs and tissues along the head-leg axis of body in the JF-60 and JF-103. (a) Esophagus, (b) Trachea, (c) Thyroid and (d) Thymus.

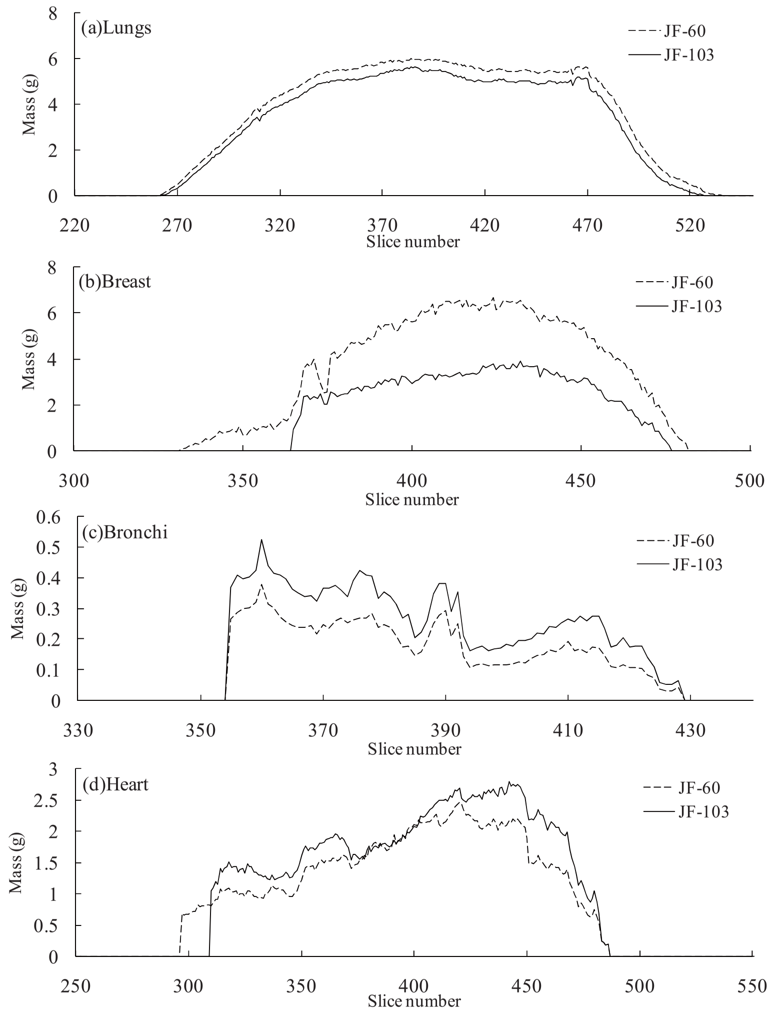

Figure E-14 Mass distribution of some organs and tissues along the head-leg axis of body in the JF-60 and JF-103. (a) Lungs, (b) Breast, (c) Bronchi and (d) Heart.

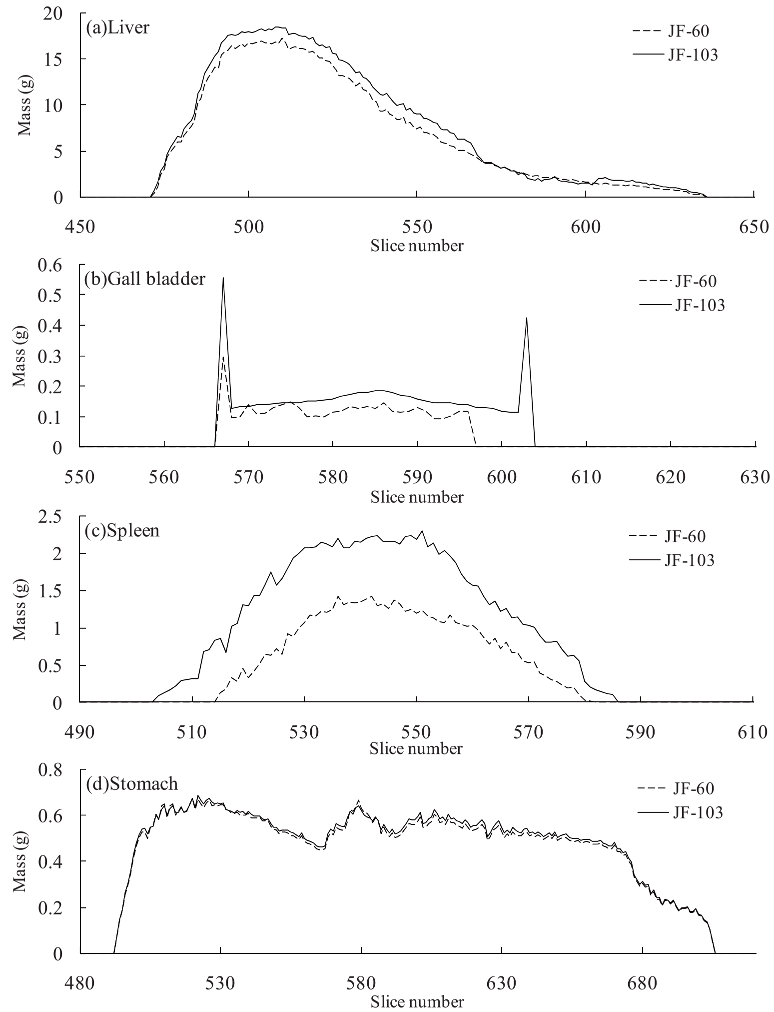

Figure E-15 Mass distribution of some organs and tissues along the head-leg axis of body in the JF-60 and JF-103. (a) Liver, (b) Gall bladder, (c) Spleen and (d) Stomach.

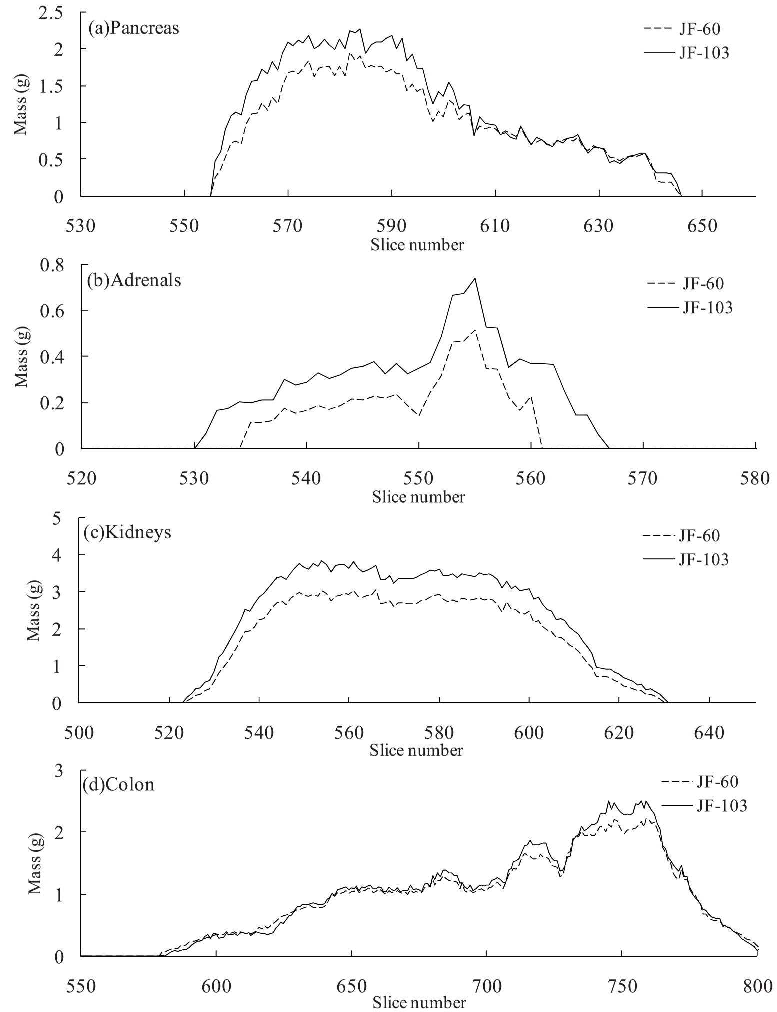

Figure E-16 Mass distribution of some organs and tissues along the head-leg axis of body in the JF-60 and JF-103. (a) Pancreas, (b) Adrenals, (c) Kidneys and (d) Colon.

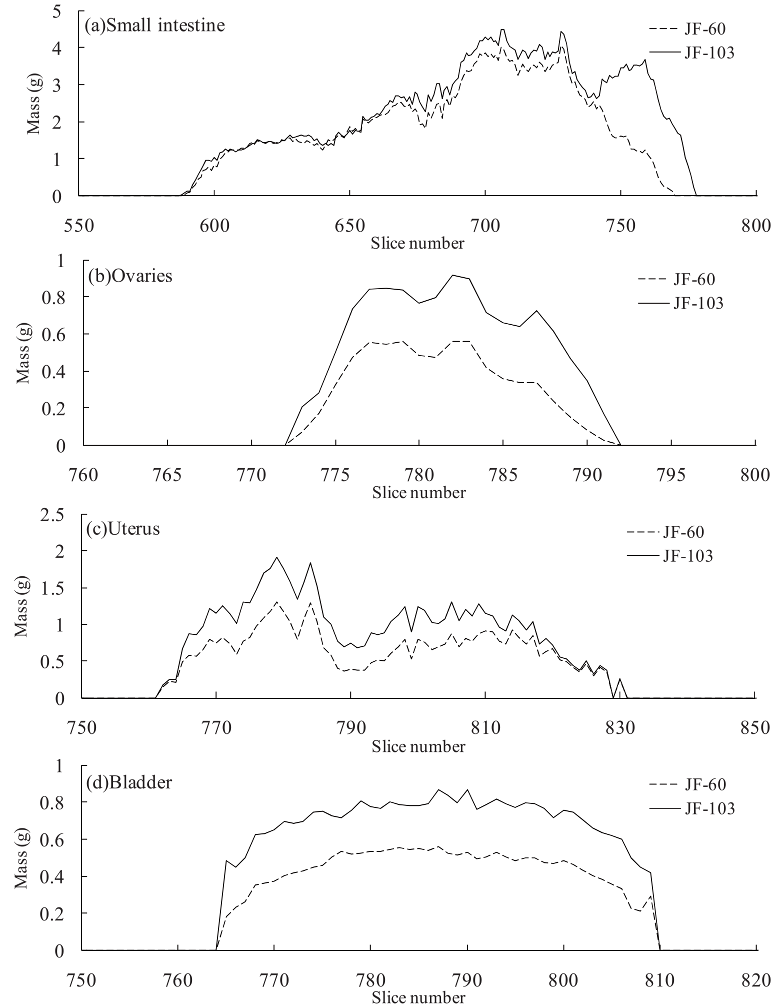

Figure E-17 Mass distribution of some organs and tissues along the head-leg axis of body in the JF-60 and JF-103. (a) Small intestine, (b) Ovaries, (c) Uterus and (d) Bladder.

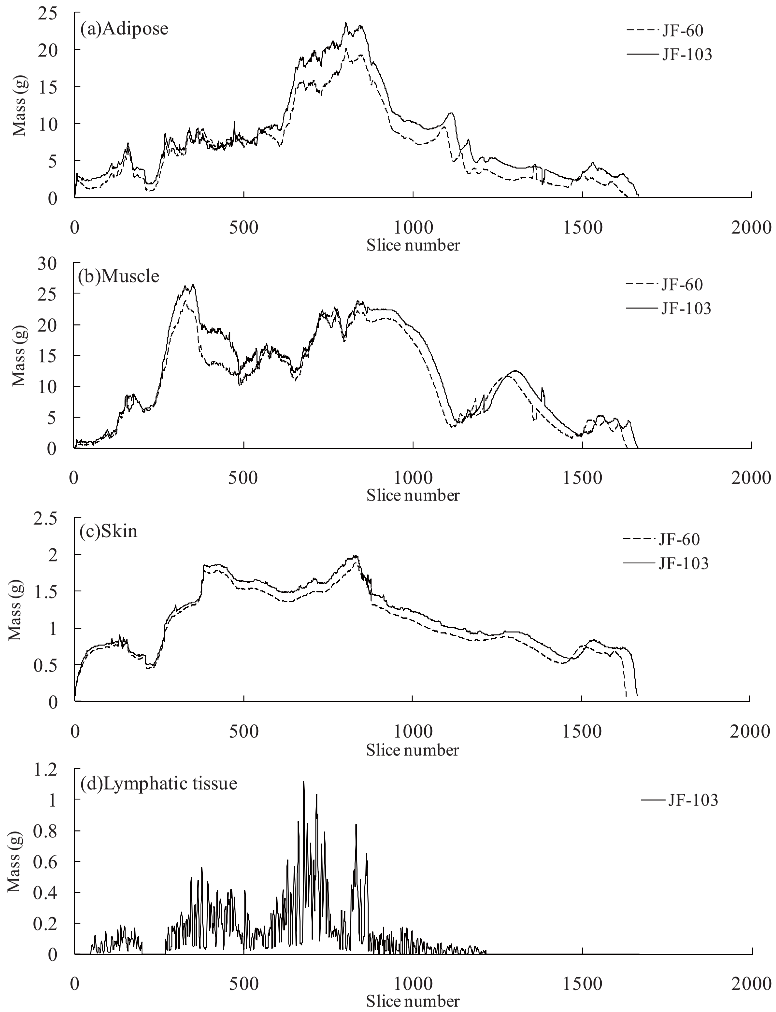

Figure E-18 Mass distribution of some organs and tissues along the head-leg axis of body in the JF-60 and JF-103. (a) Adipose, (b) Muscle, (c) Skin and (d) Lymphatic tissue.

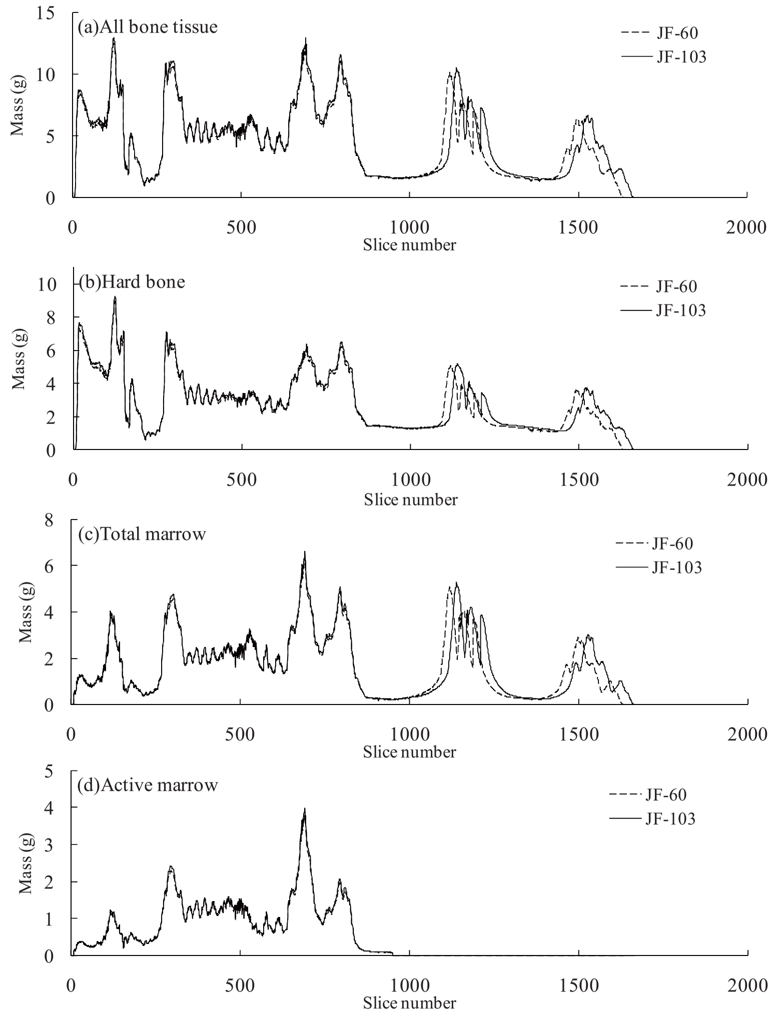

Figure E-19 Mass distribution of some organs and tissues along the head-leg axis of body in the JF-60 and JF-103. (a) All bone tissue, (b) Hard bone, (c) Total marrow and (d) Active marrow.

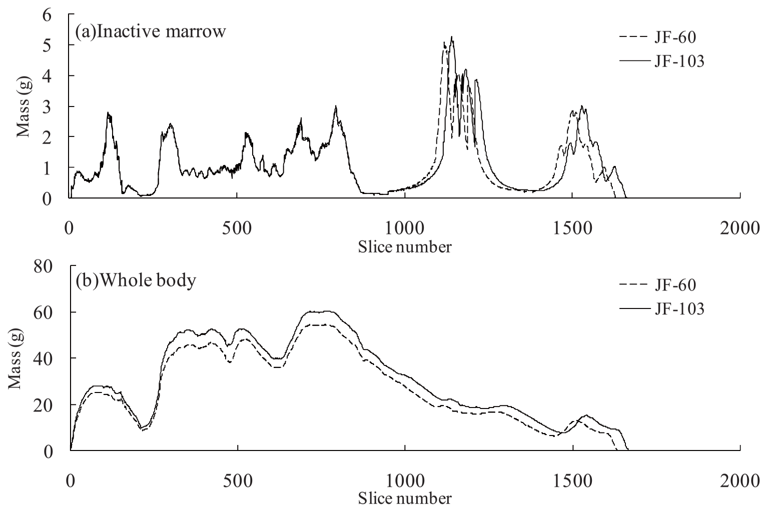

Figure E-20 Mass distribution of some organs and tissues along the head-leg axis of body in the JF-60 and JF-103. (a) Inactive marrow and (b) Whole body.

Appendix F Examples of photon SAFs in the JM-103, JF-103, JM-60 and JF-60 phantoms

This appendix presents examples of photon SAFs for some combinations of selected source regions and target organs in the JM-103 and JF-103 phantoms. The SAFs in JM-103 and JF-103 are given as absorbed fractions per unit mass (kg) of target organs, and are calculated for 6 selected photon energies (0.02, 0.03, 0.05, 0.1, 0.5 and 1 MeV). The SAFs[36)] evaluated using the JM-60 and JF-60 are also shown in the figures for comparison.

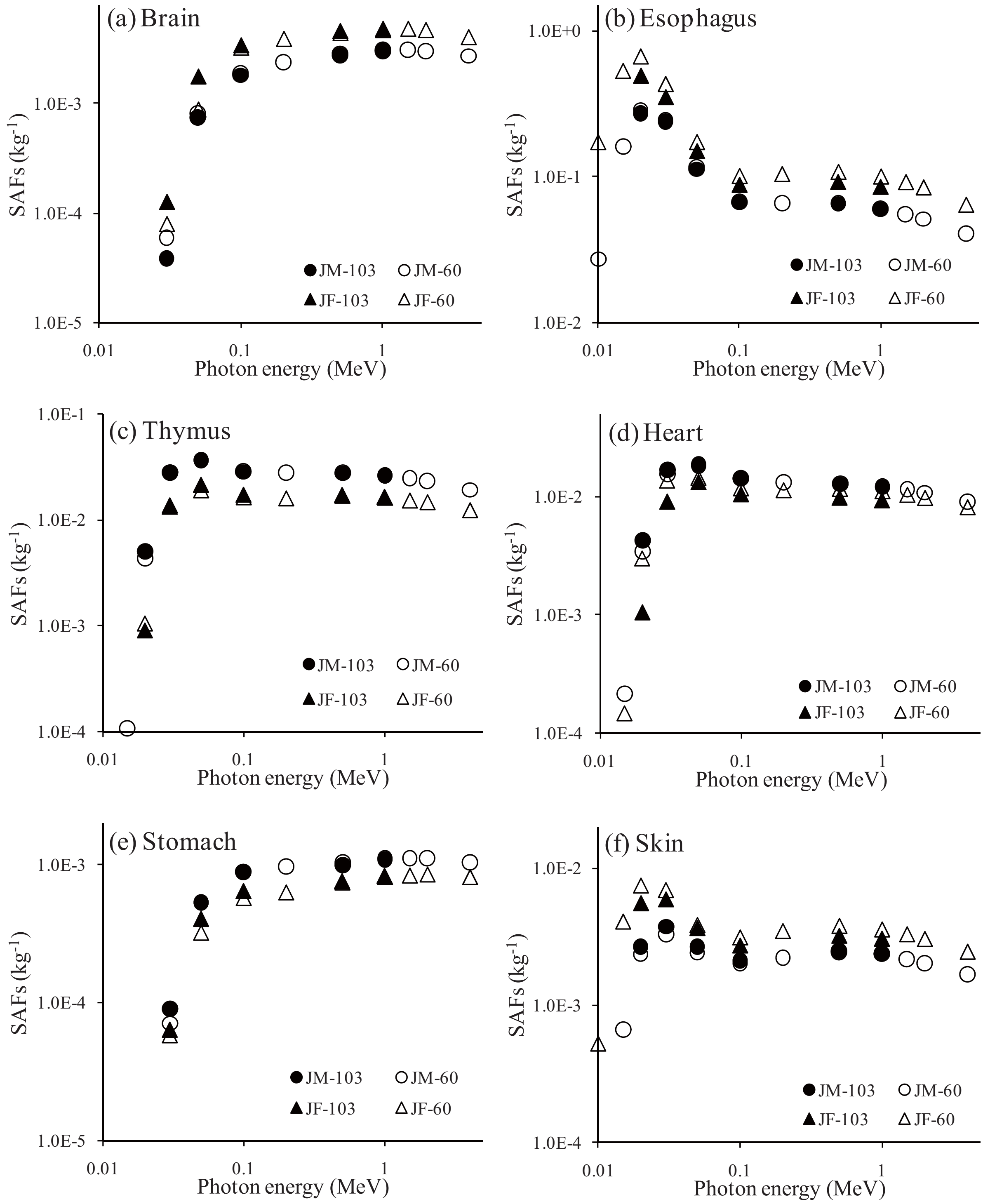

Figure F-1 SAFs for source in thyroid and for target in (a) brain, (b) esophagus, (c) thymus, (d) heart, (e) stomach and (f) skin.

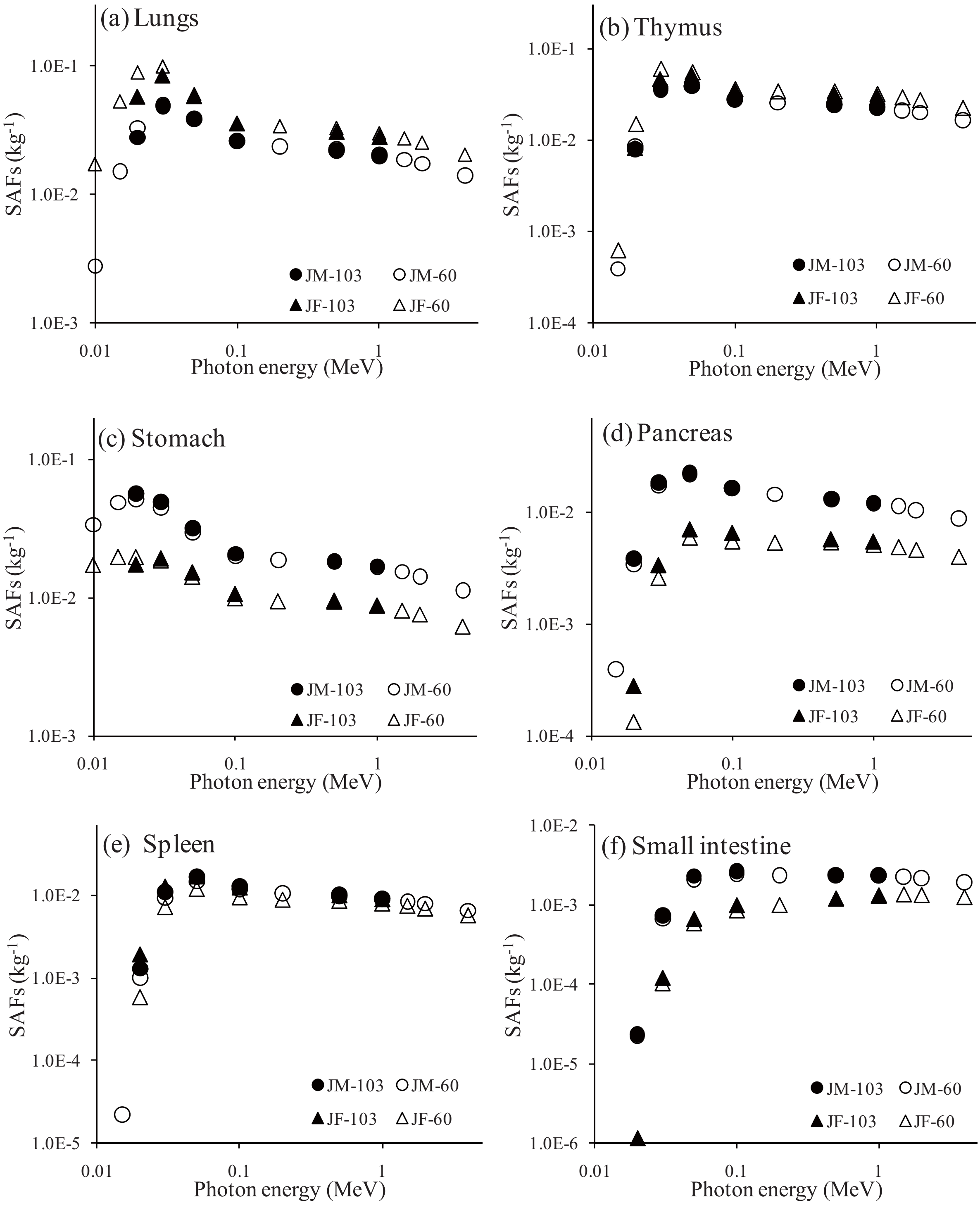

Figure F-2 SAFs for source in esophagus and for target in (a) lungs, (b) thymus, (c) stomach, (d) pancreas, (e) spleen and (f) small intestine.

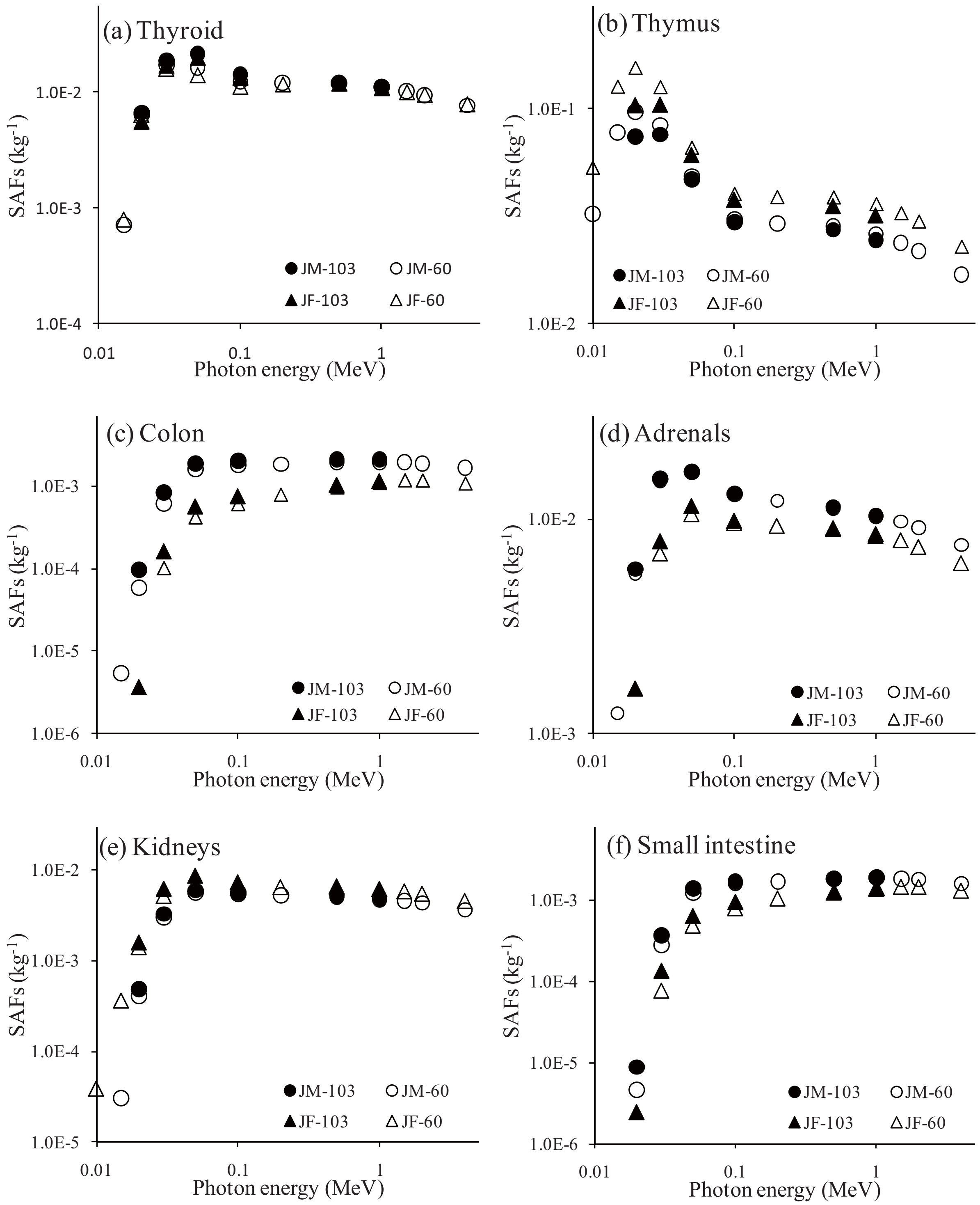

Figure F-3 SAFs for source in lungs and for target in (a) thyroid, (b) thymus, (c) colon, (d) adrenals, (e) kidneys and (f) small intestine.

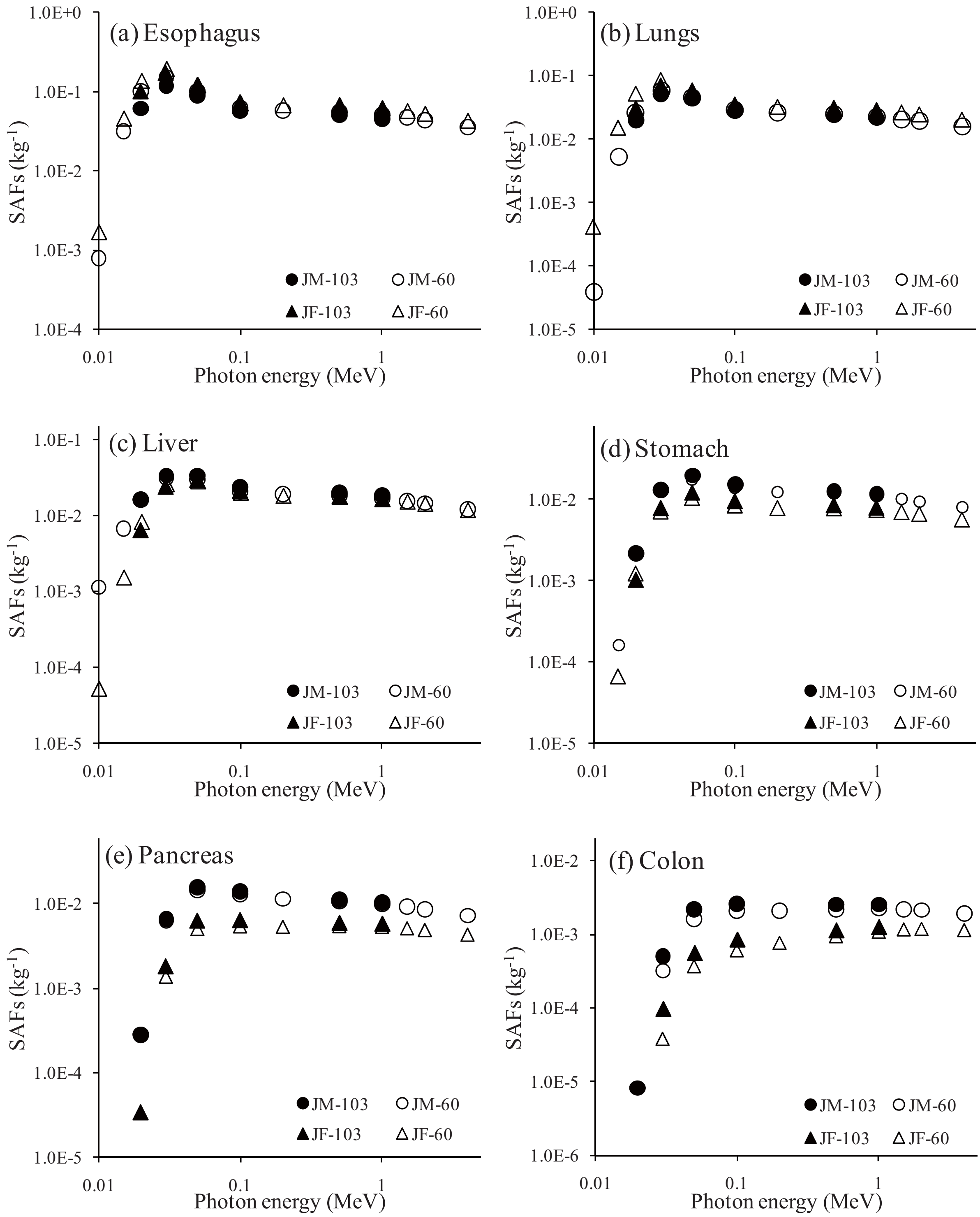

Figure F-4 SAFs for source in heart content and for target in (a) esophagus, (b) lungs, (c) liver, (d) stomach, (e) pancreas and (f) colon.

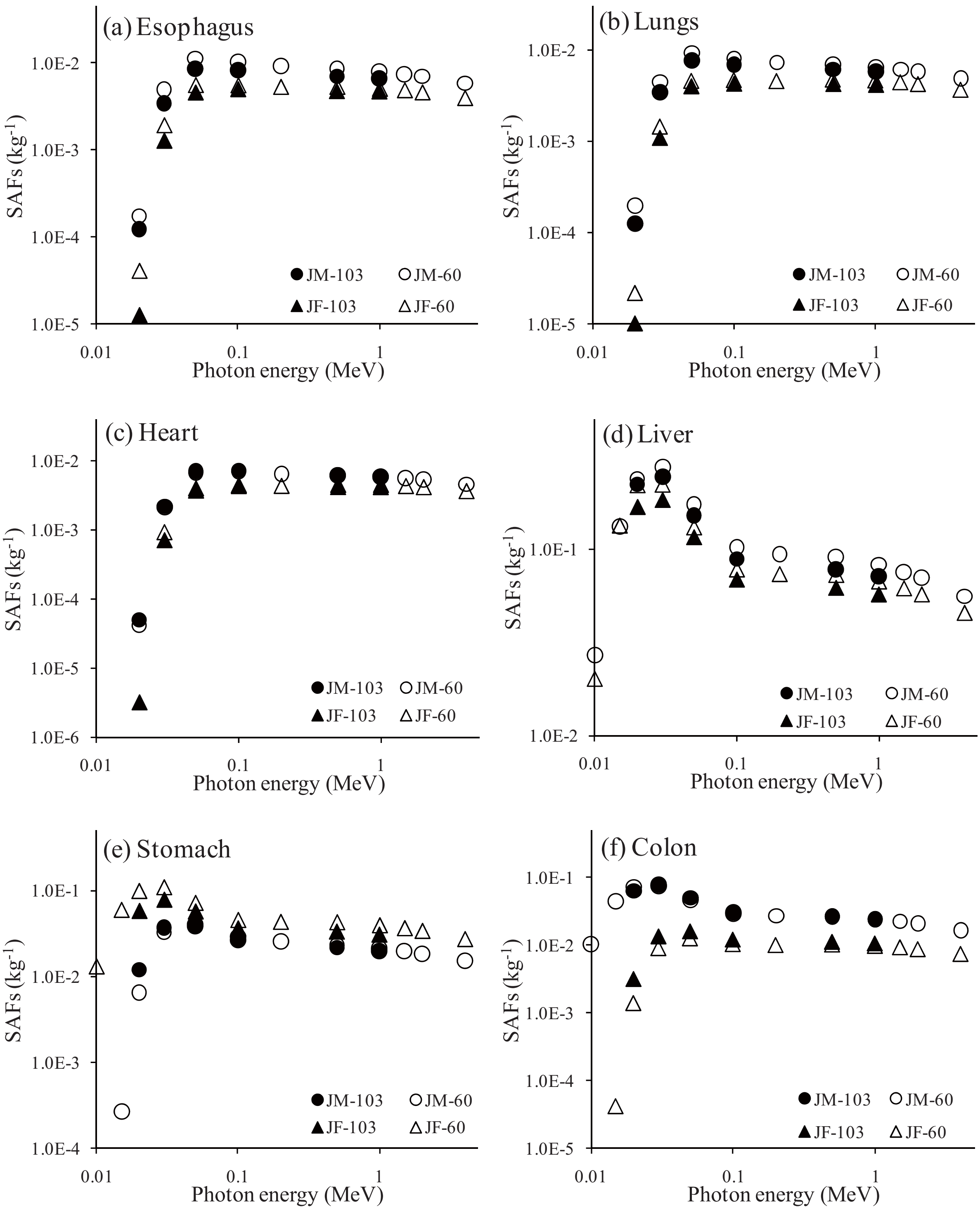

Figure F-5 SAFs for source in gall bladder content and for target in (a) esophagus, (b) lungs, (c) heart, (d) liver, (e) stomach and (f) colon.

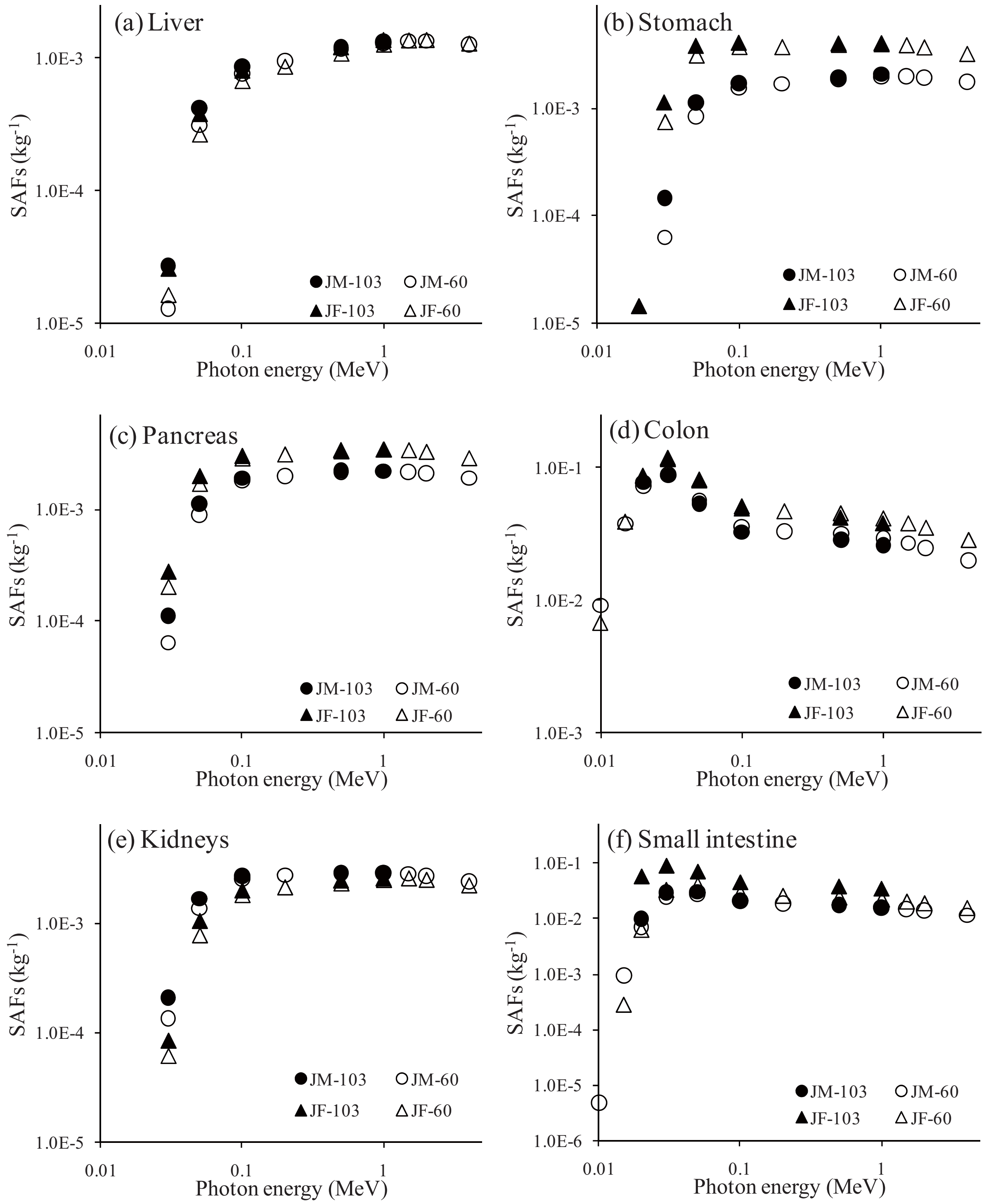

Figure F-6 SAFs for source in bladder content and for target in (a) liver, (b) stomach, (c) pancreas, (d) colon, (e) kidneys and (f) small intestine.

Appendix G Examples of organ doses against external photon exposures in the JM-103, JM-60, JF-103 and JF-60 phantoms

In this appendix, examples of dose conversion coefficients against external photon exposures in the JM-103 and JF-103 phantoms are shown in the figures. The dose conversion coefficients are given as absorbed dose per unit air-kerma free-in-air, and are calculated for 8 incident photon energies (0.03, 0.06, 0.08, 0.1, 0.15, 0.5, 1.0 and 5.0 MeV) for six irradiation geometries (AP, PA, LLAT, RLAT, ROT and ISO). The dose conversion coefficients[34)] by the JM-60 and JF-60 phantoms are also presented in the figures for comparison.

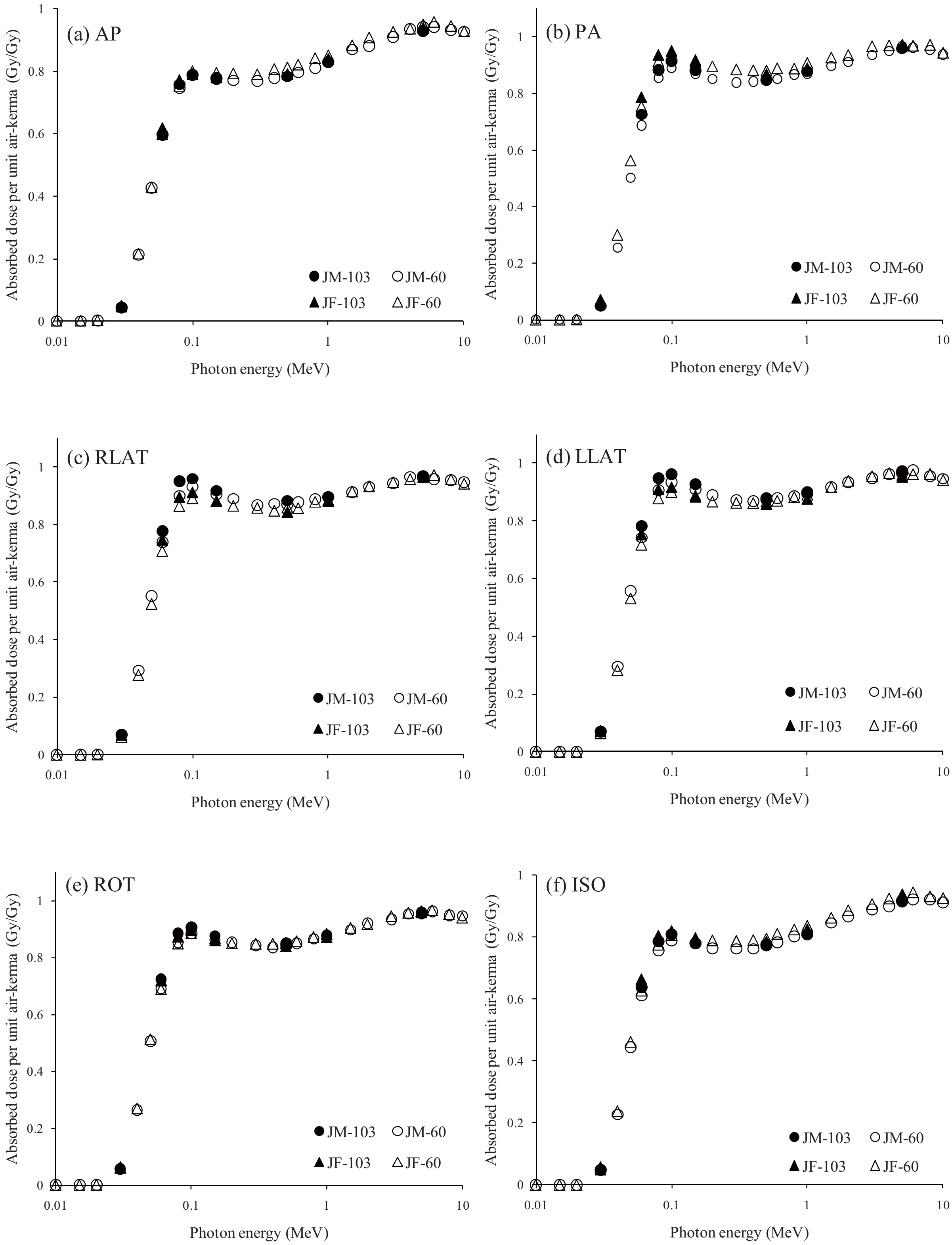

Figure G-1 Brain absorbed doses per unit air-kerma for six kinds of idealized irradiation geometries. (a) AP, (b) PA, (c) RLAT, (d) LLAT, (e) ROT and (f) ISO.

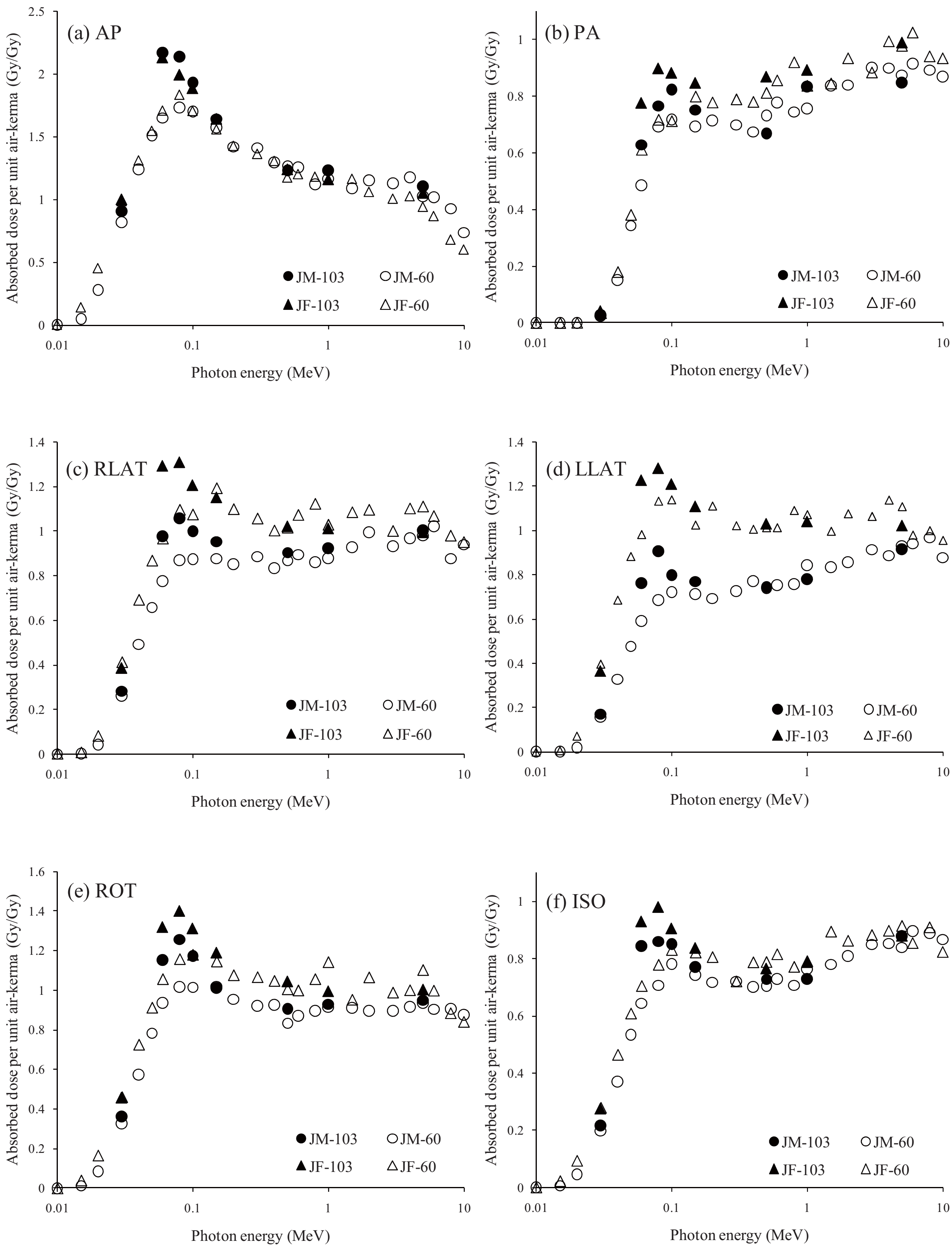

Figure G-2 Thyroid absorbed doses per unit air-kerma for six kinds of idealized irradiation geometries. (a) AP, (b) PA, (c) RLAT, (d) LLAT, (e) ROT and (f) ISO.

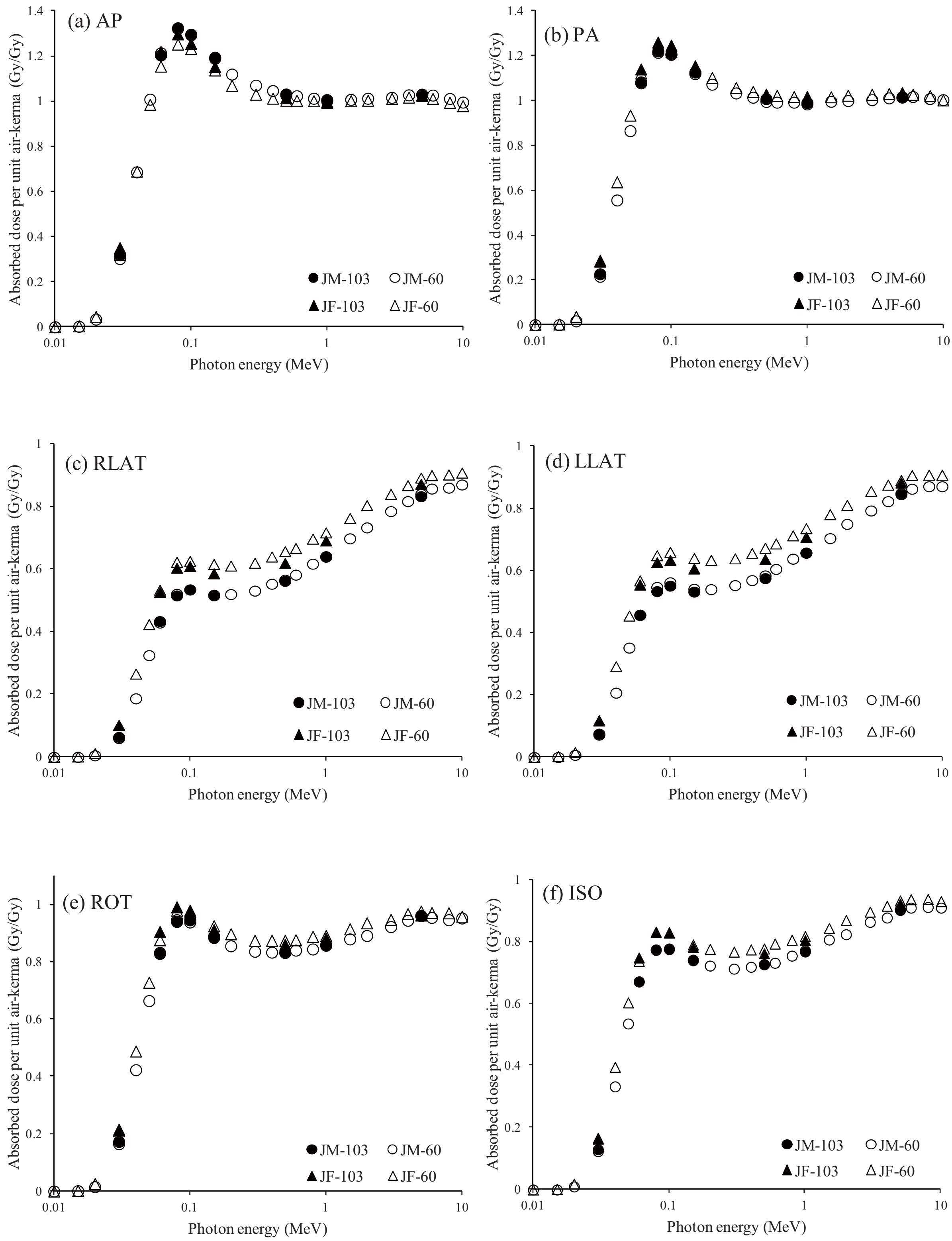

Figure G-3 Lung absorbed doses per unit air-kerma for six kinds of idealized irradiation geometries. (a) AP, (b) PA, (c) RLAT, (d) LLAT, (e) ROT and (f) ISO.

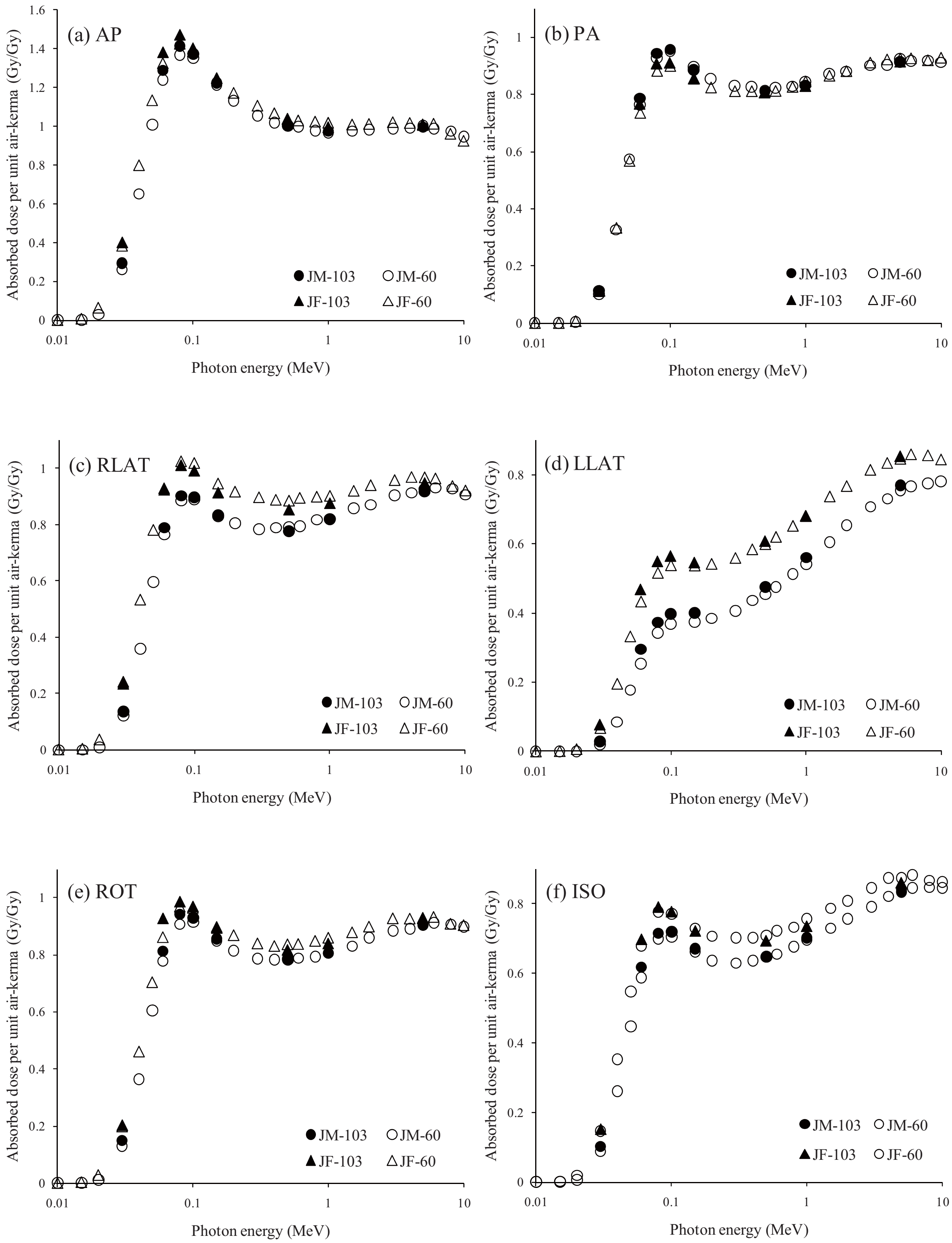

Figure G-4 Liver absorbed doses per unit air-kerma for six kinds of idealized irradiation geometries. (a) AP, (b) PA, (c) RLAT, (d) LLAT, (e) ROT and (f) ISO.

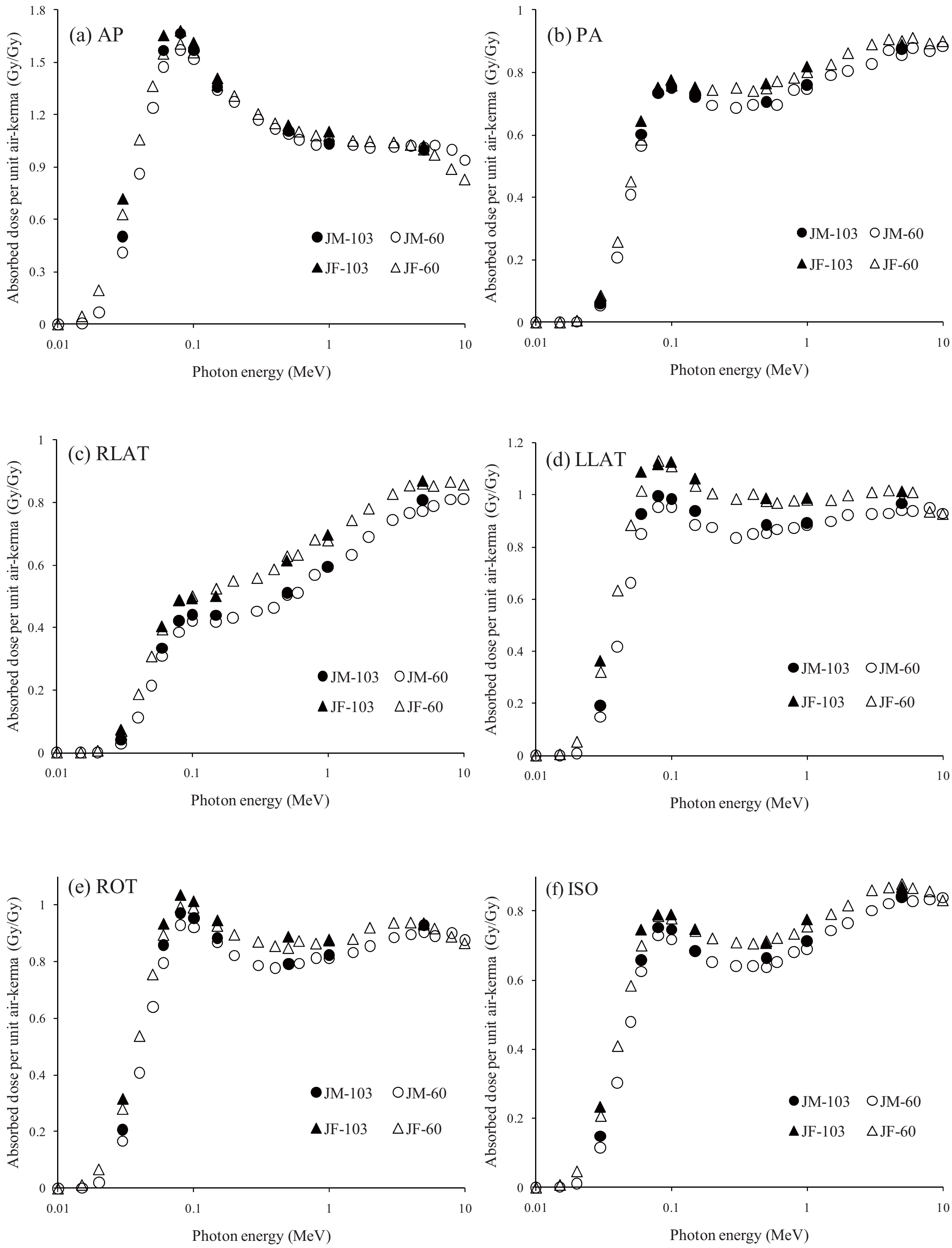

Figure G-5 Stomach absorbed doses per unit air-kerma for six kinds of idealized irradiation geometries. (a) AP, (b) PA, (c) RLAT, (d) LLAT, (e) ROT and (f) ISO.

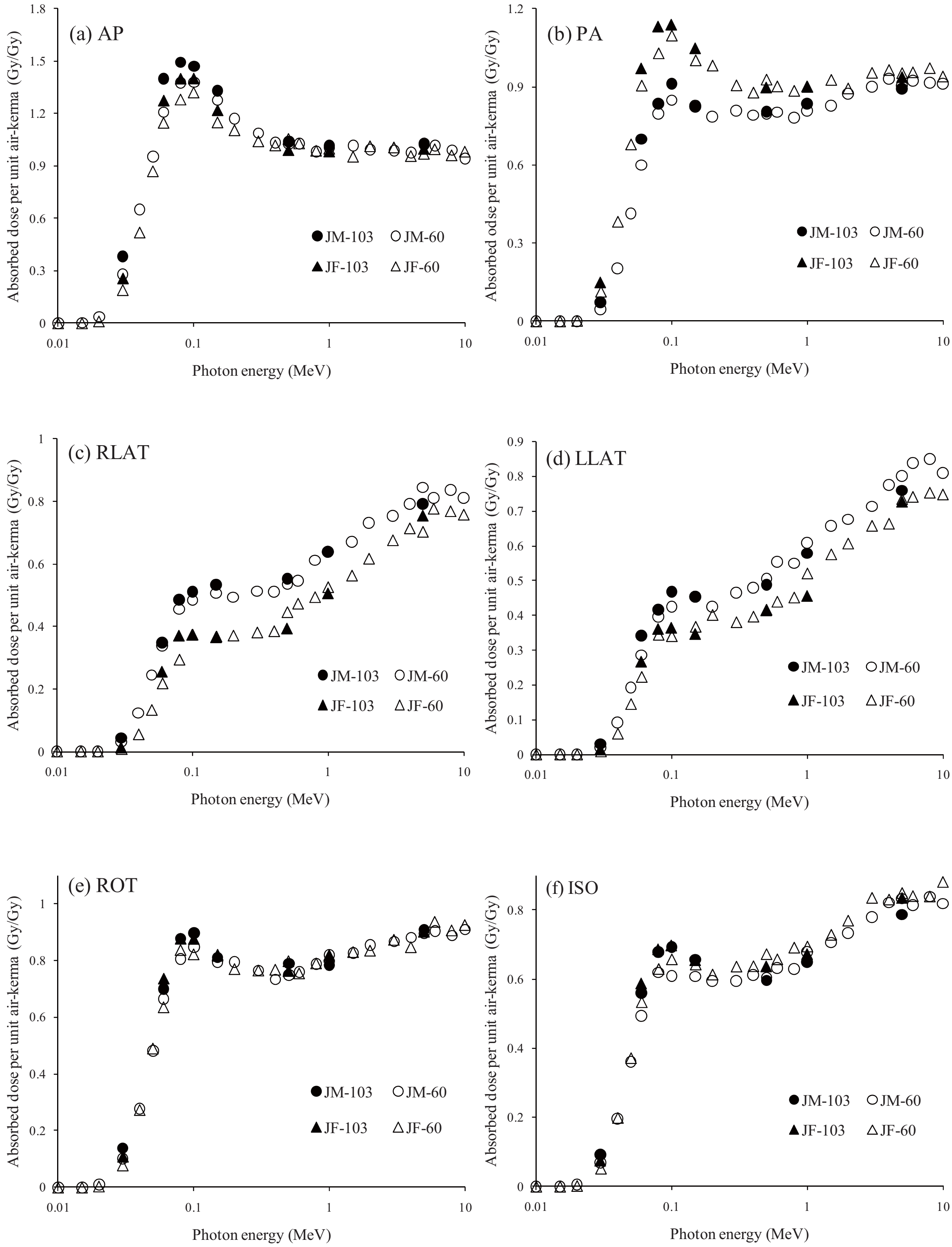

Figure G-6 Bladder absorbed doses per unit air-kerma for six kinds of idealized irradiation geometries. (a) AP, (b) PA, (c) RLAT, (d) LLAT, (e) ROT and (f) ISO.

国際単位系（SI）

表１．SI 基本単位

基本量	SI 基本単位 名称	記号
長さ	メートル	m
質量	キログラム	kg
時間	秒	s
電流	アンペア	A
熱力学温度	ケルビン	K
物質量	モル	mol
光度	カンデラ	cd

表２．基本単位を用いて表されるSI組立単位の例

組立量	SI 基本単位 名称	記号
面積	平方メートル	m^2
体積	立法メートル	m^3
速さ，速度	メートル毎秒	m/s
加速度	メートル毎秒毎秒	m/s^2
波数	毎メートル	m^{-1}
密度，質量密度	キログラム毎立方メートル	kg/m^3
面積密度	キログラム毎平方メートル	kg/m^2
比体積	立方メートル毎キログラム	m^3/kg
電流密度	アンペア毎平方メートル	A/m^2
磁界の強さ	アンペア毎メートル	A/m
量濃度 (a)，濃度	モル毎立方メートル	mol/m^3
質量濃度	キログラム毎立法メートル	kg/m^3
輝度	カンデラ毎平方メートル	cd/m^2
屈折率 (b)	（数字の） 1	1
比透磁率 (b)	（数字の） 1	1

(a) 量濃度（amount concentration）は臨床化学の分野では物質濃度（substance concentration）ともよばれる。
(b) これらは無次元量あるいは次元１をもつ量であるが、そのことを表す単位記号である数字の１は通常は表記しない。

表３．固有の名称と記号で表されるSI組立単位

組立量	SI 組立単位 名称	記号	他のSI単位による表し方	SI基本単位による表し方
平面角	ラジアン(b)	rad	1 (b)	m/m
立体角	ステラジアン(b)	sr(c)	1 (b)	m^2/m^2
周波数	ヘルツ (d)	Hz		s^{-1}
力	ニュートン	N		$m\ kg\ s^{-2}$
圧力，応力	パスカル	Pa	N/m^2	$m^{-1}\ kg\ s^{-2}$
エネルギー，仕事，熱量	ジュール	J	N m	$m^2\ kg\ s^{-2}$
仕事率，工率，放射束	ワット	W	J/s	$m^2\ kg\ s^{-3}$
電荷，電気量	クーロン	C		s A
電位差（電圧），起電力	ボルト	V	W/A	$m^2\ kg\ s^{-3}\ A^{-1}$
静電容量	ファラド	F	C/V	$m^{-2}\ kg^{-1}\ s^4\ A^2$
電気抵抗	オーム	Ω	V/A	$m^2\ kg\ s^{-3}\ A^{-2}$
コンダクタンス	ジーメンス	S	A/V	$m^{-2}\ kg^{-1}\ s^3\ A^2$
磁束	ウエーバ	Wb	Vs	$m^2\ kg\ s^{-2}\ A^{-1}$
磁束密度	テスラ	T	Wb/m^2	$kg\ s^{-2}\ A^{-1}$
インダクタンス	ヘンリー	H	Wb/A	$m^2\ kg\ s^{-2}\ A^{-2}$
セルシウス温度	セルシウス度(e)	℃		K
光束	ルーメン	lm	cd sr(c)	cd
照度	ルクス	lx	lm/m^2	$m^{-2}\ cd$
放射性核種の放射能 (f)	ベクレル (d)	Bq		s^{-1}
吸収線量, 比エネルギー分与, カーマ	グレイ	Gy	J/kg	$m^2\ s^{-2}$
線量当量, 周辺線量当量, 方向性線量当量, 個人線量当量	シーベルト (g)	Sv	J/kg	$m^2\ s^{-2}$
酸素活性	カタール	kat		$s^{-1}\ mol$

(a)SI接頭語は固有の名称と記号を持つ組立単位と組み合わせても使用できる。しかし接頭語を付した単位はもはやコヒーレントではない。
(b)ラジアンとステラジアンは数字の１に対する単位の特別な名称で、量についての情報をつたえるために使われる。実際には、使用する時には記号rad及びsrが用いられるが、習慣として組立単位としての記号である数字の１は明示されない。
(c)測光学ではステラジアンという名称と記号srを単位の表し方の中に、そのまま維持している。
(d)ヘルツは周期現象についてのみ、ベクレルは放射性核種の統計的過程についてのみ使用される。
(e)セルシウス度はケルビンの特別な名称で、セルシウス温度を表すために使用される。セルシウス度とケルビンの単位の大きさは同一である。したがって、温度差や温度間隔を表す数値はどちらの単位で表しても同じである。
(f)放射性核種の放射能（activity referred to a radionuclide）は、しばしば誤った用語で"radioactivity"と記される。
(g)単位シーベルト（PV,2002,70,205）についてはCIPM勧告2（CI-2002）を参照。

表４．単位の中に固有の名称と記号を含むSI組立単位の例

組立量	SI 組立単位 名称	記号	SI 基本単位による表し方
粘度	パスカル秒	Pa s	$m^{-1}\ kg\ s^{-1}$
力のモーメント	ニュートンメートル	N m	$m^2\ kg\ s^{-2}$
表面張力	ニュートン毎メートル	N/m	$kg\ s^{-2}$
角速度	ラジアン毎秒	rad/s	$m\ m^{-1}\ s^{-1}=s^{-1}$
角加速度	ラジアン毎秒毎秒	rad/s^2	$m\ m^{-1}\ s^{-2}=s^{-2}$
熱流密度，放射照度	ワット毎平方メートル	W/m^2	$kg\ s^{-3}$
熱容量，エントロピー	ジュール毎ケルビン	J/K	$m^2\ kg\ s^{-2}\ K^{-1}$
比熱容量，比エントロピー	ジュール毎キログラム毎ケルビン	J/(kg K)	$m^2\ s^{-2}\ K^{-1}$
比エネルギー	ジュール毎キログラム	J/kg	$m^2\ s^{-2}$
熱伝導率	ワット毎メートル毎ケルビン	W/(m K)	$m\ kg\ s^{-3}\ K^{-1}$
体積エネルギー	ジュール毎立方メートル	J/m^3	$m^{-1}\ kg\ s^{-2}$
電界の強さ	ボルト毎メートル	V/m	$m\ kg\ s^{-3}\ A^{-1}$
電荷密度	クーロン毎立方メートル	C/m^3	$m^{-3}\ sA$
表面電荷	クーロン毎平方メートル	C/m^2	$m^{-2}\ sA$
電束密度，電気変位	クーロン毎平方メートル	C/m^2	$m^{-2}\ sA$
誘電率	ファラド毎メートル	F/m	$m^{-3}\ kg^{-1}\ s^4\ A^2$
透磁率	ヘンリー毎メートル	H/m	$m\ kg\ s^{-2}\ A^{-2}$
モルエネルギー	ジュール毎モル	J/mol	$m^2\ kg\ s^{-2}\ mol^{-1}$
モルエントロピー, モル熱容量	ジュール毎モル毎ケルビン	J/(mol K)	$m^2\ kg\ s^{-2}\ K^{-1}\ mol^{-1}$
照射線量（Ｘ線及びγ線）	クーロン毎キログラム	C/kg	$kg^{-1}\ sA$
吸収線量率	グレイ毎秒	Gy/s	$m^2\ s^{-3}$
放射強度	ワット毎ステラジアン	W/sr	$m^4\ m^{-2}\ kg\ s^{-3}=m^2\ kg\ s^{-3}$
放射輝度	ワット毎平方メートル毎ステラジアン	$W/(m^2\ sr)$	$m^2\ m^{-2}\ kg\ s^{-3}=kg\ s^{-3}$
酵素活性濃度	カタール毎立方メートル	kat/m^3	$m^{-3}\ s^{-1}\ mol$

表５．SI 接頭語

乗数	接頭語	記号	乗数	接頭語	記号
10^{24}	ヨタ	Y	10^{-1}	デシ	d
10^{21}	ゼタ	Z	10^{-2}	センチ	c
10^{18}	エクサ	E	10^{-3}	ミリ	m
10^{15}	ペタ	P	10^{-6}	マイクロ	µ
10^{12}	テラ	T	10^{-9}	ナノ	n
10^{9}	ギガ	G	10^{-12}	ピコ	p
10^{6}	メガ	M	10^{-15}	フェムト	f
10^{3}	キロ	k	10^{-18}	アト	a
10^{2}	ヘクト	h	10^{-21}	ゼプト	z
10^{1}	デカ	da	10^{-24}	ヨクト	y

表６．SIに属さないが、SIと併用される単位

名称	記号	SI 単位による値
分	min	1 min=60s
時	h	1h =60 min=3600 s
日	d	1 d=24 h=86 400 s
度	°	1°=(π/180) rad
分	’	1’=(1/60)°=(π/10800) rad
秒	”	1”=(1/60)’=(π/648000) rad
ヘクタール	ha	$1ha=1hm^2=10^4m^2$
リットル	L，l	$1L=1l=1dm^3=10^3cm^3=10^{-3}m^3$
トン	t	$1t=10^3$ kg

表７．SIに属さないが、SIと併用される単位で、SI単位で表される数値が実験的に得られるもの

名称	記号	SI 単位で表される数値
電子ボルト	eV	$1eV=1.602\ 176\ 53(14)\times10^{-19}J$
ダルトン	Da	$1Da=1.660\ 538\ 86(28)\times10^{-27}kg$
統一原子質量単位	u	1u=1 Da
天文単位	ua	$1ua=1.495\ 978\ 706\ 91(6)\times10^{11}m$

表８．SIに属さないが、SIと併用されるその他の単位

名称	記号	SI 単位で表される数値
バール	bar	$1\ bar=0.1MPa=100kPa=10^5Pa$
水銀柱ミリメートル	mmHg	1mmHg=133.322Pa
オングストローム	Å	$1\ Å=0.1nm=100pm=10^{-10}m$
海里	M	1 M=1852m
バーン	b	$1\ b=100fm^2=(10^{-12}cm)2=10^{-28}m^2$
ノット	kn	1 kn=(1852/3600)m/s
ネーパ	Np	SI単位との数値的な関係は、対数量の定義に依存。
ベル	B	
デジベル	dB	

表９．固有の名称をもつCGS組立単位

名称	記号	SI 単位で表される数値
エルグ	erg	$1\ erg=10^{-7}$ J
ダイン	dyn	$1\ dyn=10^{-5}N$
ポアズ	P	$1\ P=1\ dyn\ s\ cm^{-2}=0.1Pa\ s$
ストークス	St	$1\ St=1cm^2\ s^{-1}=10^{-4}m^2\ s^{-1}$
スチルブ	sb	$1\ sb=1cd\ cm^{-2}=10^4cd\ m^{-2}$
フォト	ph	$1\ ph=1cd\ sr\ cm^{-2}\ 10^4lx$
ガル	Gal	$1\ Gal=1cm\ s^{-2}=10^{-2}ms^{-2}$
マクスウェル	Mx	$1\ Mx=1G\ cm^2=10^{-8}Wb$
ガウス	G	$1\ G=1Mx\ cm^{-2}=10^{-4}T$
エルステッド (c)	Oe	$1\ Oe \triangleq (10^3/4\pi)A\ m^{-1}$

(c) ３元系のCGS単位系とSIでは直接比較できないため、等号「 ≙ 」は対応関係を示すものである。

表10．SIに属さないその他の単位の例

名称	記号	SI 単位で表される数値
キュリー	Ci	$1\ Ci=3.7\times10^{10}Bq$
レントゲン	R	$1\ R=2.58\times10^{-4}C/kg$
ラド	rad	$1\ rad=1cGy=10^{-2}Gy$
レム	rem	$1\ rem=1\ cSv=10^{-2}Sv$
ガンマ	γ	1 γ =1 nT=10-9T
フェルミ		1フェルミ=1 fm=10-15m
メートル系カラット		1メートル系カラット = 200 mg = 2×10-4kg
トル	Torr	1 Torr = (101 325/760) Pa
標準大気圧	atm	1 atm = 101 325 Pa
カロリー	cal	1cal=4.1858J（「15℃」カロリー），4.1868J（「IT」カロリー）4.184J（「熱化学」カロリー）
ミクロン	µ	$1\ µ=1µm=10^{-6}m$

（第8版，2006年改訂）